A pH SENSOR BASED ON A FLEXIBLE SUBSTRATE

by

WEN-DING HUANG

Presented to the Faculty of the Graduate School of

The University of Texas at Arlington in Partial Fulfillment

of the Requirements

for the Degree of

DOCTOR OF PHILOSOPHY

THE UNIVERSITY OF TEXAS AT ARLINGTON

May 2010

ACKNOWLEDGEMENTS

I would like to express my deepest appreciation and gratitude to my supervising professor Dr. Jung-Chih Chiao who gave me opportunities to work on interdisciplinary research projects, and always encourage me to improve my capabilities in the knowledge of my research, logic, and langrage. Without his support, guidance and enthusiasm, I could not have chance to get into MEMS and biomedical research fields. Without his research experience and advising, this dissertation couldn't been finished. His support and encouragement throughout the thesis enlighten me to finish this work.

I would like to thank my dissertation committees: Dr. Jonathan Bredow, Dr. Ronald L. Carter, Dr. Weidong Zhou, and Dr. H.F. Tibbals for their interest in my research and for taking time to serve in my dissertation committee. My sincere appreciation also extends to Dr. Shou-Jiang Tang and Ms. Deborah Hogg from UT Southwestern Medical Center for their highly professional suggestions and help on the animal experiments.

I would like to thank the technicians and facility support from UTA NanoFab. Without their experience, this project and devise will never be finished and successful. Furthermore, I wish to thank all of my friends at UTA and colleagues in iMEMS group. Your friendship and support are my valuable assets.

Finally, I would like to express my appreciation and thanks to dear Weilin and my family for their unceasing support and encouragement throughout my career.

April 13, 2010

ABSTRACT

A pH SENSOR BASED ON A FLEXIBLE SUBSTRATE

Wen-Ding Huang, PhD

The University of Texas at Arlington, 2010

Supervising Professor: Jung-Chih Chiao

pH sensor is an essential component used in many chemical, food, and bio-material industries. Conventional glass electrodes have been used to construct pH sensors, however, have some disadvantages. Glass electrodes are easily affected by alkaline or HF solution, they require a high input impedance pH meter, they often exhibit a sluggish response. In some specific applications, it is also difficult to use glass electrodes for *in vivo* biomedical or food monitoring applications due to the difficulty of size miniaturization, planarization and polymerization based on current manufacturing technologies.

In this work, we have demonstrated a novel flexible pH sensor based on low-cost sol-gel fabrication process of iridium oxide (IrO_x) sensing film (IROF). A pair of flexible miniature IrO_x/AgCl electrode generated the action potential from the solution by electrochemical mechanism to obtain the pH level of the reagent. The fabrication process including sol-gel, thermal oxidation, and the electro-plating process of the silver chloride (AgCl) reference electrode were reported in the work.

The IrO_x film was verified and characterized using electron dispersive analysis (EDAX), scanning electron microscope (SEM), and x-ray diffraction (XRD). The flexible pH sensor's

performance and characterization have been investigated with different testing parameters such as sensitivity, response time, stability, reversibility, repeatability, selectivity and temperature dependence. The flexible IrO_x pH sensors exhibited promising sensing performance with a near-Nernstian response of sensitivity which is between –51.1mV/pH and –51.7mV/pH in different pH levels ranging from 1.5 to 12 at 25°C.

Two applications including gastroesophageal reflux disease (GERD) diagnosis and food freshness wireless monitoring using our micro-flexible IrO_x pH sensors were demonstrated. For the GERD diagnosing system, we embedded the micro flexible pH sensor on a 1.2cmx3.8cm of the capsule size of wireless sensor implanted inside the esophagus. Our pH electrode can monitor the pH changes of gastric juice in real time when the reflux happening in the esophagus. Our micro flexible pH sensor performed clear responses in each distinct pH reflux episode quickly and accurately comparing with the other commercial pH monitoring system.

For the food freshness monitoring applications, we used the flexible pH sensor as a freshness indicator to monitor the pH changing profile during the food spoilage procedure. The sensor was then embedded with radio frequency identification (RFID) based passive telemetry enabling remote monitoring of food freshness. In the result, our pH-wireless RFID system presented 633Hz/pH of the sensitivity in the frequency calibration. The calibration of stability and dynamical response of the RFID system were also demonstrated before the test on food freshness monitoring. Finally, a white fish meat for long term spoilage procedure monitoring was applied and tested by using our wireless IrO_x pH sensing system. Our RFID pH sensing module is able to monitor, collect and transmit the pH information continuously for 18 hours during the food spoilage procedure.

In this dissertation, a micro size of IrO_x/AgCl pH sensor was fabricated on a flexible substrate. The physical properties of the IrO_x thin film was verified in the work. The different sensing capability such as the sensitivity, stability, reversibility, response time, repeatability, selectivity, and temperature dependence was then demonstrated in this work. After the different

in-vitro tests, the pH sensor were embedded with our passive RFID circuitry for the in-vivo GERD diagnosis and food freshness monitoring application. Our wireless pH sensing system was able to deliver the accurate and quick pH sensing data wirelessly.

In conclusion, our deformable IrO_x pH electrodes have been demonstrated with the advantages of accommodating and conforming sensors in small spaces or curved surfaces. This miniature IrO_x pH sensor can respond to distinct potentials of the various pH levels as traditional glass electrodes, however, the miniature, bio-compatible and flexible substrate and the ability to be integrated in batterryless telemetry enable the pH sensor to be applied on many new medical, bio-chemical and biological field.

TABLE OF CONTENTS

LIST OF ILLUSTRATIONS

Figure Page

LIST OF TABLES

CHAPTER 1

INTRODUCTION

1.1 Motivation

The pH measurement is the most widely performed test which reflects the grade of solvents in chemical laboratory since 1909. Therefore, pH sensor has become an essential component used in many applications such as chemical, food, and bio-material industries. In the 90 years since the first use of the electrode to determine hydrogen ion concentration, the glass type electrode has been a matured routine tool to classify the pH level of the chemical solvents. The glass pH electrodes performed good sensitivity, selectivity, stability and long life time in pH sensing test. However, glass electrodes have several disadvantages due to the physical nature of the glass membrane. Glass material is easily affected or dissolved by alkaline or Hydro-Fluoride (HF) acid. Moreover, the size of electrode is bulky which hard to reduce the size for micro-scale or implant testing requirement such as in food or bio-medical in-vivo testing environment. The brittle nature of the glass also increases the risk of leaving sharp debris during the experiment. Therefore, to achieve small sizes and reliable performance in pH sensing applications, a deformable, biomechanically-compatible and implantable pH sensors then are needed.

1.2 Proposed Approach

To achieve small sizes and robust design, ion-sensitive field-effect transistor (iSFET) pH sensors [1.1-1.5], optical fiber pH sensors [1.1, 1.6-1.11], hydrogel film pH sensors [1.12-1.14], and solid state pH sensors [1.1, 1.15-1.18] have been proposed. iSFET sensors have power consumption concerns due to the FET operation requirement [1.19]. Hydrogel film pH sensors utilize the physical properties of the pH-response swelling and shrinking polymer to

measure resistance changes [1.12]. The sensor structure design and polymer layer fabrication process could be complicated and expensive [1.13]. Optical pH sensors also have power consumption issues due to the use of light sources. The system including optical devices could be expensive and unsuitable for implantation [1.1, 1.7-1.8, 1.10-1.11].

1.3 Innovation Work

In order to achieve cost effectiveness, simpler fabrication and lower power consumption, a metal-oxide pH sensor with deformable flexible substrate was proposed in our work. Various solid state metal oxides have been investigated for pH sensing electrodes [1.1, 1.15] including PtO_2, IrO_x, RuO_2, OsO_2, Ta_2O_5, RhO_2, TiO_2 and SnO_2 as the pH sensing films. The pH sensitivity, selectivity, working range, and hysteresis indicate sensing performance. IrO_x, RuO_2 and SnO_2 have been demonstrated with more advantages in sensor performance for various applications [1.22]. RuO_2 [1.18, 1.20] and SnO_2 [1.21] show near Nernstian responses in wide pH ranges. However, SnO_2 and RuO_2 presented hysteresis and drift problems leading to potential calibration issues and unstable responses [1.20, 1.21]. PtO_2 and Ta_2O_5 can only perform the limited pH sensing range from 5 to 10 [1.15]. Furthermore, higher redox cation interference is mentioned on TiO_2, RuO_2, RhO_2, PtO_2 and OsO_2 sensing film [1.15, 1.20].

According to some literature researches, Iridium oxide film (IROF) has been proposed with outstanding stability over wide pH ranges, rapid responses, less potential drift and high durability, which have also been demonstrated at high temperature up to 250ºC [1.23].

In this work, we developed a miniature pH sensor array based on flexible Kapton substrates using iridium oxide sol-gel fabrication techniques. The purpose was to develop a smart electronic litmus pH sensing film. The amorphous iridium oxide thin film was formed by dip-coating and sequential heat treatment techniques [1.24] which have been used in industry. We investigated design considerations, fabrication processes and experimental results of the deformable miniature pH sensors.

1.4 Dissertation Architecture

There are three major parts presented in this dissertation. First part will be the fabrication and the performance test of the IrO_x pH sensor which is from chapter 2 to chapter 4. The objectives of the first part are to build a low cost, small size, non-glass base, and quick response of pH sensor. According to the goals of the sensor design, we used the low-cost IrO_x sol-gel process to simplify the fabrication procedure. The IrO_x sol-gel film showed the good pH sensing performances by doing in vitro test of sensitivity, stability, response time, reversibility, repeatability, selectivity, and temperature dependence. In the first section, we finish a micro size of IrO_x pH sensor on flexible substrate. The good pH sensing performances were then demonstrated in these chapters. Finally, In order to target on the wound healing or other high pH sensitive applications, we built and demonstrated a 4x4 pH sensor array for dynamical pH distributing detection. The multi-solutions, temporal, and spatial test were presented and applied.

In the second parts of dissertation, we are going to present two applications of our flexible pH sensor on freshness indicator, and GERD diagnosis. A flexible IrO_x pH sensor was embedded with a passive battery-less RFID circuitry to reach the wireless pH sensing. The first application is the smart wireless freshness indicator. Our pH sensor was used to monitor the food quality. The freshness indicator can be attached with the food package, and monitor the food condition in order to reduce the risk of spoilage or contamination during the delivery or storage. In the GERD diagnosis, the in vitro and in vivo test were applied and demonstrated in chapter 5. Our wireless pH sensing system was able to catch the gastric juice reflux wirelessly, quickly and precisely. It can reduce the risk of esophagus cancer happening.

In the chapter 6, we proposed the possibility of the pH sensing by using smaller electrode size in order to target on micro- or nano- scale of the pH measurement potential. In order to target on the applications of medical environment such as the wound healing monitoring, we demonstrated three sizes of the exposure area on the sensor. The sensitivity

kept similar even that the sensor size is in micro scale. These two works represented that our flexible pH sensor is able to used and applied on the medical or bio-medical applications in the future. Finally, two future works for new applications are proposed by using the iridium oxide material. One is the nerve simulator needle, and another is the immune-sensor. The IrO_x material contains excellent physical properties such as the high conductivity, porosity, and redox capability. These applications can be able to apply for bio-medical or industrial in the next generation.

CHAPTER 2

LITERATURE REVIEW OF IRIDIM OXIDE

2.1 Iridium (Ir) and Iridium oxide (IrO_x)

The iridium (Ir) has been confirmed as a noble metal which is stable in all pH levels of aqueous solutions [2.1]. Iridium has very high resistance to aggressive chemical reagents such as the aqueous solutions of caustic alkalis, acids and oxidizing agents [2.1]. In finely divided state, iridium most probably takes place through the formation of complex ions in which iridium has a valence of +3 (ex. Ir_2O_3) or +4 (ex. IrO_2). At atmospheric pressure and 25ºC iridium can absorb 807 times its own volume of hydrogen. When used as an anode, iridium is not usually attacked, even in the presence of chlorine liberated by electrolysis. Oxygen is adsorbed onto the metal surface when an iridium anode is polarized in the presence of dilute sulfuric acid or dilute caustic soda, even when the potential is low. When used as a cathode, iridium absorbs hydrogen, which gradually penetrates into the metal [2.1]. On heating in air or oxygen, iridium will be tarnished, and owned to superficial oxidation to IrO_2; at temperatures of 750-1000ºC, iridium loses weight through volatilization, most likely as IrO_4; the anhydrous oxide Ir_2O_3 is normally hard to prepare. The hydrated form of Ir (III) is $Ir_2O_3 \cdot xH_2O$ which is soluble in acids and alkaline, and is easily oxidized to Ir (II) of $IrO_2.2H_2O$ by the common oxidizing agents such as air.

Therefore, iridium can be oxidized and tarnished to different types of iridium oxide (IrO_x) depending on the different fabrication methods. The characteristics of IrO_x are generally very sensitive to its structure and composition which very depends on varies fabrication methods. Basically, for the stable structure of IrO_2 as shown in Fig. 2.1, it crystallizes in the tetragonal rutile structure [2.2]. The rutile structure has edge-sharing octahedrally coordinated metal ions

which are form chains along the [001] direction. The feature of the rutile structure is that the O-O bonds are not equal, so the base of the octahedron is not square, the shared edge being shorter than the edge parallel to the c axis.

According to the differences of structure and composition of iridium oxide (IrO_x) films and their influence on the kinetics and mechanism effect, the various applications was proposed [2.3] such as the oxygen deficiency of the iridium oxide as Ir_2O_3-Ir(III) and Ir_2O_2-Ir(II). The experimental results show that the charge carrier concentration and plasma frequency of iridium oxide increase significantly as oxygen is removed from the unit cell. In addition, highly conducting iridium oxide films are excellent electro-catalysts for O_2 evolution and serve as stable anode materials for C_{12} evolution.

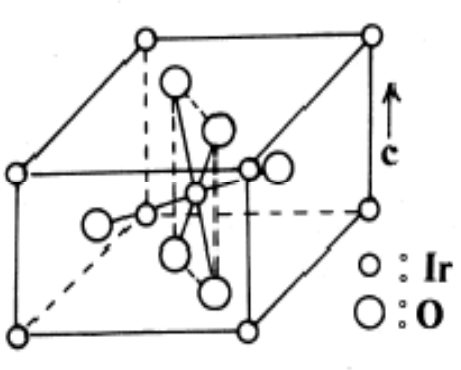

Figure 2.1 The arrangement of the atoms inside a unit cell of tetragonal IrO_2 [2.2].

To form an IrO_x, thermal and electrochemical base of preparing methods are the standard process in different fabrication methods. Generally speaking, anodic iridium oxide film (AIROF) can be done by electrochemical fabrication. The poorly crystallized structure and highly hydrated surface are the basic properties of these kinds of iridium oxide films [1.22]. Sputtering iridium oxide (SIROF) and sol-gel (SG) IrO_x are based on thermal preparing method. Annealing oxidation is required in the fabrication process. The different heating profile and temperature point will change the morphology of the iridium oxide [2.4]. The different structure of iridium oxide can be an important factor for different applications. For example, the higher crystalline IrO_x structures were used to improve the electro-chromic properties such as light dispersion for

the better absorption of the solar cell in energy harvesting system [2.4]. However, for the pH sensing requirement, a stable sensing film with low crystalline properties of IrO_x is required because the stability of the surface quality is controlled by the crystallization of the structure. The lower crystalline structure is a physically stable structure which the iridium atom is aligned and stacked in the same order. Therefore, regarding higher crystalline properties containing more disorder iridium oxide atoms, the structure of the higher crystallization will be very loose which is not suitable for long term sensing.

2.2 Iridium Oxide Fabrication Methods

2.2.1 Electro-deposition

In the IrO_x electrodeposition fabrication process, iridium oxide film can be deposited on a variety of electronically conducting substrates, such as Ti, Pt, or glassy carbon. This method is useful to produce the micro-electrode and is less expensive than electrochemical and thermal oxidization since it doesn't require Ir substrates. Yamanaka [2.5] deposited IrO_x film on indium tin oxide (ITO) conductive polymer by using iridium tetrachloride ($IrCl_4$), hydrogen peroxide (H_2O_2), oxalic acid (CH_3COOH) and potassium carbonate (K_2CO_3) as a soluble iridium precursor. IrO_x was deposited by driving 2-3 A/m^2 current for 15 minutes at 10°C either on anode or cathode. The results show the deposited film has very small crystals about 15 Angstrom diameters. However, in this fabrication process, the pH value of the deposition solution, solution temperature and current density control may easily affect the deposition efficiency. A precise costly power supply system such as potentiostat is also required in the electro-deposition process for thickness and film quality control. The crystallization of the IROF is not strong as the film from thermal oxidation fabrication process. Those concerns are easy to complicate and influence the film quality of IrO_x.

2.2.2 Electro-chemical deposition

In the electro-chemical deposition, a hydrous iridium oxide layer is grown on the surface of pure iridium when it is electrochemically activated in an electrolyte. The IrO_x can be prepared

by cycling its potential called cyclic voltammetry (CV) method in a solution such as H_2SO_4 or NaOH. In cyclic voltammetry experiment, the working electrode (Iridium) potential is ramped linearly versus time like linear sweep voltammetry. Cyclic voltammetry takes the experiment a step farther than linear sweep voltammetry which ends when it reaches a set potential. When cyclic voltammetry reaches a set potential, the working electrode's potential ramp is inverted. The complete process is finished by the internal material oxidation-reduction as shown in Fig. 2.2. During the fabrication, the current will increase by precise control from potentiostat until the potential reaches the reduction potential of the analyte at point (3), then falls off as the concentration of the analyte is depleted close to the electrode surface. If the redox couple is reversible then when the applied potential is reversed, it will reach the potential that will reoxidize the product formed in the first reduction reaction, and produce a current of reverse polarity from the forward scan. As a result, a thin film of iridium oxide created by redox potential and electrochemical reaction will be obtained and compounded on the surface of the working electrode (Ir). This single process can be repeated multi-time in order to get thicker layer of IrO_x.

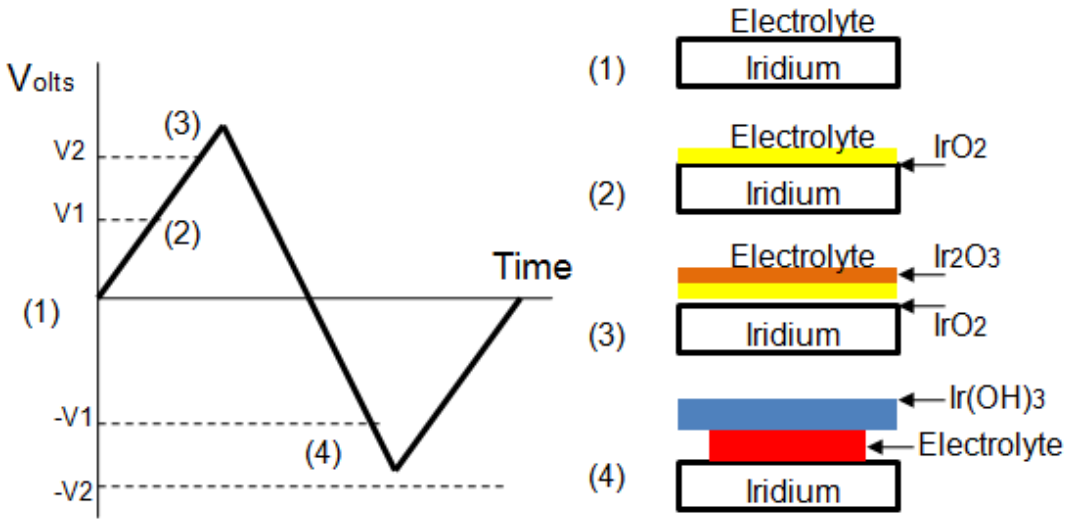

Figure 2.2 The multi-layer iridium oxide film by using cyclic voltammetry fabrication.

The morphology of the hydrous IrO_x film depends on the electrolyte. This kind of IrO_x is hydrous, very porous and provides a high degree of transport for water, protons and other ions

[2.6]. However, in this fabrication process, the current also need to be under very precise controlled, and potential must exceed critical upper (E^+_g) and lower (E^-_g) potential limits during each deposition cycles [1.22]. The costly potentitiostat and pure iridium oxide substrate are needed by using this fabrication.

2.2.3 Sputtering

Sputtering deposition of IrO_x electrodes has become quite popular. However, the SIROF deposition process is costly due to the target cost. At room temperature, the SIROF appear amorphous and a distinctive rutile pattern emerges from films deposited at 200ºC and above. The most stable films are generally deposited at very slow rates (<2 nm/min) controlled by the parameter set up of sputtering machine. Therefore, the oxygen and argon pressure ratios, position of the target, deposition rate, and RF powers during the fabrication processes all affect the pH sensing parameters such as potential drifts and redox interferences [1.22].

2.2.4 Thermal deposition - Iridium oxidation

On heating in air or oxygen, iridium metal will be oxidized to IrO_x. Michael L. Hitchman [2.7] presented the oxidation of Ir wire in air at 800°C. Thermally prepared Iridium oxide film can be made much thicker than AIROFs, and provide more reliable potential values. Generally, thermally prepared IrOx films are comparable in nature to SIROF. Both are anhydrous films called “dry” oxide film as they are less hydrous than AIROF. However, thermally prepared procedure limits the fabrication material because of the highly heating treatment especially for the use of polymer and photoresist as sacrificial material, which often cannot survive at a temperature above 200ºC. Beside the material issue, the film surface has a tendency to crack after the high temperature treatment. The adhesion property of the cracked film then becomes an issue.

2.2.5 Thermal deposition – Sol-Gel (SG) IrO_x deposition

The sol-gel IROF deposition process has been demonstrated with dip coating [2.8, 2.9] and heat treatment [2.4] procedures. K. Nishio, [2.8] established a method for the preparation of

iridium oxide thin films by the sol-gel dip-coating process where iridium tetrachloride ($IrCl_4$) was used as a starting material. The coating solution was prepared by reacting iridium chloride, ethanol and acetic acid. The iridium oxide coating was formed at a 2.0 cm/min withdraw rate, and IROF films did not contain impurities under the heat-treated at 300ºC. Iridium oxide is strongly crystallized at temperatures above 450ºC. This shows we can control the parameters of withdraw rate and annealing temperature to have an appropriate iridium oxide sensing film by using the sol-gel fabrication technology. The dip coating process, and low temperature treatment not only provide simpler and economical fabrication approach, but also allow the fabrication based on micro-scale, and polymer substrate.

2.3 pH Sensing Mechanism of Iridium Oxide

Five different explanations of the electrode mechanism for these oxides have been formulated:

- Simple ion exchange on a surface layer containing OH^- groups. This mechanism is known from the common glass electrode.
- A redox equilibrium between two different solid phases, i.e. a lower and a higher valence oxide, or an oxide and a pure metal phase, such as the antimony electrode:

$$Sb_2O_2 + 6H^+ + 6e^- \Leftrightarrow 2Sb + 3H_2O$$

- A redox equilibrium involves only one solid phase whose hydrogen content can be varied continuously by passing current through the electrode. This is known as a solid solution or intercalation reaction. The process scheme may be written as:

$$H_xMO_n + yH^+ + ye^- \Leftrightarrow H_{x+y}MO_n$$

- A single phase oxygen intercalation electrode may similarly be envisaged, though no examples of pH electrodes involving oxygen-deficit phases have been demonstrated.

- A steady-state corrosion of the electrode material may, in some cases, cause a pH dependent potential.

Three possible mechanisms have been proposed for pH dependent redox intercalation equilibrium between two oxidation states of the iridium oxide [2.10] as

$$Ir_2O_3 + 6H^+ + 6e^- \leftrightarrow 2Ir + 3H_2O \quad (1)$$

$$IrO_2 + 4H^+ + 4e^- \leftrightarrow Ir + 2H_2O \quad (2)$$

$$2IrO_2 + 2H^+ + 2e^- \leftrightarrow Ir_2O_3 + H_2O \quad (3)$$

$$E = E^0 - 2.303\frac{RT}{F}pH = E^o \pm 0.05916\,pH \quad (4)$$

where E^0 is the standard electrode potential with a value of 926 mV vs. standard hydrogen electrode (SHE) or 577 mV vs. Ag/AgCl reference electrode. *F* is the Faraday's constant with a value of 96,487 coul/equiv, and *R* is the gas constant with a value of 8.314 joules/deg. *RT/F* is equal to 25.688 at 25°C. The pH potential sensitivity is –59 mV/pH if space charges are formed [1.22, 2.10-2.11] which is called the Nernstian response. From Fig. 4.4, a near ideal Nerstian slope of –52.3 mV/pH is obtained experimentally. The intercept at pH=0 showing when E equal to E^0 is between 513 mV to 523 mV vs. Ag/AgCl reference electrode also close to the theoretical value. However, there are some effects which may cause the potential difference with the theoretical value of pH sensing mechanism. E^0 value is not always the same in different electrodes. The variation of E^0 may be caused by the variation in the stoichiometry of the oxide compound, and the difference of oxidation state of iridium oxide [1.22]. In addition to the solid phase and intercalation equilibriums, Fog and Buck [1.15] presented that pH response could be also due to ion exchange in surface layer containing OH^- groups. The general equilibrium from Burke [2.12] and Olthuis [2.13] for proton exchange is

(5)

$$[-Ir^{IV}-(OH)_x-Ir^{IV}-]_n+2ne^-+3nH^+ \leftrightarrow [-Ir^{III}-(OH)_{x-3}\bullet 3H_2O-Ir^{III}-]_n$$
$$Ir_2O(OH)_3O^{3-}{}_3+3H^++2e^- \leftrightarrow 2Ir(OH)_2O^-+H_2O \quad (6)$$

The equilibrium of (6) indicated that the theoretical possibility of the sensitivity may be higher than |─59| mV/pH.

2.4 Discussions

In the basic reviews of the physical properties, fabrication methods, and pH sensing mechanisms of Iridium oxide, we are able to decide the requirements which are suitable for the innovated pH sensor design. For the physical properties, we want to build a physically stable IrO_x thin film for long term using. Therefore, the lower crystalline structure of IrO_x is required and needed. The physically stable structure for the iridium atom is aligned and stacked in the same order, and the condensing density is higher than the highly crystalline IrO_x film. For the fabrication methods, according to the requirement of polymer substrate, we should use the lower annealing temperature during the fabrication process. The thermal oxidation method won't be suitable because of the thermal limitation of polymer's nature property. Furthermore, the higher oxidation temperature also causes higher crystalline structure which will be presented on the next section. According to those requirements, the sol-gel method is the suitable fabrication process for the innovated pH sensor. The advantages of sol-gel fabrication include flexible parameter control for fabrication such as the dip-coating, withdraw rate, annealing temperature, and low-cost coating agent. Those factors are related to the film quality of iridium oxide such as the response time or sensitivity of the sensor. For the pH sensing mechanism, it also related to surface quality of the sensing film. Basically, the sensing sensitivity may follow the theoretical Nernstian response. The relationship and chemical reactions between the electrochemical potential and pH level is defined and performed as the equation shown in Eq. (1)-(4). The higher or lower sensing sensitivity represent the surface structure such as the porous, and thickness of the layer.

In this dissertation, we presented the IrO_x sol-gel method as our fabrication process. An amorphous and minor-crystalline of the iridium oxide thin film was formed and tested. The theoretical and experimental result will be proposed on the next two sections.

CHAPTER 3

SENSOR FABRICATION PROCESS

Our pH sensor was fabricated by standard photolithography and lift-off processes. All of the metal layers were deposited by electron-beam evaporation. First, a layer of 7-nm thick Cr was deposited on a piece of Kapton polyimide substrate, followed by a 0.1-μm thick layer of Au. Iridium oxide sensing film was formed by the sol-gel process [2.8] which will be discussed in the next section. 7-nm thick Cr and 3-nm thick Pt were evaporated for adhesion. A 30-nm thick silver layer then was deposited by electron-beam evaporation. Silver chloride (AgCl) reference electrodes were formed by electroplating. The working and reference electrode areas are 2×2 mm². The fabrication procedure is illustrated in Fig. 3.1.

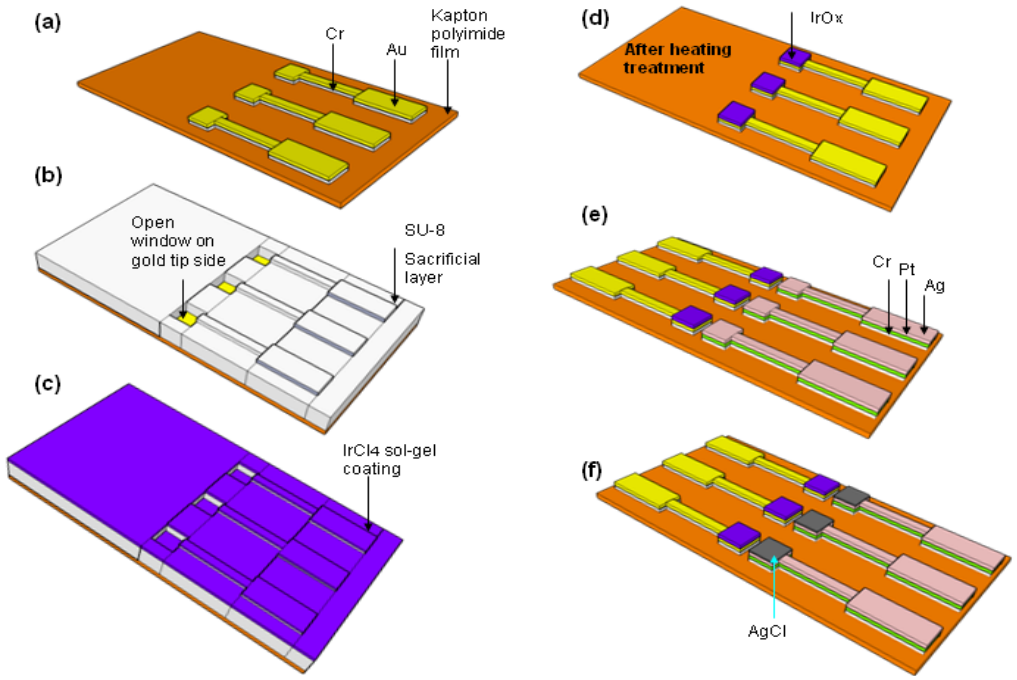

Figure 3.1 Fabrication processes: (a) Cr and Au deposition on a Kapton polyimide substrate, (b) SU-8-100 deposition for the sacrificial layer, (c) $IrCl_4$ sol-gel process, (d) thermal treatment, (e) Cr, Pt and Ag deposition and (f) AgCl electroplating.

3.1 Iridium Oxide Sol-Gel Process

3.1.1 Coating agent

The sol-gel coating solution was based on the recipe for rigid substrates described in [2.8]. One gram of anhydrous iridium chloride ($IrCl_4$) was dissolved in 42 ml of ethanol (C_2H_5OH) followed by adding 10 ml of acetic acid (CH_3COOH) in the solution. The solution was stirred continuously by a magnetic rod at the bottom of the beaker for at least one hour. Fig. 3.2 shows the flowchart of the IrO_x sol-gel process. The chemical reaction took place as follow:

$$2IrCl_4 + 3H_2O \xrightarrow{300^oC} Ir_2O_3 + 6HCl + Cl_2 \qquad (7)$$

In this recipe, the $IrCl_4$ will be just floating on the ethanol when the agent was mixed. The acetic acid was added in order to keep the solution at low pH level. The lower pH level will let the solution stable to avoid the other chemical reaction happening during the mixing procedure [2.8]. The dip coating process was then applied in order to get more condensers surface comparing with other method such as the spray or spin coating process. The detail of dip-coating and annealing process will be explained on the next section.

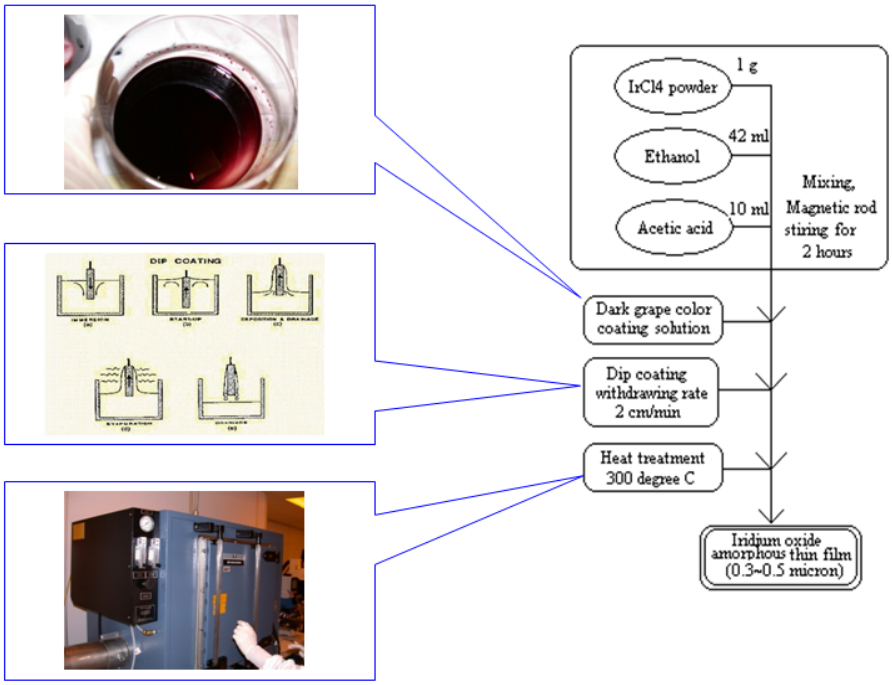

Figure 3.2 IrO_x sol-gel process.

3.1.2 Dip coating process

3.1.2.1 Film formation

In the sol-gel process, there are some ways to coat the thin film on the substrate such as the spin coating, dip coating, and spray method. The condensing agents such as the polymer or photoresist normally use the spin coating method. The advantage of spin coating is that a film of liquid tends to become uniform in thickness during the sample in the spin-off process. Once the surface becomes uniform, the thickness tends to remain the viscosity, and the thickness won't diffuse varying by different substrate [2.9]. The procedures of the spin coating are deposition, spin-up, spin-off, and evaporation. However, in our application, our coating agent is based on the ethanol which is easy evaporated in few seconds. Therefore, when the coating agent is deposited, then the agent just evaporates. The particle inside the agents will not be coated uniform. On the other hand, the spray method is depended the human control which by hand or nozzle. The deposition area is hard to control, and the particles will not be spread uniformly.

For dip coating method, it is suitable for the agents which have higher evaporation property. The continuous dip coating process is shown in Fig 3.3. Basically, the dip coating process is divided in to five steps: immersion, start-up, deposition, drainage, and evaporation [2.9]. The thickness of the deposited film is related to the position of the streamline dividing the upward- and downward-moving layers [2.9]. There are six forces: (1) viscous drag upward by the moving sample, (2) force of gravity, (3) resultant force of the surface tension, (4) inertial boundary force, (5) surface tension gradient, and (6) disjoining or conjoining pressure in order to control and govern the deposition position and streamline [2.9].

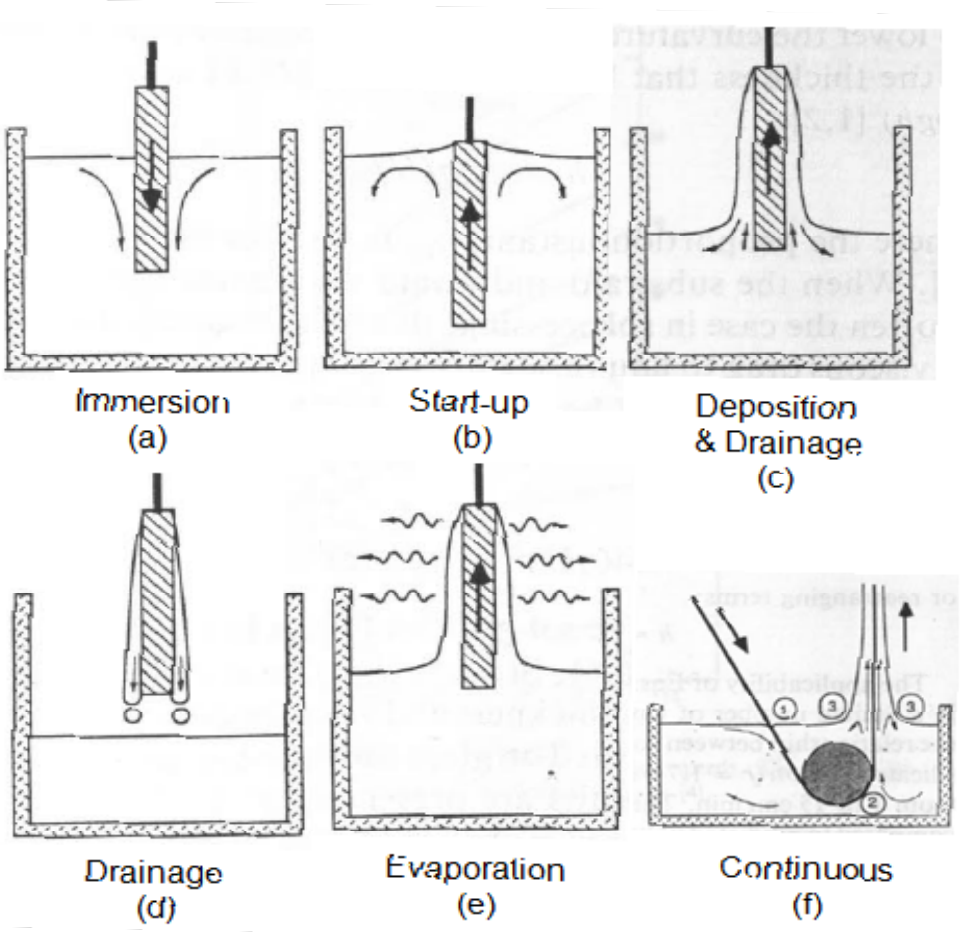

Figure 3.3 Six stages of the dip coating process from: (a) to (e), and (f) continuous withdrawing [2.9].

3.1.2.2 Withdraw rate and film thickness

In our application, the thickness of the film is an important parameter because the surface charge density is higher if the film is thicker. The charge density can be able to represent the capability of the surface electron charge as a capacitor. The thickness is also related to the response time of the pH sensing performance which we will present on the chapter 3. During the dip coating process, the relationship between the liquid viscosity (η), thickness (h), gravity force (ρgh), and substrate speed (U) is shown by:

$$h = c_1 \bullet (\frac{\eta U}{\rho g})^{1/2} \qquad (8)$$

where the proportionality constant c_1 is about 0.8 for Newtonian liquids. The equation (8) represented that the faster withdraw speed will make thicker thickness of the deposition. In our requirement, the thickness should maintain properly due to the surface charge related to the response time. However, in opposite, the thicker layer will represent poorer porosity which will reduce the sensitivity of the sensing performance. Therefore, in order to control the sensing sensitivity and response speed, we should create a proper thickness which is to maintain the response time, but still have enough surface porosity to keep the constant sensing sensitivity. The experiment data is proposed on the next section.

3.1.2.3 Experiment

In this experimental test, we applied different withdraw rates at 2 cm/min, 5 cm/min, 10 cm/min, and 12 cm/min during the dip coating process. By using our homemade dip coater as shown in Fig. 3.4; which provided a good withdrawing stability by a stable stepper motor speeding control based on Microsoft Visual Basic (VB) program interface, the thickness of IrO_x thin film did follow the theoretical equation (3). The thickness is increasing from 0.1μm to 1.2μm when the withdraw rate increased as shown in Table 2.1. In order to find a proper withdraw rate, we also measured the sensitivity test for each speed. Finally, we will use the 10 cm/min of withdraw rate because we can get thicker thickness with a better sensitivity value.

Table 3.1 Experimental data for different thicknesses with different withdraw rate

Withdraw rate	Thickness(μm)	Ave. Sensitivity(mV/pH)
2 cm/min	0.05-0.1	39.8
5 cm/min	0.6	51.7
10 cm/min	**1.10-1.20**	**55.9**
12 cm/min	1.2	55.3

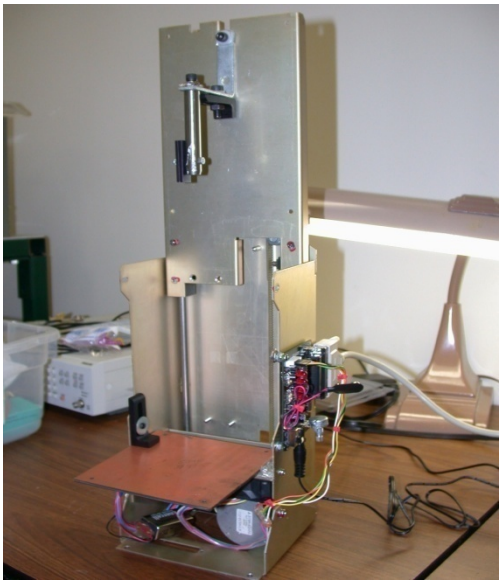

Figure 3.4 Homemade dip coater.

3.1.3 Annealing process

In the previous section, the surface quality is investigated and represented by the thickness of the sensing film related to the different coating method and agents. In this section, for the sol-gel process, the influence of temperature treatment is investigated because the heating temperature is also an important parameter which is related to the surface quality. Regarding our requirement of the sensor design, an amorphous, stable, and non-crystalline of the sensing film is required. We will compare the design methodology under different temperature treatments. The material structure during the heating process will be also represented in this section. Finally, the experimental result will be proposed in this and next chapter.

3.1.3.1 Structure transformation

There are two major systems defined and concerned in material structure. One is the amorphous system, and another one is crystalline system. In our fabrication process, the $IrCl_4$ is a powder form which can address in to the amorphous system. In this dissertation, we will introduce the detail structure change during the annealing treatment in amorphous IrO_x system.

In the complete temperature range of the annealing process from 0°C to 700°C, there are three regions represented by different physical and chemical change called shrinkage. The Region-1 is proposed in the temperature range from 0°C to 150°C. The weight loss is caused by the endothermic process attributed by the desorption of the physically adsorbed water. The water molecular is gone because of the thermal desorption. The structure of the material becomes a skeleton structure which has lower thermal expansion coefficient, and is a higher condensed structure.

In the Region-2 which the heating temperature is between the 150°C to 510°C, the shrinkage primarily caused by the removal of organics, polymerization, and structural relaxation. For the removal of organics, various C-H, C-O, M-OR stretching vibration will reduce the relative intensities of the sharp bands. The more condensed structure is produced because the temperature is higher. The phenomenal also shows the skeletal density accompanying with the weight loss. For the structural relaxation, the process is due to more free volume released by the mechanisms of the water desorption or organics removal. This phenomenon allows the structure approaching the material configuration characteristic of the metastable condition. The material molecule may be rearranged within the skeletal phase to higher coordination sites. Thus, the new structure of the material may be represented by a good alignment of lattice. The surface properties will be more rigid, but less flexibility. The surface is somehow easy to crack on particular orientation [2.8].

In the Region-3, the predominant shrinkage mechanism is to produce the strong viscous sinter. In this phenomenon, the shrinkage rate is proportional to the surface energy divided by the surface pore size and viscosity. The sintering kinetics is related to the surface energy which will create the different porous structure. Normally, the sintering phenomenon happens at the temperature above about 600°C. Heating to 1100°C, the surface area is reduced, and some atom groups or bonds may loss or change the angle because of the lack of exposed surface area available for rehydration [2.8]. In our application, the annealing

temperature is about 300°C-350°C which locate at Rigion-2. The removal of organic and structural relaxation will dominate the mechanisms of structure change of the IrO_x thin film. The surface may theoretically have minor skeleton structure and weight loss. In the chapter 4, we have the result comparison with the sample heated at 550°C.

H. Andreas [3.1] also presented that the IrO_x surface quality such as the charge density and film morphology are related to different withdraw rate, the quality of dip coating process, and different annealing temperature.

3.1.3.2 Experiment

After the dip coating process, the sample was baked on the hot plate at 120ºC for about 3 minutes in order to dry the coating agent on the opening window. The SU-8 100 sacrificial layer were then torn off by using tweezers, and the sample was then ready for annealing treatment process without the SU-8 polymer layer.

In the heating treatment of our process, the sample was thermally treated with a heating profile starting at 25^{o}C to 300^{o}C in a 2-hour period. The temperature stayed at 300^{o}C for 5 hours. To obtain amorphous iridium oxide film, the surface needs to only be heated at below 350^{o}C [2.8-2.10]. The furnace was then cooled down in a 10-hour period to 25^{o}C. Fig. 3.5 shows the morphology of the IrO_x surface at peak treatment temperatures of (a) 300^{o}C and (b) 550^{o}C using the ZEISS Supra 55 VP scanning electron microscope (SEM). At 300^{o}C, an amorphous surface was formed without cracks which means the surface still kept at the structure eventually the water desorption. Fig. 3.5(a) shows uniform and smooth surface; even at the boundaries to the gold layer where cracks form often due to thermal treatment. In opposite, the iridium oxide thin film crystallized at 550°C [2.8] and the surface cracked at multiple places across the film, as shown in Fig. 3.5(b). This phenomenon showed the structure was transformed to skeleton form. The lattice of IrO_x was rearranged, and aligned because of the weight lost and structural relaxation which is Rigion-2 that we mentioned in the previous section. Therefore, for the pH sensor applications, a uniform film surface is required. After

experimenting at different temperatures, it showed that the 300°C heat treatment would provide good film quality.

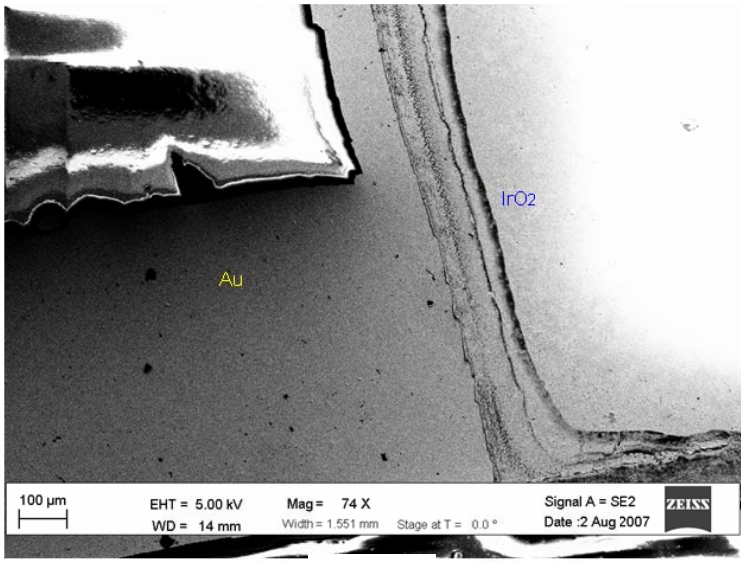

(a)

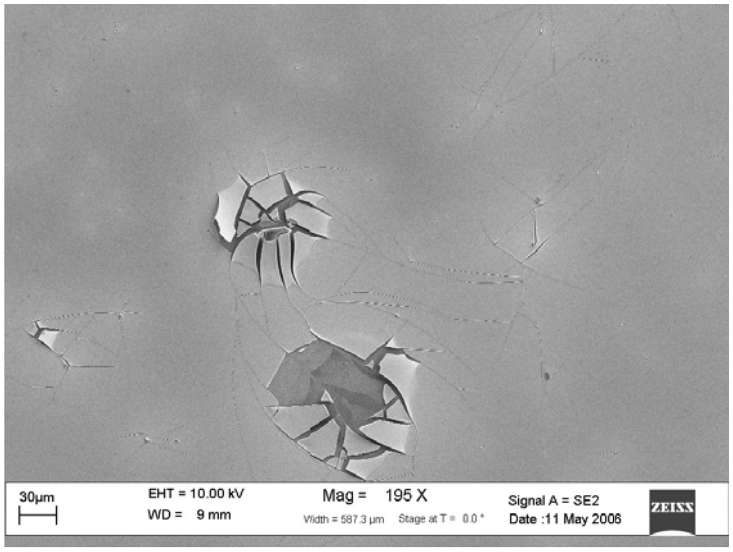

(b)

Figure 3.5 SEM photos of the IrO_x films treated at (a) 300°C (amorphous) and (b) 550°C (crystalline).

3.2 Silver Chloride (AgCl) Reference Electrode Electro-Plating Process

Electrochemical anodization process was used on an anodic silver electrode with a platinum cathode electrode in 0.1-M HCl solution. An electrical current of 0.5 mA was applied on electrodes in HCl solution for 5 seconds. Fig. 3.6 shows the AgCl electro-plating setup. During the electrolysis, a brown silver chloride layer was formed on the silver surface of the polyimide substrate as shown in Fig. 3.7(a). The electrode surface was rinsed by DI water and then immersed in 3-M KCl solution for 24 hours to saturate and stabilize potentials [3.2]. Fig. 3.7(b) shows the electrodes after the saturation process. Fig. 3.8 shows the SEM of the AgCl surface. It shows gap between each AgCl crowd is only about less than 1μm as shown in Fig. 3.8(a). The Fig. 3.8(b) shows the different zoom scale of the SEM photo. The surface is even and clean without any crack.

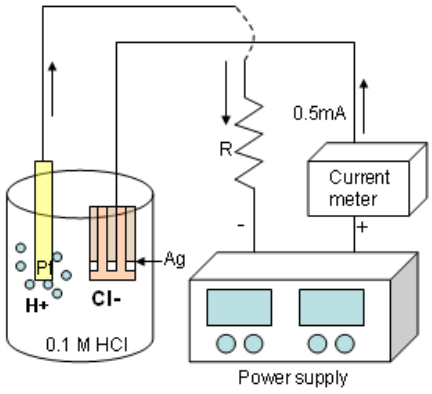

Figure 3.6 Electroplating setup for AgCl reference electrode.

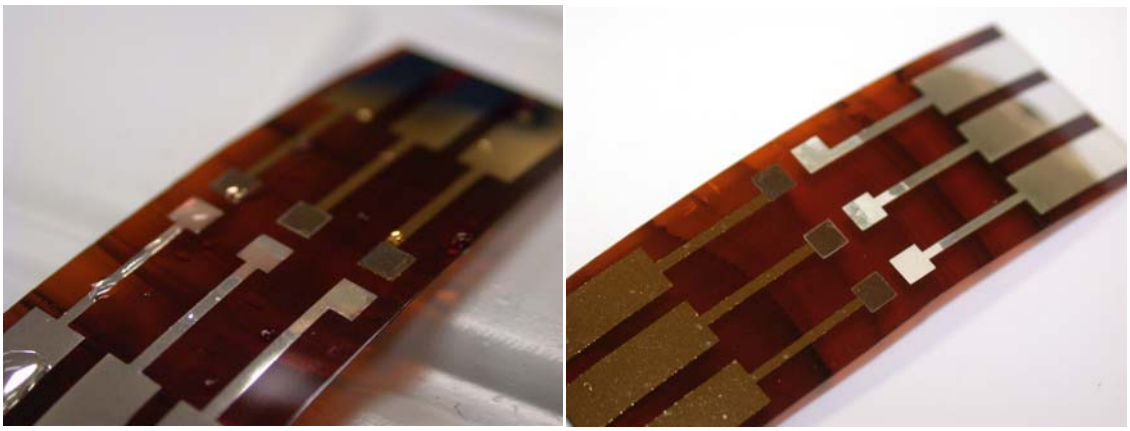

(a) (b)

Figure 3.7 AgCl electroplating layer (a) before and (b) after the KCl saturation process.

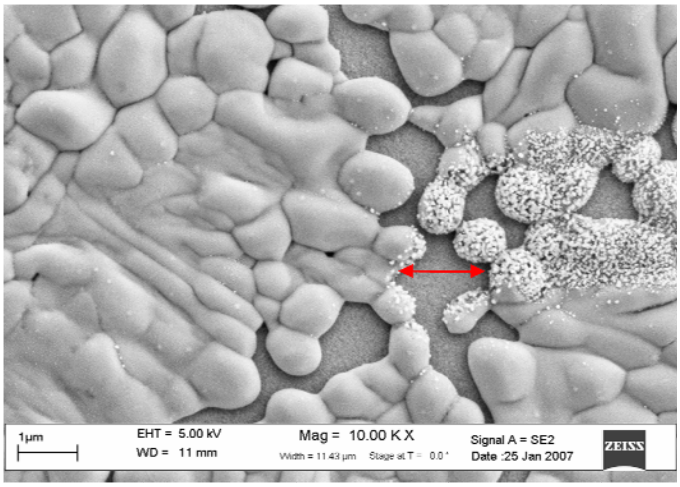

(a)

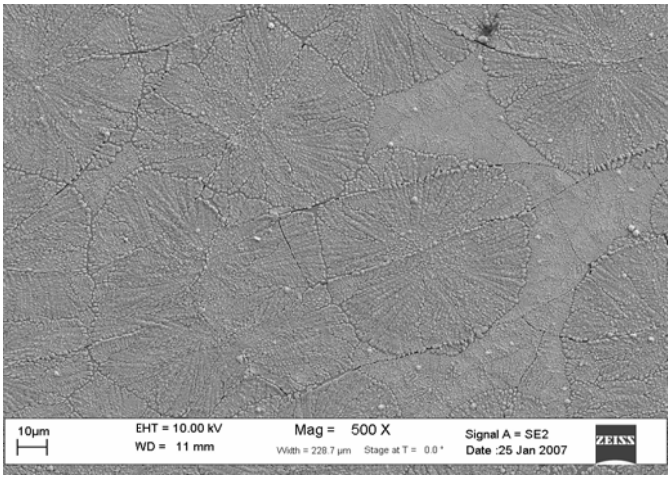

(b)

Figure 3.8 SEM picture of AgCl in the scale of (a) 10KX, and (b) 500X.

3.3 Discussions and Conclusions

In order to form an even, stable and amorphous iridium oxide thin film, the sol-gel process is used and investigated. The dip coating process was then applied during the sol-gel process because the high evaporation of ethanol based solvent is used as the coating agent. The surface molecule will be coated in more even and condensed quality than other methods such as the spin coating and spray method. The relationship between the withdraw rate and thickness were also investigated and proved in both theoretical and experiment result. For the

annealing process, 300°C of the heating temperature is applied to form an amorphous structure of IrO_x thin film which is more stable and uniform for the sensor application. The X-Ray diffraction analysis (XRD) and electron dispersive analysis (EDAX) will be proposed on the next chapter.

For the AgCl fabrication, we applied a traditional electro deposition process on the polymer flexible substrate. The good adhesion and condensation of the AgCl surface were shown in SEM picture. The surface was then soaked in KCl agent in order to keep the stability of the standard constant potential.

In conclusion, an entire IrO_x sol-gel fabrication process was investigated and completed. The dip coating method is applied with the 10cm/min of withdraw rate which reached a proper pH sensing sensitivity and response time. The amorphous structure was formed by proper annealing temperature. For AgCl electroplating process, the surface is even and uniform. The pH sensor based on the IrO_x/AgCl is ready for the test.

CHAPTER 4

RESULTS AND DICUSSIONS

4.1 Testing Setup

Fig. 4.1 shows the measurement setup. An Agilent 34401A digital multi-meter with GPIB interface operated with a LabVIEW program was used for real-time analog potential recording. In between the IrO_x pH sensor and multi-meter, a unit gain amplifier made by Texas Instrument TLC074 op-amp was added as the buffer to provide an appropriate impedance match. A commercial pH meter was used to verify the pH values of testing solution. During the experiment, our pH sensor was immersed in acid or alkaline based diluted test solution. We used hydrochloric acid (HCl) for acidic tests while potassium hydroxide (KOH) solutions were used for alkaline tests. The potential and pH values were displayed and recorded in a computer simultaneously.

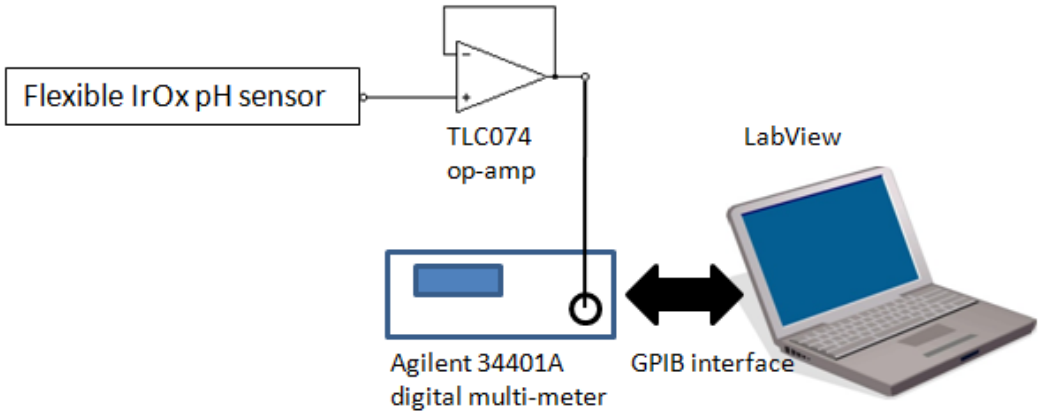

Figure 4.1 pH titration and measurement setup.

4.2 Electron Dispersive Analysis (EDAX) and X-ray Diffraction (XRD) Analysis

In order to confirm the existence and quality of IrO_x film after sol-gel fabrication, the electron dispersive analysis (EDAX) and X-ray diffraction (XRD) analysis were applied in this work. The sample was prepared for energy-dispersive x-ray analysis using the EDAX 4000 system in a Zeiss Supra 55 VP scanning electron microscope (SEM). Fig. 4.2 shows the energy-dispersive x-ray analysis result of the sol-gel IrO_x film. The ratio between iridium and oxygen was measured 2.4. Some other small amounts of elements such as chlorine, silicon and carbon detected were probably due to contamination from the solution and the device carrier under the sensor in the SEM.

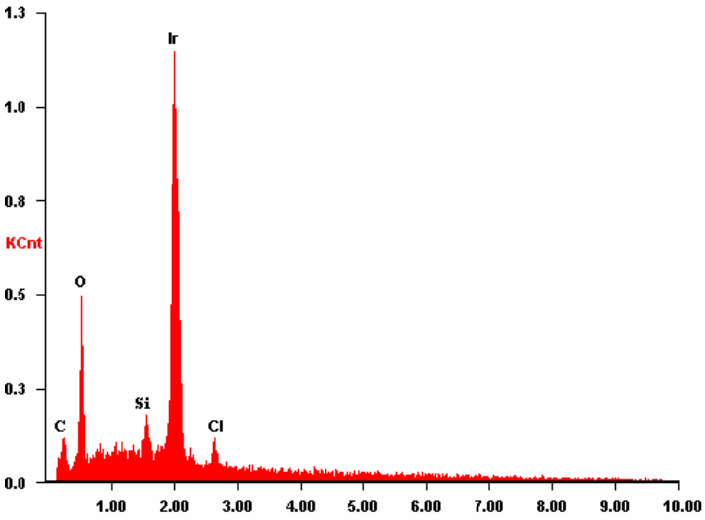

Figure 4.2 Energy-dispersive x-ray analysis result of the sol-gel IrO_x film.

In order to confirm the iridium oxide thin film formation, x-ray diffraction (XRD) patterns were performed using Siemens D-500 x-ray diffractometer. Fig. 4.3 shows the XRD patterns at annealing temperatures of 350°C and 550°C. The crystallization of iridium oxide normally begins at 400°C [2.8]. We compared the results with 5-hour 350°C and 550°C heating treatments. The iridium oxide crystal structure from XRD patterns shown in Fig. 4.3 agreed with the results shown in the literatures [2.4, 4.1]. The data showed a lower temperature treatment

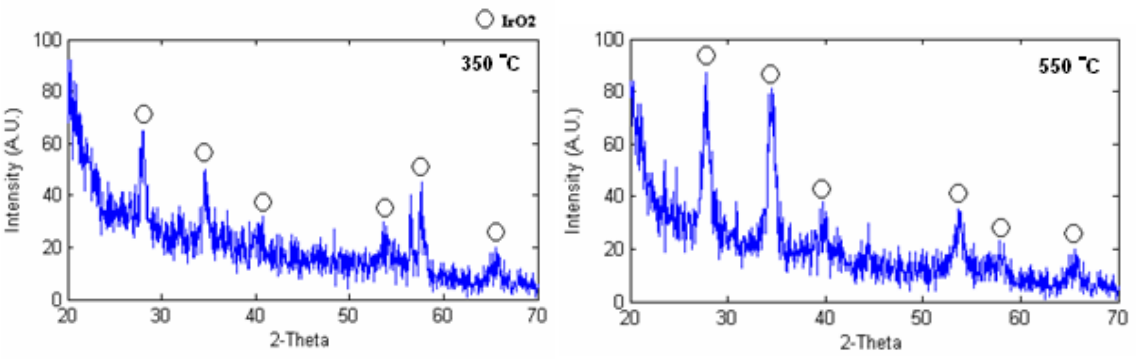

(a) (b)

Figure 4.3 XRD patterns for IrO_x with thermal treatment at (a) 350°C and (b) 550°C.

produced weaker diffraction due to lower crystallinity. This indicated our iridium oxide thin film was close to amorphous and fine grain structures. Our data showed clearly stronger diffraction peaks for the 550°C annealing temperature. The wide line widths and peak shifts were probably due to local disorders and/or micro-crystallinity [4.1] which we discussed in the previous chapter.

4.3 Sensitivity

The sensitivity of IrO_x pH sensor was tested and validated by dipping the sensor in different pH levels of solutions at the room temperature. 0.1 M of HCl and KOH were used to adjust the pH level of testing solution. We tested each sensor electrode three times in the same solution in order to demonstrate the near-Nernstian response and the consistency of our electrodes. The sensors were immersed in the solution, and then taken out to be washed with DI water, dried by compressed air and tested again. The tests were conducted by measuring the sensor in the most acidic solution (pH=1.5) first and gradually increasing the pH levels of solution to the most alkaline level (pH 12.10).

Fig. 4.4(a) shows the potential responses with eight different pH levels of solution from 1.5 to 12.10. The results showed consistent sensitivity –51.1mV/pH, –51.6mV/pH, and –51.7mV/pH with high correlation coefficient r^2 values between 0.95 and 0.959. Fig. 4.4(b) shows the reverse pH responses tested with eight different solutions from 12.10 to 1.5. The sensitivity

results were –48.9mV/pH, –50.1mV/pH and –51.1mV/pH. The r^2 values of these linear regressions were between 0.95 and 0.953.

Comparing with the sensitivity of anodic iridium oxide film (AIROF) [1.22, 2.13], the sensitivity of the IrO_x film done by sol-gel thermal oxidation process was less. The main reason is that AIROF have higher porous surface which causes the presence of many hydroxyl groups to ensure high ionic conduction [2.13, 4.2]. The anhydrous IrO_x film such as sputtered iridium oxide film (SIROF) [4.3] and sol-gel (SG) [2.4, 2.8 ,3.1] have very little numbers of hydrophilic site which is responsible for proton and electron transfer during redox process in the oxide film, because the surface of SIROF or SG-IrO_x film is covered by oxide completely without any porosity. Therefore, the anhydrous IrO_x film doesn't show the extra effect of sensitivity caused by the dissociation of hydroxyl groups [2.13]. In this test, our flexible pH electrode showed a consistent sensitivity, compared to the electrode formed by other methods which typically have sensitivities in the range of 50–70mV/pH [1.22, 4.4-4.7].

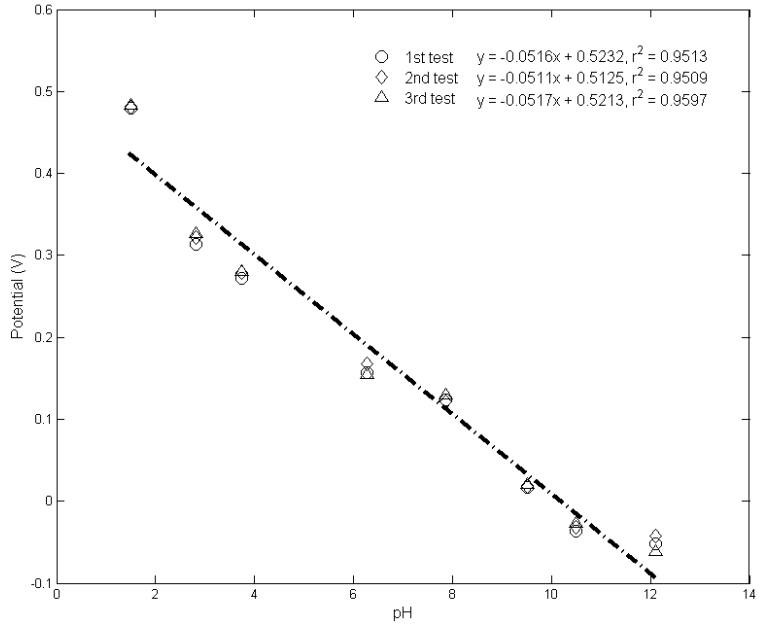

(a)

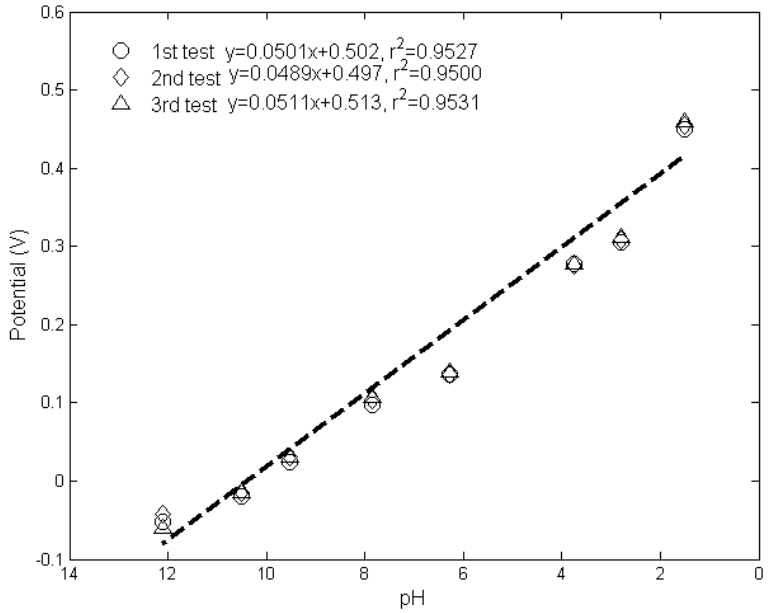

(b)

Figure 4.4 Measured Nernstian potential sensitivity responses of IrO_x flexible pH sensor from (a) pH=1.5 to pH=12.10, and (b) from pH=12.10 to pH=1.5.

4.4 Response Time

The response time of our flexible pH sensor was measured in three different tests. The first test was from acid to alkaline conditions by quickly dripping KOH into an acidic solution while the sensor was in the solution. The second one was from alkaline to acid conditions by quickly dripping HCl into an alkaline solution with the sensor in the solution. The third one was tested by dripping diluted HCl droplets directly on the dry sensing electrode surface of the sensor. The sensor response time has not been universally defined since the environmental parameters are quite different under different sensing scenarios. In our work, the response time is defined as the time needed for the potential change to reach 90% within the equilibrium value of potential [1.22].

Fig. 4.5(a) shows about 0.9 second of response time with measured potential step change of our flexible pH electrode from pH 3.9 to pH 11 verified by commercial pH electrode. Fig. 4.5(b) shows the result from pH 12 to pH 3.5. The response time is about 2 second. Fig. 4.5(c) shows the result from dry surface condition to pH 4.01. The response time is about 0.8 second. In this work, our flexible pH sensor performed about 0.9 to 2 second of response time.

To compare with the 5-15 seconds of response time reported from other literature's experiment [4.8-4.10], the response time of our IrOx flexible pH sensor was much shorter and more consistent in between the different pH level change. The short and consistent response time represent that the quality of our IrOx surface was well fabricated by the appropriate withdraw rate and annealing temperature during the sol-gel fabrication process. The Olthuis [2.13] presented that the response time may be affected by the porous properties of the film. The ion which is trapped in the porous of the iridium oxide film needs to equilibrate the solution in the bulk area. The phenomenon may affect the speed of the ion exchanging, and increase the response time.

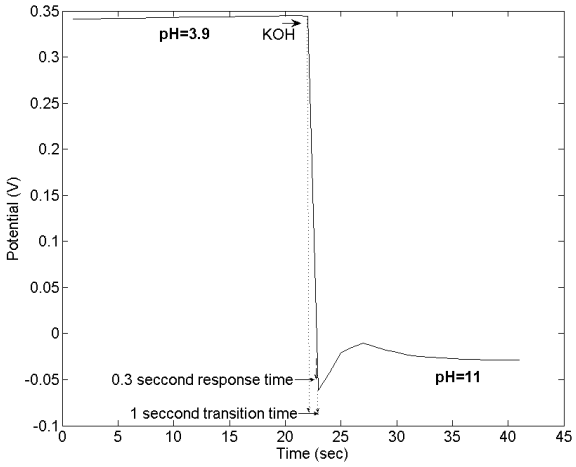

(a)

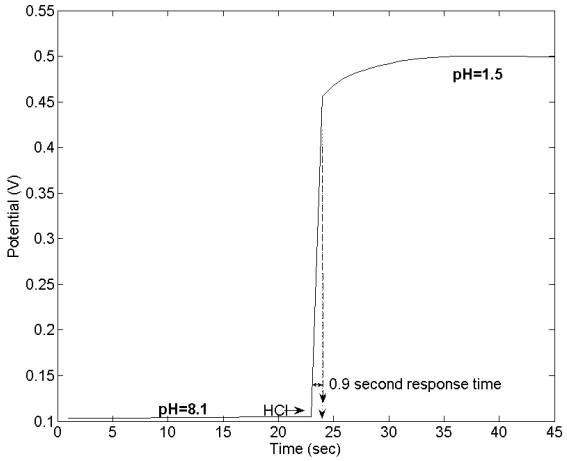

(b)

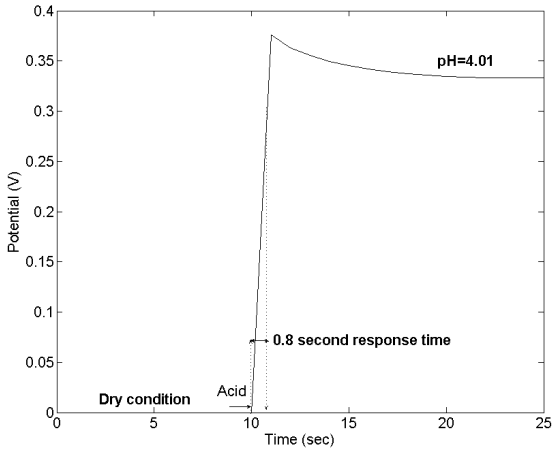

(c)

Figure 4.5 Response times in titration (a) from pH=3.9 to pH=11, (b) form pH=8.1 to pH=1.5, and (c) from dry condition to pH=4.01.

4.5 Stability and Repeatability

In the previous sensitivity test, the electrode exhibited distinct potential responses at each different pH levels. The measurements were carried out by placing the sensor in individual solutions of various pH values. The sensor was washed with DI water between the experiments. The potential generated in each solution with static pH was not affected by other environmental parameters.

Different literatures defined stability and repeatability differently for their respective applications and general terms could not be found, to the best of our knowledge. For clarification purpose, the terms are defined by us in Fig. 4.6. In the following measurements, for each pH level, our sensor was tested continuously, in a solution to identify potential fluctuation (ΔV), potential deviation (δV), and potential drift (V'), shown in Fig. 4.6(a). The ΔV is defined as a stable, small, and non-random voltage fluctuating range which happens after the detected electrochemical potential reaching the stable condition. The potential fluctuation may be caused by the noise of the recording instrument or unstable source interference such as the liquid flowing or stirring during the test. The δV is defined as a potential difference between the different testing episodes by using the same pH electrode in the same test solution. The potential deviation may be caused by the different factors such as the oxidation state, and the surface OH^- ion exchange of iridium oxide. These phenomenons may generate new equilibrium which causes the higher or surface charge [1.22, 2.12-2.13]. For the potential drift V', we defined it as the potential shift which is from the peak potential value to 90% of the equilibrium potential value as showed in Fig. 4.6(a). The potential drift may be caused by some reasons such as the procedure of ion neutralization, sensor age, temperature affection, and different fabrication method [1.22]. In this measurement, our flexible pH electrode was immersed and tested by using eight different pH buffer solutions at room temperature. In each pH level test, the sensor was tested for three times and four minutes to test sensor's stability and

repeatability. The sensor was cleaned by DI water and dried between each test of the different pH level episode.

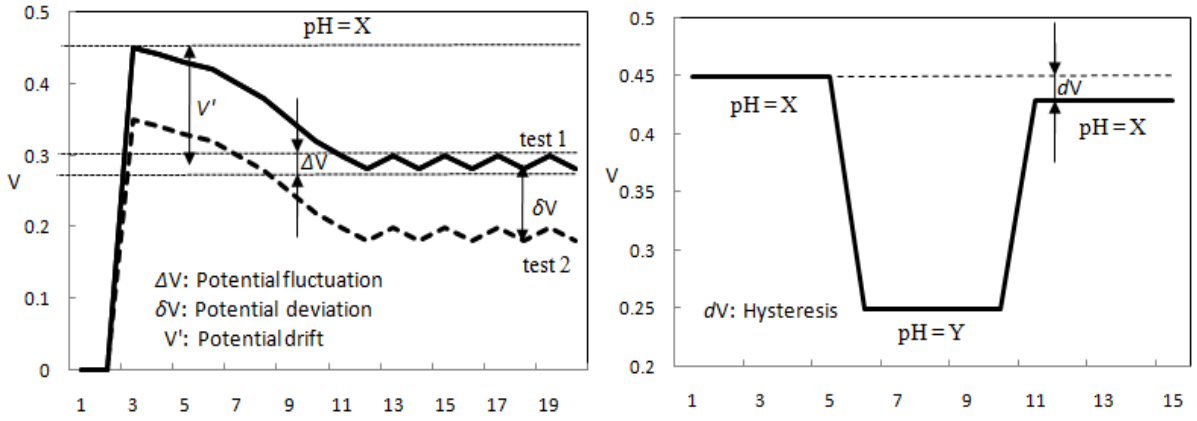

(a) (b)

Figure 4.6 The definitions of (a) potential drift & deviation, and (b) hysteresis.

Fig.4.7 shows that the result of eight different potential levels which responded to eight pH levels of solutions. The values of the potentials are almost constant for four minutes at each pH levels with only ±0.3mV to ± 1mV of potential fluctuation (*ΔV*). According to this result, the *ΔV* were small enough, and fairly well for reorganization of the distinct pH level without the noise interference. For the potential deviations (*δV*), it was about only 5mV difference at each pH level of solutions, and the value is smaller than the 15mV to 200mV presented in [4.11-4.13]. For potential drift (*V'*), our pH sensor performed about 3mV of voltage drifting from the highest potential response value to 90% of equilibrium potential value. The small *δV* and *V'* values explain that our sol-gel fabrication produced a high quality of IrO_x thin film. As we mentioned before, the oxidation state and hydration oxide film are important factors for long-term stability of the electrode. The oxidation and hydration state may be changed or created by a new equilibrium reaction because of the disturbance of the surface quality change [1.22]. In conclusion, our pH sensor performed very little potential fluctuation (*ΔV*), potential deviation (*δV*), and potential drift (*V'*) presenting the good stability and repeatability.

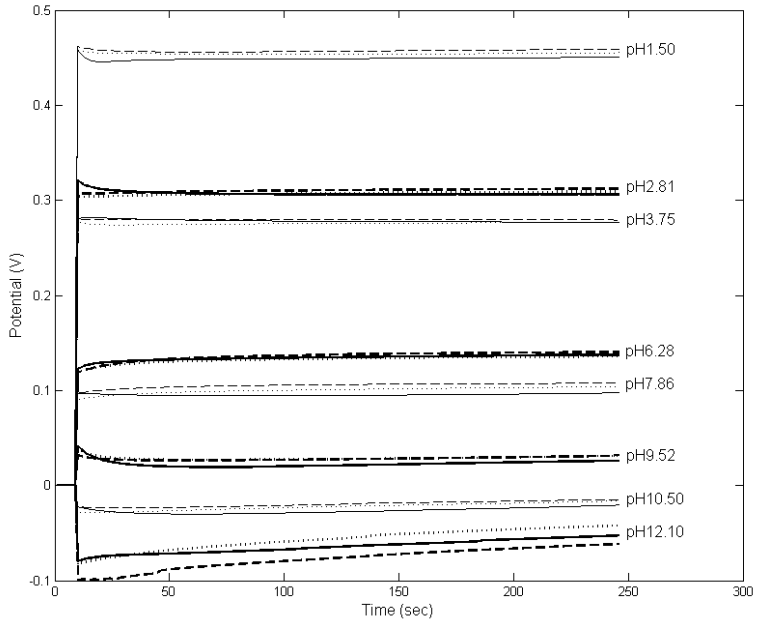

Figure 4.7 The Stability tests of eight different pH levels.

4.6 Reversibility

In the previous measurements, stability and repeatability of the sensor has been demonstrated by showing three parameters such as small potential fluctuation (ΔV), deviation (δV) and drift (V'). The sensor were cleaned by DI water and dried with compressed air between each test episode. However, in the random pH environment, the sensor will be used not only for the long term condition, but also in the random pH level conditions. Therefore, in order to test the reversibility of our sensor, our sensor was tested by using the test in a complete pH titrated loop cycle in pH=1.5-pH=13.1-pH=1.5 continuously without the surface cleaning and drying procedure. During the measurement, the output voltage at the same pH level may be different because of the delay of the pH response between the buffer solution and the insulator interface [1.20]. The phenomenon is called memory effect or hysteresis which is defined as dV showed in Fig. 4.6(b). The hysteresis phenomenon happens when the same device tested in a complete pH cycle which is from alkaline to acid then back to alkaline or vice versa. The hysteresis phenomenon of IROF or some other metal oxide films were also reported in other studies [2.13]. The phenomenon may be caused by various factors such as different oxidation state and

degree of hydration which may establish a new equilibrium in the redox reaction. Then the electrochemical potential will be changed in the reversible reaction [1.22, 2.13].

Fig. 4.8 shows that the results of reversibility test by using our flexible IrO_x pH electrode. The potential generated by the sensor represented the clear reversible cycle from pH=1.5 to pH=13.1 then back to pH=1.5 condition. The distinct and constant potentials were able to response and recognize eight different pH levels in the complete titration from acid to alkaline then back to acid again. In Fig. 4.9, we presented the standard error measurements (SEM) values of hysteresis (*dV*) range which is from about ±2mV to ±15mV at seven different pH levels. The results were less than 26mV to 30mV of hysteresis values derived from other different IrOx fabrication process [4.12-4.13], and different sensing materials such as WO_2 and RuO_2 [1.18-1.21]. To minimize the hysteresis phenomenon, the key is also only to produce a high quality of iridium oxide film which response the more precise reacting potential [1.22]. Therefore, this miniature hysteresis shows that our sol-gel fabrication process successfully developed a good quality of iridium oxide sensing film on flexible substrate, and this sensing electrode response to the pH level very precisely.

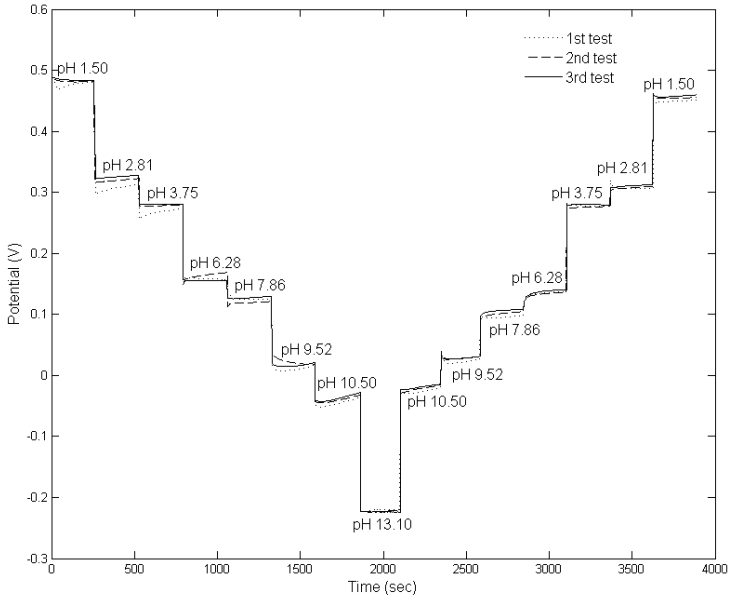

Figure 4.8 Three times of reversibility and repeatability tests with the pH 1.5 – 13.1 – 1.5 sequences.

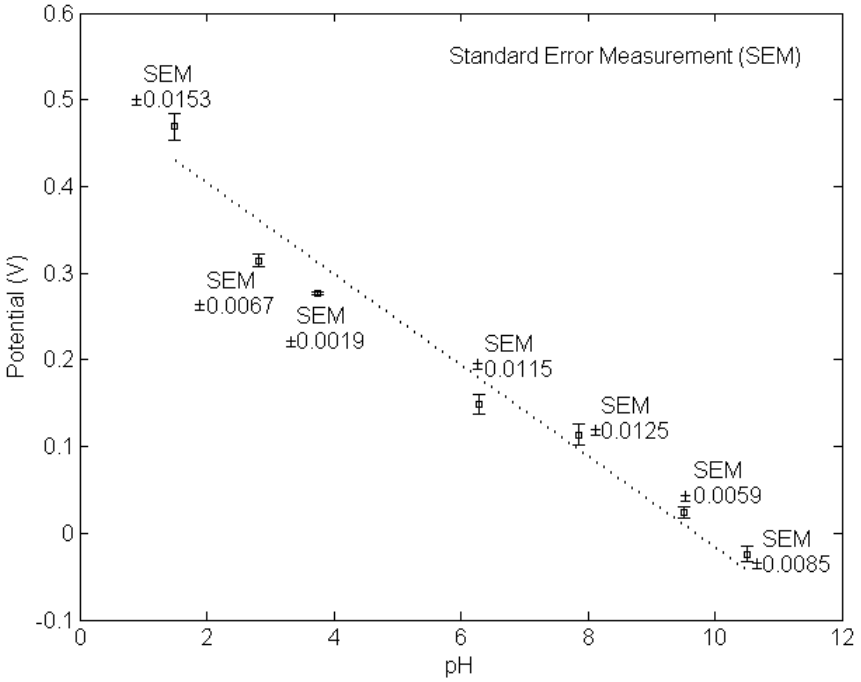

Figure 4.9 Drifting measurements at different pH levels during the reversibility test.

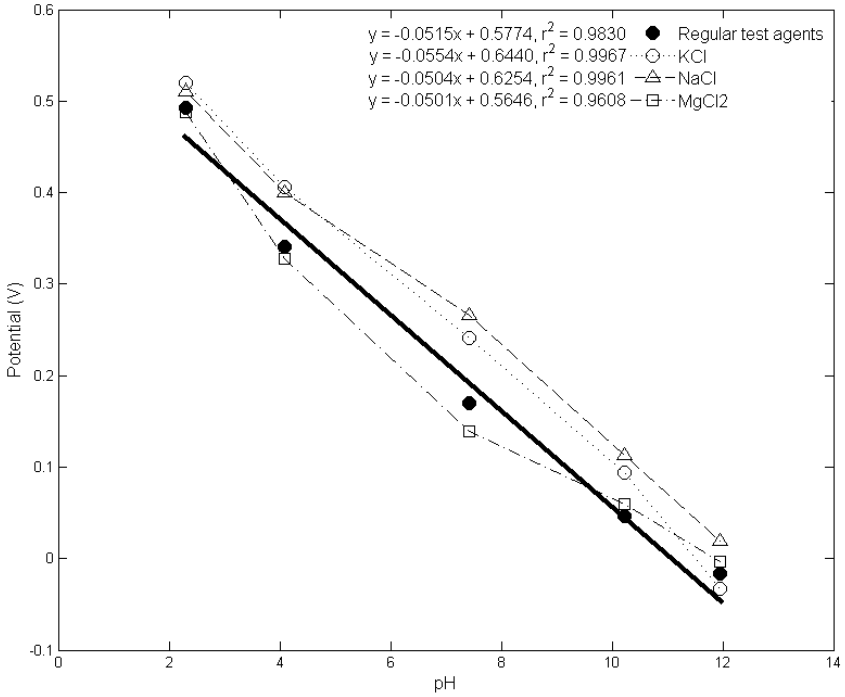

Figure 4.10 The effect of interference cation on pH sensitivity slope.

4.7 Selectivity

The effects of experimentally controlled parameters on the physical and electrochemical properties of IROF have been studied for many years. Katube et al. [4.3] presented the effect of some cations on the IrO_x pH sensing electrode. Their paper mentioned that the presence of the metal cations caused up to 8 mV of potential shift which may confuse the pH level judgment during the measurement. The ionic interference became a non-neglected problem related to different ion's effect to ion-selective electrode (ISE). The sensing selectivity of ISE should be concerned in the evaluation of sensor's performance. Therefore, the selectivity test of our flexible pH electrodes were investigated by the fixed interference method (FIM) and potentiometric selective coefficients, which were calculated by the Nikolskii-Eisenman equation is written as [4.14]

$$E = E^0{}_t \pm \frac{RT}{z_I F} \ln(a_I + K_{Ij}{}^{pot} \bullet a^{z_I / z_j}{}_j) \quad (7)$$

$$K_{Ij}{}^{pot} = \exp(\frac{z_I F}{RT}(E^0{}_j - E^0{}_I)) \quad (8)$$

where E is the experimentally determined galvanic potential difference of ISE in voltage. E^0 is the standard electrode potential with a value of 926mV *vs.* standard hydrogen electrode (SHE) or 577mV *vs.* Ag/AgCl reference electrode. F is the Faraday's constant with a value of 96,487 coul/equiv, and R is the gas constant with a value of 8.314 joules/deg. *RT/F* is equal to 25.688 at 25°C. a_i and a_j are the sample activities of the primary ion I^{z_1+} such as H^+ ,and interfering ion J^{z_j+} such as Na^+ , K^+ or Ca^{2+}. z_I and z_j are the charge number of the principal ion *I* and interfering ion *j*. $K_{Ij}{}^{pot}$ is the Nikolskii coefficient. In this section, the effect of three addition cations were compared and discussed by the pH sensitivity and selectivity coefficient. 0.1 M of NaCl, KCl, and $MgCl_2$ were used for interference cations agents. The presence of cations didn't exert large effect on the response slope, and the pH sensitivity kept in between –50.1 to –55.4

mV/pH as shown in Fig. 4.10. The selectivity coefficient of our flexible IrO_x pH electrode were calculated and summarized in Table 4.1. It is shown that the ranges of selectivity coefficients for potassium, sodium and magnesium cation are about below 8×10^{-3} factors. Comparing the result from [4.15], although our K_{Ij}^{pot} are higher, the change of pH sensitivity of our sensor still kept in the small ranges from –1 mV/pH to –5 mV/pH after the ion-interference. The different selectivity may be attributed or affected by different cation's mobility in the solution [4.4]. The literature data [4.16-4.17] also shows that the proper and acceptable range of K_{Ij}^{pot} is about less than 10^{-2} for the ion-selective electrodes.

Table 4.1 The selectivity coefficients of the electrode.

0.1 M of interference ion in pH=4.05 buffer	**Slope mV/pH(Before)**	**Slope mV/pH(After)**	K_{Ij}^{pot} **(selectivity Coeff.)**	**Log** K_{Ij}^{pot}
K^+	–51.5	–55.4	5.6×10^{-3}	–2.24
Na^+	–56	–50.2	8.3×10^{-3}	–2.07
Mg^{2+}	–48.5	–47	8.02×10^{-4}	–3.09

4.8 Temperature Dependence

In this section, the temperature dependence of IrO_x pH sensor was investigated and presented. Based on the Nerestian Eq.(4) introduced in section 2.3, at fixed number of pH value and chloride concentration, *E/T* should exhibit a linear relationship. According to the equation, the temperature change may cause the fluctuation of the pH value as we described in stability test part. Therefore, to investigate the temperature dependence is very important in the pH sensor calibration procedure. In this measurement, our pH sensor was tested by using four different pH levels of buffer solutions in three distinct temperatures separately. The sensor was cleaned and air dried between each testing episode.

Fig. 4.11(a) shows the temperature response of the flexible IrO_x pH sensor at 3.8°C, 21.2°C, and 50.8°C in the pH range from 2 to 10. The temperature coefficients are

approximately from 0.3 to 2 mV/°C which are smaller than other sensing material [4.18]. The smaller temperature coefficient represents that the pH sensor have minor temperature dependence under the test in different pH levels and temperature environment. The linearity response is also presented in Fig. 4.11(b) at three different temperatures' condition. The results showed consistent sensitivity –78.9 mV/pH, –74 mV/pH and –73.7 mV/pH with high correlation coefficient r^2 values between 0.98 and 0.99 at three different temperature levels. The test of temperature dependence provides important information for sensor calibration before the measurement.

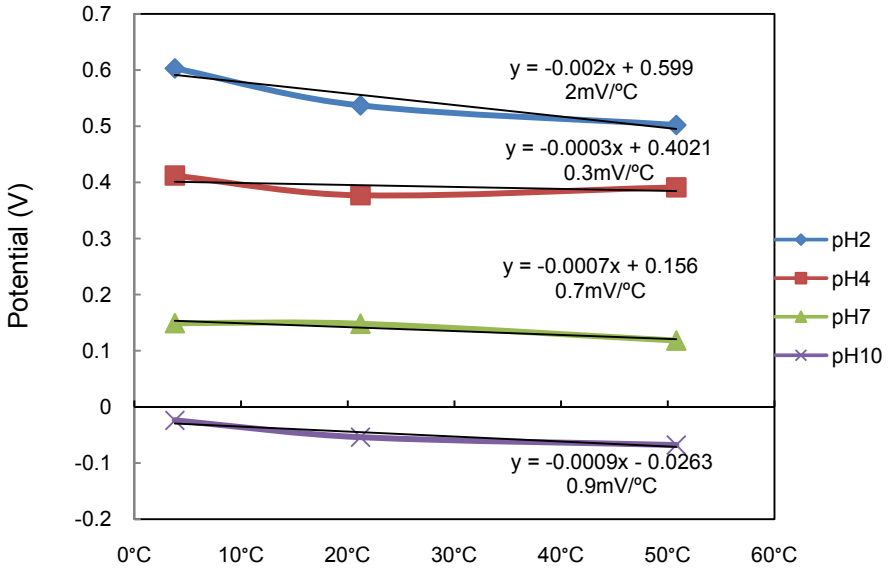

(a)

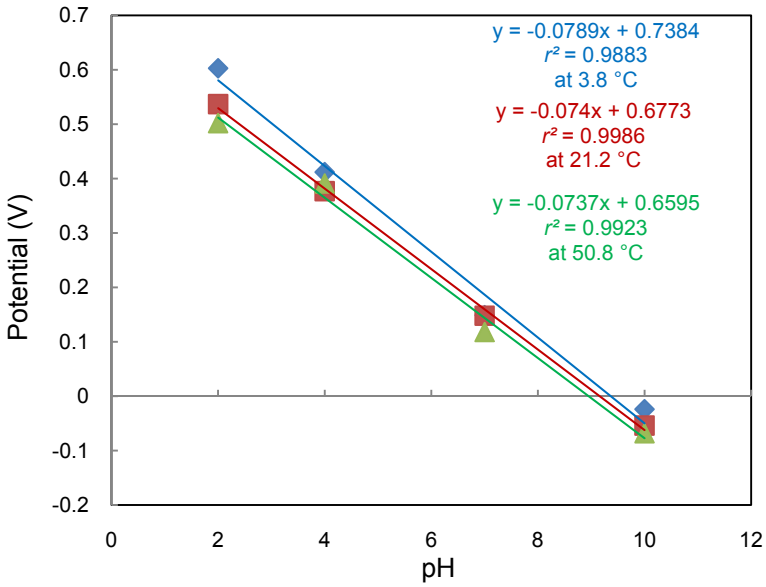

(b)

Figure 4.11 The temperature dependence represented by (a) temperature coefficients and (b) linear response in three different temperatures.

4.9 Flexible IrO_x pH Sensor Array

4.9.1 4x4 (16) pH micro IrO_x electrodes on the flexible substrate

In this section, we demonstrated a 4x4 pH sensor array fabricated on a 5cmx5cm size of polyimide flexible substrate by using the same fabrication process which was presented in chapter 3. This size of each working and reference electrodes are 1mmx1mm which are smaller than the previous design as shown in Fig. 4.12. The purpose of this design of sensor array is to target at the ability of micro-scale pH sensing for bio-medical applications which require more precise, dynamical, and smaller variously pH sensing conditions such as the wound condition, cell milieu, and fermentative monitoring. In these applications, pH levels may be changed by many small factors such as the temperature, flowing diffusion, various concentration, and other factors which will caused the variation of the micro ecology, chemical reaction, and biological derivatives. By using the micro pH sensor array, any of events happened in micro- or nano-scale will be caught and recorded in order to do the properly treatment to each applications.

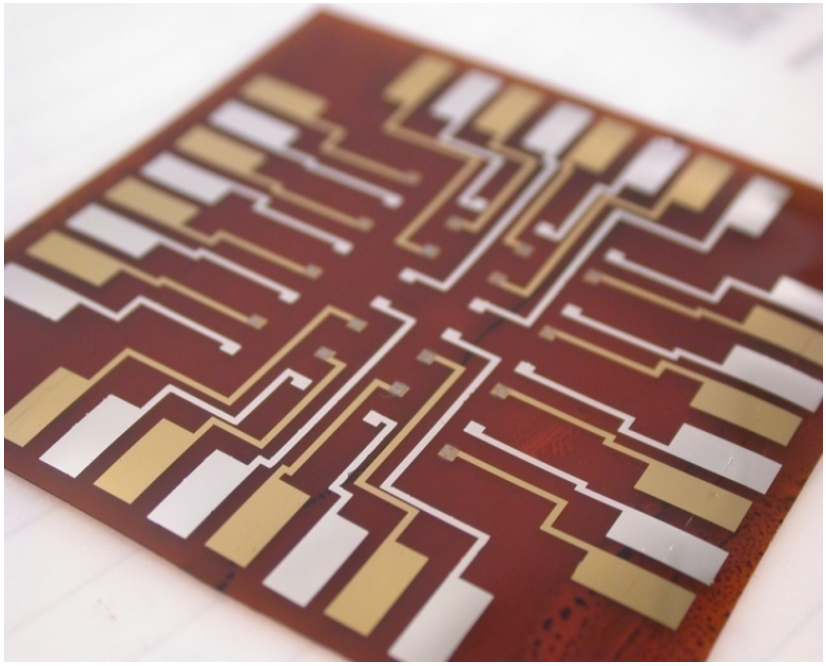

Figure 4.12 4x4 pH sensor array on flexible substrate.

4.9.2 pH distribution demonstration

4.9.2.1 Multi-solution test

In this section, we demonstrated a test including different pH levels of liquids by using our IrO_x pH sensor array simultaneously. We tested the agents of pH=2, 4, 7, 10, 12, tap water, and orange juice on seven different sensors of our 4x4 pH sensor array. The liquid was dripped on each sensor by using the burette, and the response potential was then recorded by using NI USB6210 DAQ card with LabView program in the computer as shown in Fig. 4.13.

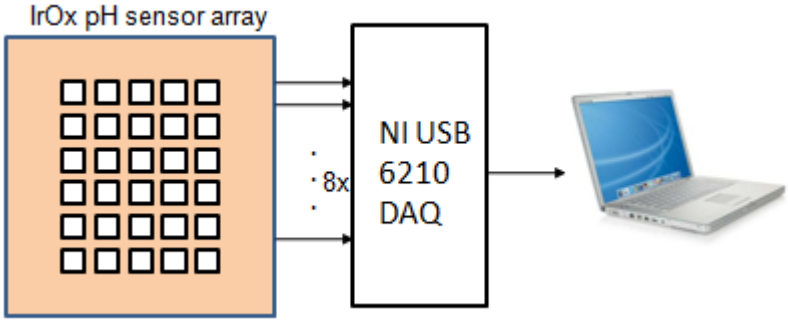

Figure 4.13 Measurement setup for 4x4 IrO_x pH sensor array.

As shown in Fig. 4.14, seven distinct potentials represented seven different pH levels of testing solutions, and keep at the constant level for 10 minutes. Comparing with the traditional pH sensor, our sensor array is able to sense multi-solution simultaneously but not just the only one bulky glass electrode for single solution test.

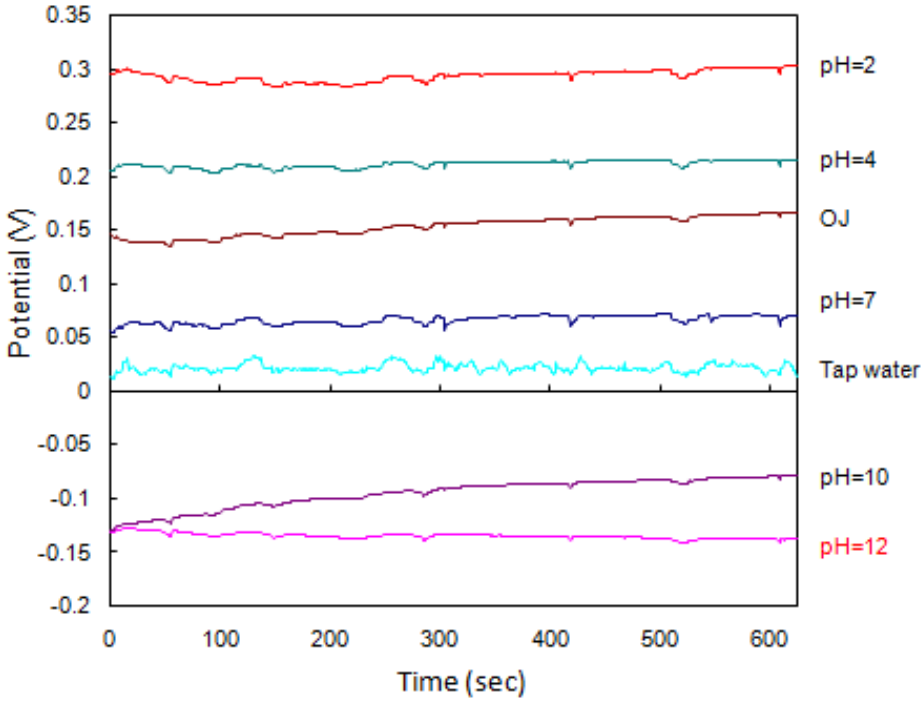

Figure 4.14 The test of seven pH agents by pH sensor array.

4.9.2.2 Temporal test

For multi-solution test, the sensor array demonstrated the sensing ability for multi-solution test. In this section, we reported a temporal test which can simulate and demonstrate the solution diffusion crossing the surface of pH sensor array. We dripped the same level of pH agents on 8 sensors separately. The time of dripping interval was about 1 minute. Fig. 4.15(a) and (b) show the temporal test at pH=2, 4, 7, 10, and 12 of solution in about 30 minutes. The sensor was dried and washed by DI water between each different test episode. As shown in Fig. 4.15, the clearly potentials responded to the different pH level solutions which were dripped on eight sensors, and the interval timing was also presented. Fig. 4.16 shows the distribution of pH level and timing for eight sensors simultaneously. The arrows show that the time delay shifting are around 1-3 minutes in each pH level testing episode. By doing the test, we proved that our pH sensor array is able to detect and response to the dynamical variation of pH level from a small area.

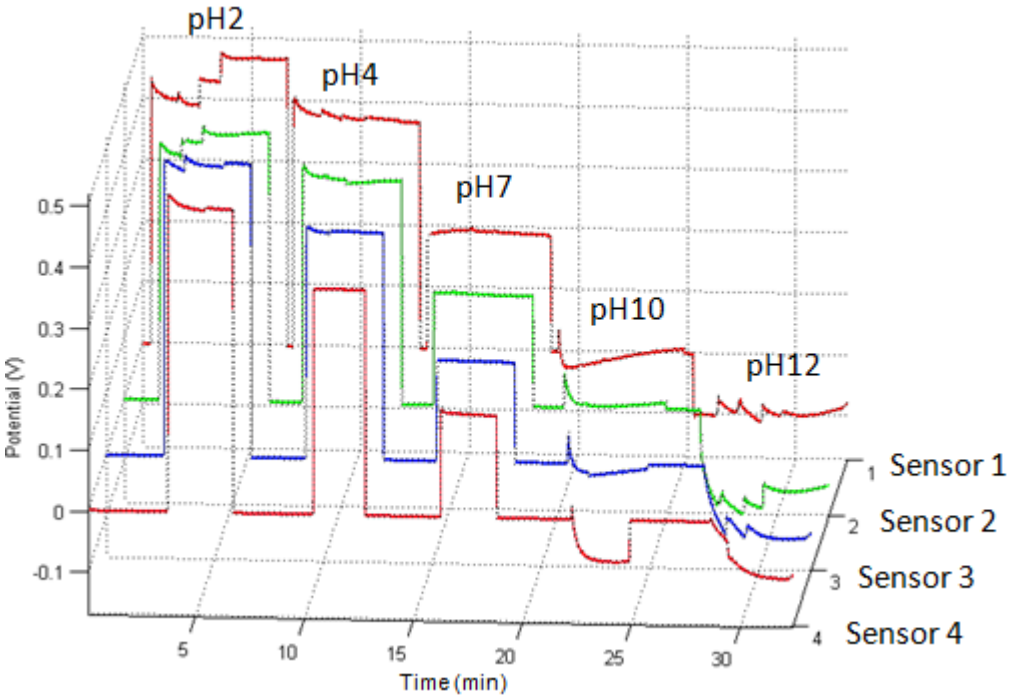

(a)

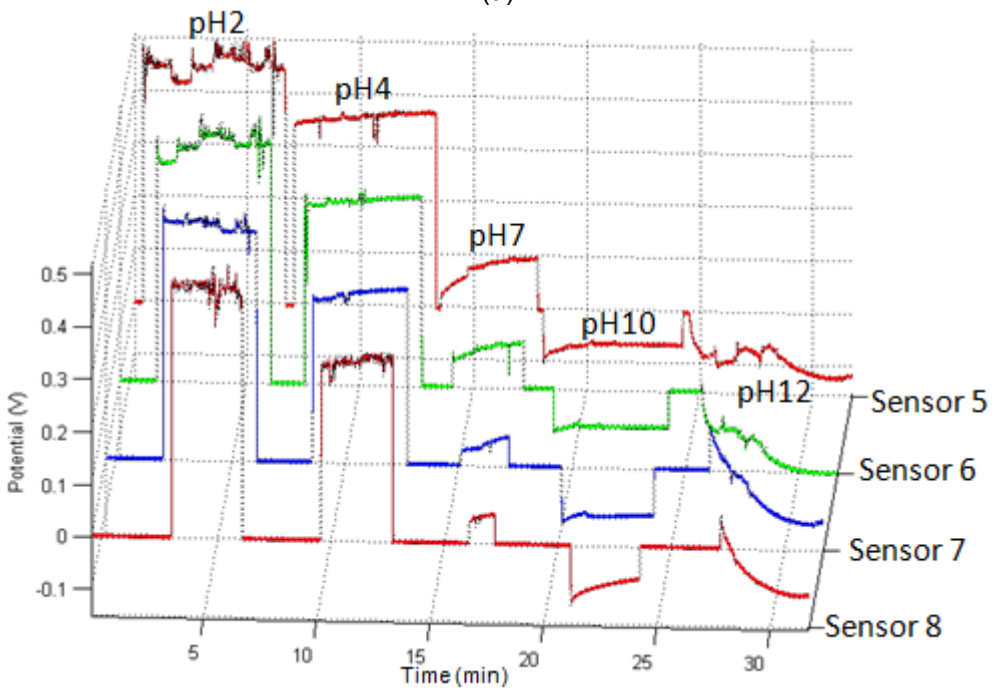

(b)

Figure 4.15 Temporal tests on (a) sensor No.1-4, and (b) sensor No.5-8.

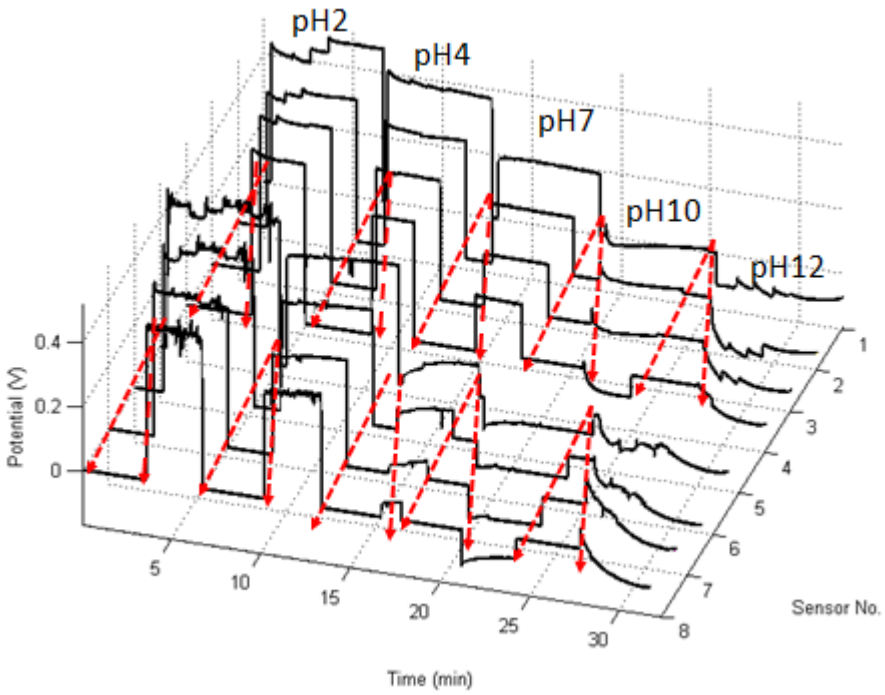

Figure 4.16 Dynamical pH-temporal tests.

4.9.2.3 Spatial test

In this section, we demonstrated the spatial test by using four sensors on pH sensor array. The purpose of the spatial test is to demonstrate the dynamical multi-selectivity and repeatability of this pH sensor array. For the bio-medical application, the pH sensor array may be used for not only the monitoring of dynamical pH distribution, but also the dynamical multi-pH level monitoring such as the cell feature or drug reorganization. The pH level may be different in each testing agent. According this requirement, we applied a layer of PDMS polymer to separate each sensing area. The size of each exposure area on the sensor is about 2 mm diameter as shown in Fig. 4.17. In this experiment, we used pH=2, 4, 5, 7, 10, and 12 of the buffer solutions for each episode test, and this test was repeated for three times in order to test the sensor's repeatability. The buffer solution was dripped in the exposed area separately, and each test was kept for four minutes. The sensor was then cleaned and dried for the next test. In Fig. 4.18, four sensors represented clear responding potential separately to show the selectivity. Three testing episodes also demonstrated the sensor's repeatability with the constant potential

response for each pH level of solution. Therefore, according to the spatial test, the massive liquid detecting may be able to apply, and the array design will definitely save the charge in labor, instrument, and space.

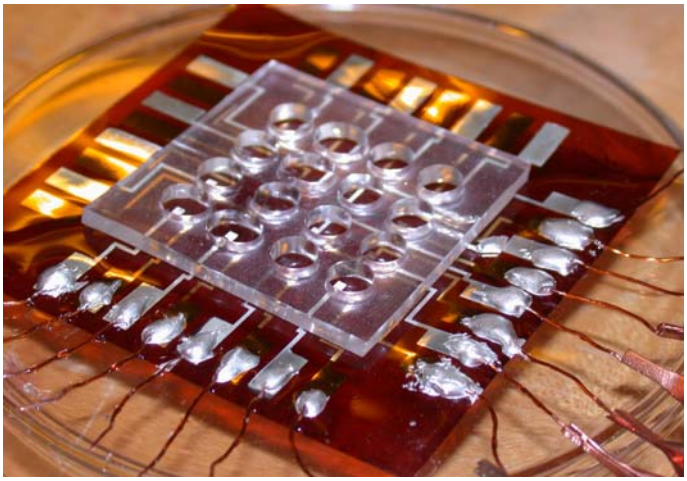

Figure 4.17 Spatial tests by using PDMS polymer as the testing window.

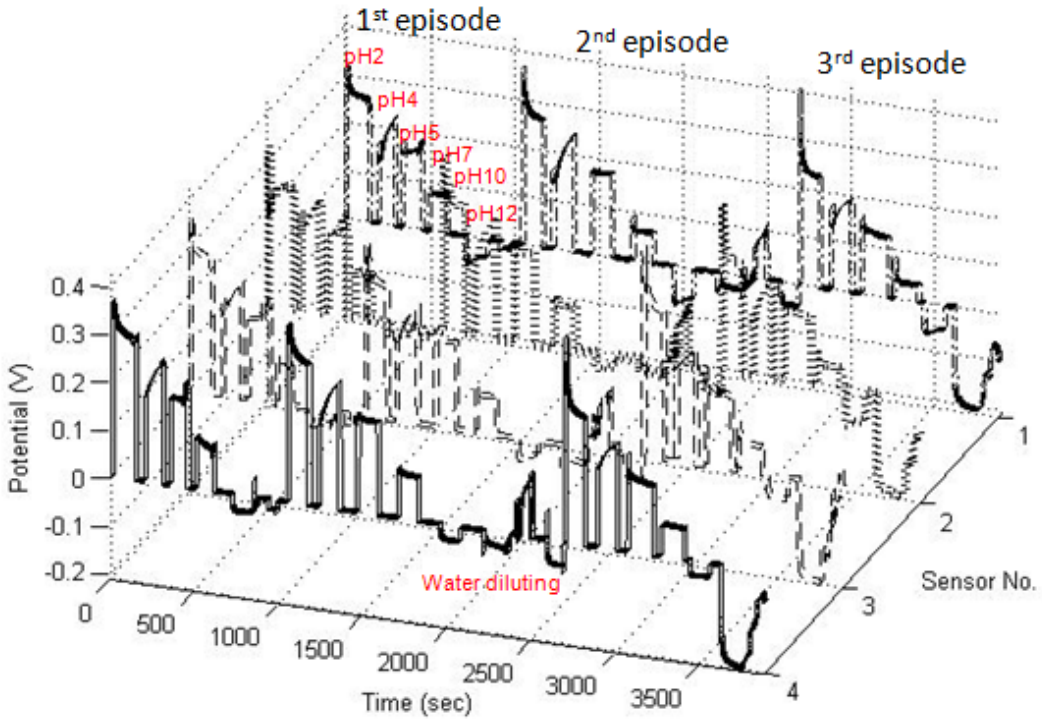

Figure 4.18 Spatial test of our pH sensor array.

4.9.3 Conclusions

In this section, we fabricated a 4x4 IrO_x pH sensor array on flexible substrate. This sensor array was tested by different ways in order to demonstrate the innovation pH measurement of the pH sensing method. In the first experiment, our sensor array presented an ability which is for simultaneous multi-solution test. In the second experiment, the nature pH level diffusion and distribution were mimicked by doing the temporal test. Our pH sensor array was able to demonstrate one minute of interval time delay which represented the dynamical ion concentration changing and switching on the detecting surface. The dynamical pH variations were able to recorded and monitored by using our IrO_x pH sensor array. Finally, the spatial tests were presented in order to target on bio-chemical or bio-medical test. The selectivity and repeatability test for multi-solutions were proved in this experiment. In conclusion, our flexible pH sensor array is a new novel design for the micro-scale of pH measurement. This innovation haven't and can't been done by using the traditional glass electrode in only 2cmx2cm of sensing area.

CHAPTER 5

PROPOSED APPLICATIONS OF IROF pH SENSOR

5.1 Wireless Freshness Monitoring System

5.1.1 Motivation

Food freshness is a key characteristic of food safety. Overall, the food safety is the result of all the desirable characteristics that make food acceptable to eat. Therefore, the control and monitor of food quality are very important in transit and storage. The food safety issue is a vital concern as shown by the introduction of the Hazard and Critical Control Point (HACCP) of U.S. Food and Drug Administration (FDA). In each year, there are up to 81 million Americans suffer food-borne illnesses, and 9,100 die [5.1]. The majority of food-borne disease outbreaks result from unintentional contamination of a product as the inappropriate processing or handling. In 1985, an estimated 350 school children and staff at a Georgia elementary school developed febrile gastroenteritis associated with the bacteria Salmonella enteritis [5.1]. The food source was identified as turkey salad that had been refrigerated improperly before it was served.

To avoid the blind risk of uncertain food spoilage, three different types of sensing principles was invented in some researches' work. The most popular freshness monitor is gas sensor which can be made by metal oxide semiconductor (MOS), conducting organic polymer (CP) and piezoelectric crystal. These sensors rely on change of conductivity induced by the adsorption of gases and subsequent surface reactions [5.2-5.3]. However, the sensitivity of MOS and CP sensor are easily influenced by temperature and moisture conditions. For piezoelectric sensor, the good quality of coating process is required during the fabrication to maintain good sensitivity of the sensor [5.3]. Generally speaking, gas sensor is easily affected and depended by the environment moisture and temperature conditions. The other two types of

freshness sensors are based on enzyme [5.4-5.7] and temperature [5.8] sensing principle. However, the selectivity and sensitivity of these sensors are still depended on many factors. For enzyme sensor, the different type of food require different specific enzyme sensor. For instance, total volatile basic nitrogen (TVB-N) [5.4-5.5] and Histamin [5.6-5.7] enzyme sensor are widely using for seafood freshness monitoring and sensing. [5.9] reported the different spoilage mechanism also happen at different race of fish in different water area. In addition, glutamate dehydrogenase and glucose oxidase (GOD) [5.10] are widely using for freshness monitoring on fruit, vegetable, and related food products such as juice or wine. In conclusion, to monitor different kinds of food require different enzyme freshness indicators. For temperature sensor, it is easily affected and confused by the environment temperature. The temperature information is not accurate enough to present the freshness grade of the food. In conclusion, the sensitivity and selectivity of the enzyme and temperature sensors are strongly depended on the specific species of food sources and environment conditions. Furthermore, the enzyme sensors also require complicated fabrication process such as the polymer treatment, temperature control, and chemical compound mixing to keep the sensing performance [5.4]. The chemical agents, specific treatment, and complicated fabrication process will increase the producing cost which is very difficult for commercializing and industrial applications. Therefore, in order to build a simpler, more accurate, and more general using freshness monitoring system, we applied the pH level profile sensing mechanism on the food spoilage procedure.

The freshness indicator is a new approach to monitor the condition of food especially for high risk items such as seafood, poultry, meat and dairy. Currently, some of commercial freshness indicators [5.11] only contain the information of the expiration date and food temperature. Some of researches used pH sensitive dye [5.12] to detect the food spoilage. Those indicator systems have less accuracy and information to show the food spoilage. Furthermore, without the wireless, in transit or warehouse, it’s very difficult to monitor and collect the correct information from every single food package.

To reach a simple, accurate, and low cost freshness monitoring system, we proposed and fabricated a passive pH-RFID tag based on a flexible IrO_x/AgCl as a freshness sensing electrode. First, we fabricated the IrOx/AgCl material on a bio-compatible polymer by using the simple and low cost sol-gel fabrication process presented in our previous sections. Second, a passive RFID circuit [5.13] has been then designed to cooperate with our flexible IrO_x pH sensor. The pH-RFID sensor transponder harvests radio frequency (RF) power transmitted from an external reader, and sends the modulated pH data as frequency shifts back to the reader. Finally, a prototype of the batteryless, wireless, real-time, and bio-compatible pH-RFID tag for freshness monitoring is presented in this work. We proposed the easiest, most accurate, and lowest cost way to monitor the food quality during the storage or delivery through the RFID technology.

5.1.2 Approach

5.1.2.1 Flexible freshness (pH) indicator

In this work, we have designed and fabricated a miniature iridium oxide (IrO_x) pH sensor on flexible substrate as Fig.3.6. Both iridium oxide sensing films and Ag/AgCl reference electrodes were formed on a flexible polyimide substrate by sol-gel, dip-coating and thermal oxidation processes. The pH-dependent redox equilibrium of two materials generated potential difference when pH was changed. We used our IrO_x pH sensor as the indicator to recognize the time line in the meat spoilage process.

5.1.2.2 The relationship between the pH and food spoilage

After livestock is killed, the oxygen stops to deliver into muscle which induces several different biochemical reaction changes. These changes contribute various meat flavors and stages of spoilage. Generally speaking, meat property variations follow three stages [5.14]:

Step 1: Rigor mortis (pH reduces)

Because of the lack of oxygen in the dead muscle, the glycogen will be decomposed and become the lactic acid. On the other hand, the Adenosine Tri Phosphate (ATP) is

hydrolyzed to be phosphoric acid too. The pH level of the muscle group will reduce, and muscle becomes hard. We call the phenomenon “Rigor Mortis”.

Step 2: Autolysis (pH slightly increases)

After the rigor mortis, the muscle will be dissolved to become the smaller molecule by enzyme. The muscle will become much softer as called off-rigor. The protein in the dead muscle also dissolves to be the amino acid which includes different types of structure ex. Amine. On this moment, the pH level of muscle group will increase.

Step 3: Spoilage (pH increase)

With amino acid producing, some microbes start to grow and absorb the amino acid and proteins. There are different chemicals such as indole, skatole, ammonia, and sulfide created after the absorbing processes created by bacteria. The ammonia-based chemicals increase pH level of the meat/fish and bad odors.

5.1.3 Method

Described above, we are able to relate the pH variations of the fish meat to three transitions during the spoilage process. In this section, we demonstrated the comparison of the fish meat properties under different temperatures. One Tilapia fillet was covered and stored in refrigerator at 5°C, as shown in Fig. 5.1(a) for about 18 hours. Another Tilapia fillet was tested at the room temperature of 25°C as shown in Fig. 5.1(b). Two pairs of flexible IROF pH sensors were placed on the bottom of the fish meat in the both samples. The sensing potentials responded from fish meats were detected and recorded by our IrO_x flexible pH sensor continuously in about 18 hours. After the demonstration of freshness sensor, we connected our non-invasive radio frequency identification (RFID) circuit with IrO_x pH sensor to wirelessly sense the spoilage process which we just described in the previous paragraph.

(a) (b)

Figure 5.1 The test of our freshness indicator in different temperature at (a) 5°C and (b) 25°C.

5.1.4 Wireless-freshness monitoring system

This RFID wireless pH sensing module includes a flexible IrO_x pH electrode, RFID transponder (tag) circuit, and reader circuit. The sensing concept relies on inducting coupling between coil antennas (L) and capacitance (C) to form the resonant frequency to reach the coupling efficiency. Fig. 5.2 shows the system blocks diagram of the pH wireless sensing module.

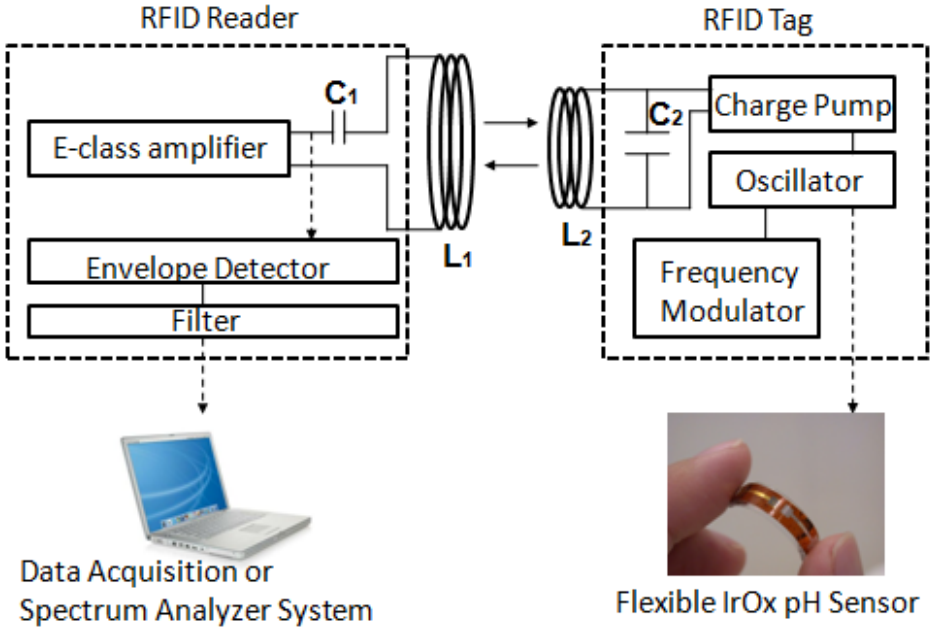

Figure 5.2 Block diagram of the passive wireless pH-RFID integrated system.

5.1.4.1 Transponder (tag) design

According to the previous work [5.13], a transponder circuit was built by two parts which are voltage multiplier [5.15] and frequency generator [5.16]. For the concept of inducting coupling, the voltage induced across the transponder antenna will also reduce by distance simultaneously. The received voltage becomes too low to operate the whole transponder circuit. Therefore, a series of diodes and capacitors was applied to form a voltage multiplier called charge pump circuit. In the output of our charge pump circuit, 2.5 V of DC voltages will be generated through a voltage regulator to support stable voltage source for our frequency generator. In order to transform the electrochemical potential generated by our pH sensor to frequency signal for our wireless sensing configuration, we designed a relaxation oscillator based on the voltage level switch at the input of the comparator [5.16] as shown in Fig. 5.3. The measured frequency decreased approximately from 22 kHz to 17 kHz responding to the pH level from 2 to 12.

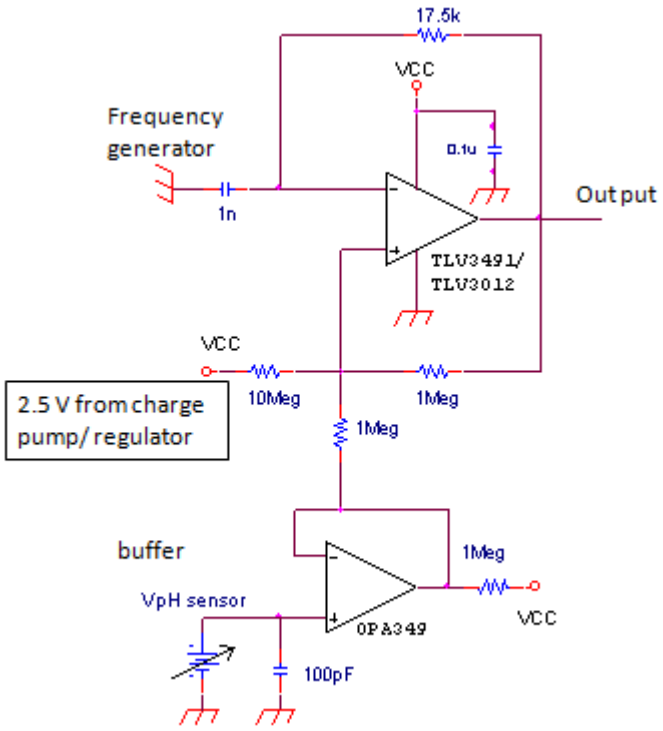

Figure 5.3 The relaxation oscillator design of the transponder circuitry.

5.1.4.2 Reader design

In our reader circuit, a class-E amplifier, envelope detector, and band-pass filter are included. The class-E amplifier [5.17-5.19] was connected to a function generator provided 0 V to 5 V of square wave with 1.34 MHz of operating frequency followed by the recommended maximum permissible exposure (MPE) of magnetic field. This operating frequency is used as carrier frequency which is adjusted to the resonant frequency of the LC circuit in a high voltage supported by this class-E amplifier at the reader coil antenna. Relying on the high efficiency of class-E amplifier, the changing of frequency signal is able to be detected and recognized by the envelope detector [5.20] through the high power support between the reader and transponder coil antenna. The band-pass filter then filters out the noise from 0.5 KHz to 75 KHz to keep the signal clean. At the final stage, a comparator was used to convert the sinusoidal signals to square wave which can be digitally processed by the spectrum analyzer or data acquisition instrument.

5.1.4.3 Wireless pH sensor

To reach the wireless pH sensing, a flexible fabricated IrO_x pH sensor is connected to the relaxation oscillator in our transponder circuit. The input of pH sensor is connected with non-inverting input of comparator. In the circuit, the shift of electrochemical potential sensing by our pH sensor at input of comparator will change the frequency output of comparator simultaneously. Then we can transfer the detected voltage level change to frequency variation which can be transmitted wirelessly using our reader circuit. The block diagram of the whole sensing setup was described in Fig. 5.2.

5.1.5 Results

5.1.5.1 pH sensor calibration

Sensitivity: We demonstrated the linearity with different potential responses for the different pH levels in order to calibrate our pH sensor before we do the food freshness test. In this experiment, an IrO_x pH sensor was tested by eight different pH buffer solutions from pH=2

to 12 separately. The result showed that the calibrated sensitivity is –49.7mV/pH with high correlation coefficient r^2 values 0.97, and the potential kept in a linear equation relationship between the range from pH=2 to 12 as showed in Fig. 5.4. Therefore, for food freshness monitoring system, we can identify and classify the pH level of the food by using the linear relationship and calibrated sensitivity.

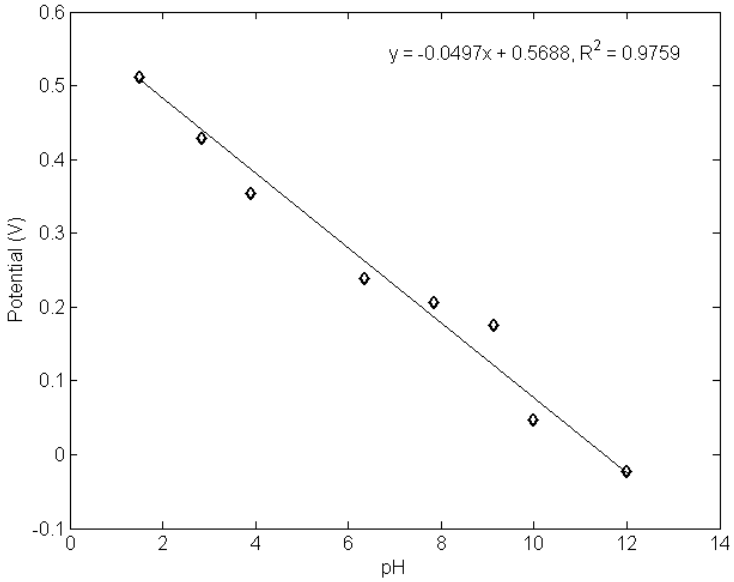

Figure 5.4 The linear potential response from pH=1.5 to pH=12.

Stability: For the food freshness monitoring procedure, it requires a stable and long term measurement and monitoring procedure. Therefore, the stability test of the pH sensor is required for freshness monitoring procedure. In this work, we used eight different buffer solutions which is from pH=1.5 to pH=12 to test our sensor. Each buffer solution was dripped on the sensor, and tested for 5 minutes. Fig. 5.5 shows that eight different potential levels which are 511 mV, 429 mV, 354 mV, 239 mV, 206 mV, 175 mV, 46.9 mV and –23 mV represent eight different pH buffer solutions at pH=1.5, 2.85, 3.9, 6.35, 7.86, 9.15, 10.15 and 12. The sensor is able to obtain the stable potential for five minutes with less 5 mV of potential drift. In this work, the stability test of our pH sensor is performed, and proved for long term food freshness detection.

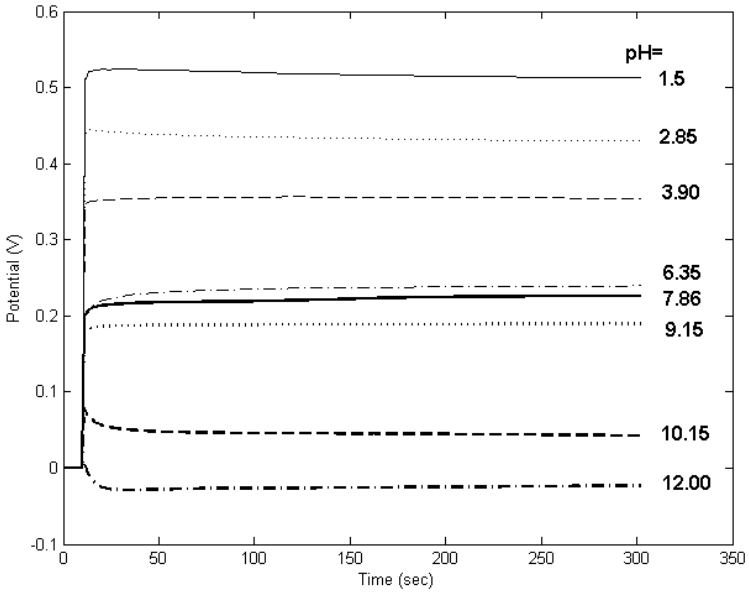

Figure 5.5 Long term stability test for our IrOx pH sensor.

Reversibility: For a long term freshness monitoring, the sensor will be used and tested under the random dynamic pH environment. Therefore, to prove the dynamical reversibility, we test the sensor by using the way of a pH cycle in pH=2.85-pH=12-pH=1.5 continuously without the surface cleaning and drying procedure. Fig.5.6 shows that the results of reversibility test by using our pH electrode. The potential responded by our sensor represented the clear reversibility from pH=2.85 to pH=12 then back to pH=1.5 condition. Each distinct and constant potential is able to response and recognize each pH level continuously. The reversibility test will help us to verify our sensor's performance under the highly dynamical and random pH changing environment such as the meat or food.

5.1.5.2 pH-wireless sensing system calibration

Wireless sensitivity calibration: In order to observe the relationship between the frequency domain and pH sensing potential, the pH-frequency sensitivity calibration is needed for wireless freshness sensor. In the test, our pH sensor was connected to the batteryless tag circuit and the sensing potentials were then transferred to frequency change by the frequency generator. The changing signals were then transmitted by inducting coupling method, and read by our reader circuit. The detected frequency signals were monitored and recorded by an

Agilent spectrum analyzer. In this experiment, we used the pH level at 2, 4, 7, 10, and 12 of buffer solutions to test our pH sensor. The potential and frequency were measured and recorded simultaneously in each pH level of buffer solution. The sensor was washed by DI water and dried by compressed air in between each testing episode. Fig. 5.7 shows the potential and frequency responses from pH=2 to pH=12 separately. The result showed that the sensitivity of sensing pH potential is –51.9mV/pH with high correlation coefficient r^2 values 0.99 which is still closed with our previous test of calibration at 3.1. For frequency detected by our circuit, the sensitivity of the pH-wireless circuitry represented 633 Hz/pH with the correlation coefficient r^2 values 0.99. The result showed that our circuit is able to transfer the pH sensing potential of different pH buffer solutions to frequency domain wirelessly. The frequency sensitivity can be read by spectrum analyzer and to recognize the different distinct pH levels. In addition, the frequency sensitivity is very important, because it can be used for pH value judgment on the end of wireless reader monitoring system.

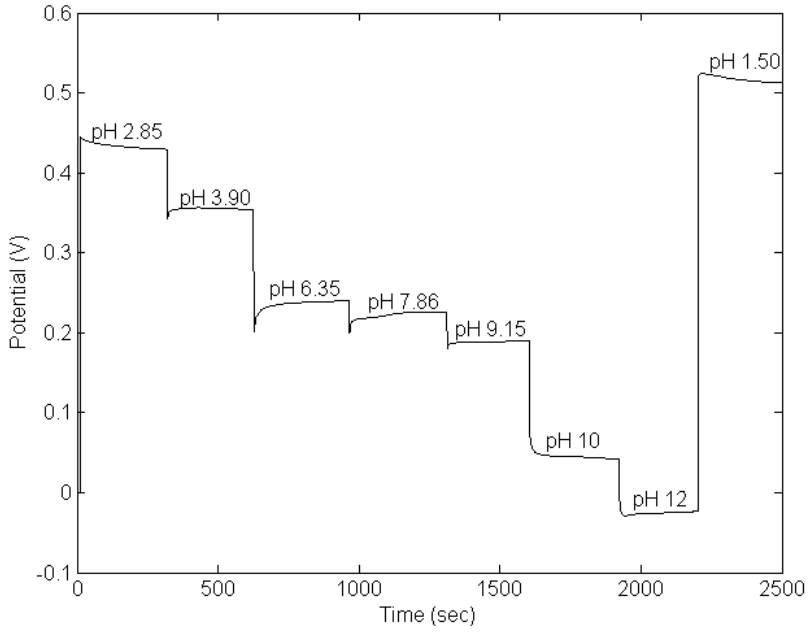

Figure 5.6 The continuous reversibility test of our IrOx pH sensor.

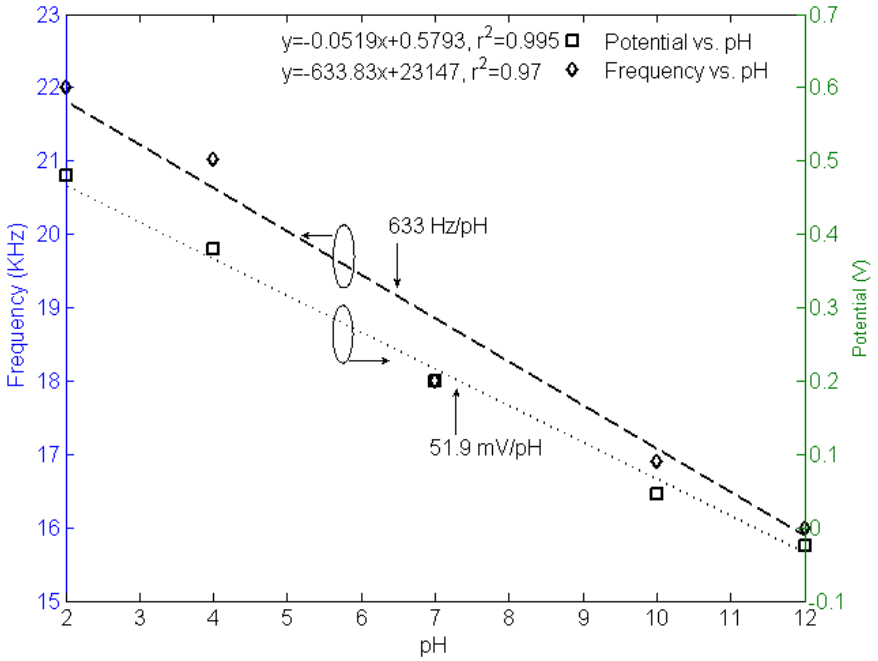

Figure 5.7 Linear response of our wireless pH sensing system in frequency and potential domain.

Wireless stability calibration: In order to present the long term performance of the pH-wireless freshness monitoring system, we used pH=2, 4, 7, 10 and 12 of the buffer solution for wireless transmission stability test. In this test, each buffer solution was dripped on our sensor and tested for 8 minutes, and the sensor was then cleaned and dried for the next testing episode. The response frequencies were recorded continuously by National Instrument USB 6216 data acquisition card simultaneously since the solution was dripped on the sensor. Fig. 5.8 shows the eight minutes of stable frequency responses for five different pH levels of buffer solution. Five different frequency levels recorded by DAQ card are 22 kHz, 20.9 kHz, 18 kHz, 16.9 kHz and 15.9 kHz corresponded to pH level at 2, 4, 7, 10, and 12 of buffer solutions separately. From this result, our pH-wireless circuit system was able to transfer and recognize the different pH sensing frequencies stably and clearly with very less noises. The noises happened at pH level 2 and 4 were about less than 50Hz which may caused by the contamination from the residual of previous testing solution. This also explained our sensor are sensitive enough even at the small amount of pH condition changes. Otherwise, our pH-

wireless freshness monitoring system provided the stable and consistent sensing ability, and it is ready for the food spoilage test.

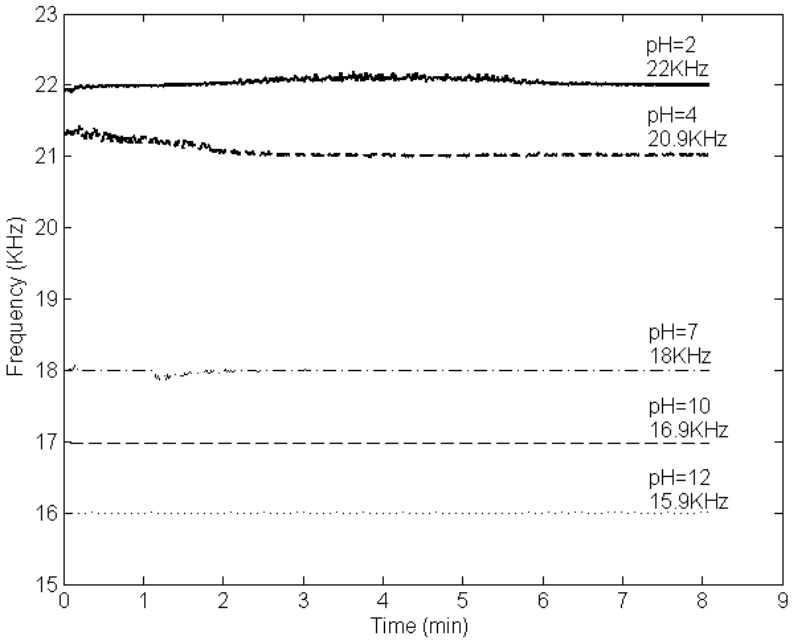

Figure 5.8 Stability test of our wireless pH sensing system.

Wireless dynamical pH level test: In this test, we are targeting on the simulation of random pH level change which may happen during the food spoilage process. The response time of the pH sensor and wireless circuitry is an important parameter showing the responding ability of our pH-wireless-freshness monitoring system. In the case, our pH sensor was tested by using the continuous titration at three pH levels of 5, 7 and 12. On the beginning, the pH=5 of testing solution was dripped on the sensing electrode for 4 seconds, and then the KOH solution was dripped in the pH=5 of testing solution. This titration episode raised the pH level of the testing solution to 7. After the frequency stable at pH=7, the same process was repeated again to reach the pH level of the solution to 12. The sensor wasn't clean during the whole experiment in order to mimic the real testing environment wirelessly. The data were recorded by NI-6216 USB data acquisition card continuously. Fig. 5.9 shows three clear frequency response steps happened when the KOH was dripped. The transition time between each pH level was about

less than 2 seconds. The response time was defined as the time needed for the potential change to reach 90% within the equilibrium value of potential [2.10]. In the result, our sensor was performed less than 1 second of response time in each titration episode. The short response time and clear frequency responses show that our pH-freshness monitoring system is able to catch the pH change precisely, dynamically and wirelessly.

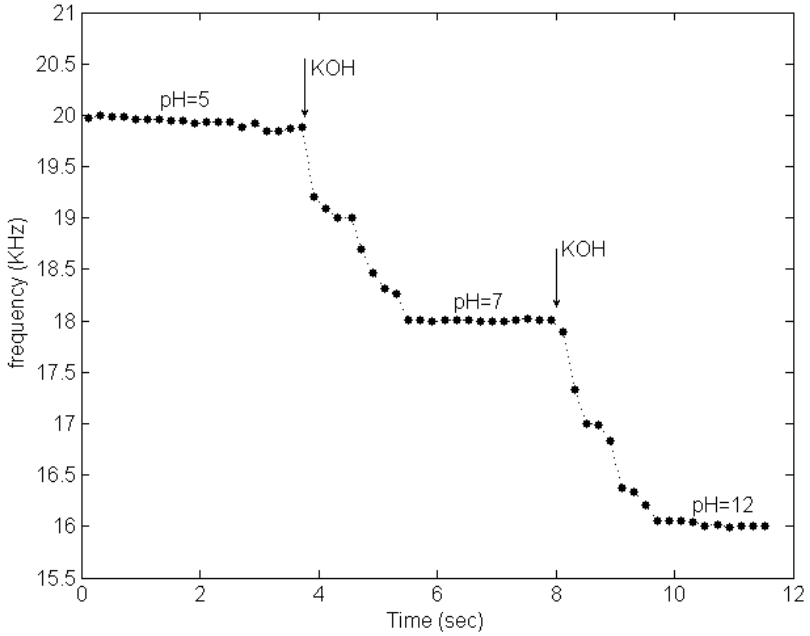

Figure 5.9 Dynamical titration and response time test of our wireless pH sensing system.

5.1.5.3 Fish spoilage test

In order to demonstrate the relationship between the pH level and spoilage process, we used one gram of Tilapia fillet as our testing sample. As shown in Fig. 5.10(a), two Tilapia samples were treated under two different temperature conditions. One Tilapia meat was stored in about 25°C of room temperature in order to induce the process of fish spoilage, and another one of Tilapia sample was stored in refrigerator which was under 5°C of constant temperature to be the comparison of the spoilage test. We put two pH sensors on the bottom of both fish samples to record and compare the pH-potential changing profiles for two different temperature

treatments on the fish meats. The potential data were recorded by Agilent 34970A multi-channel digital data acquisition system and LabView program in the personal computer.

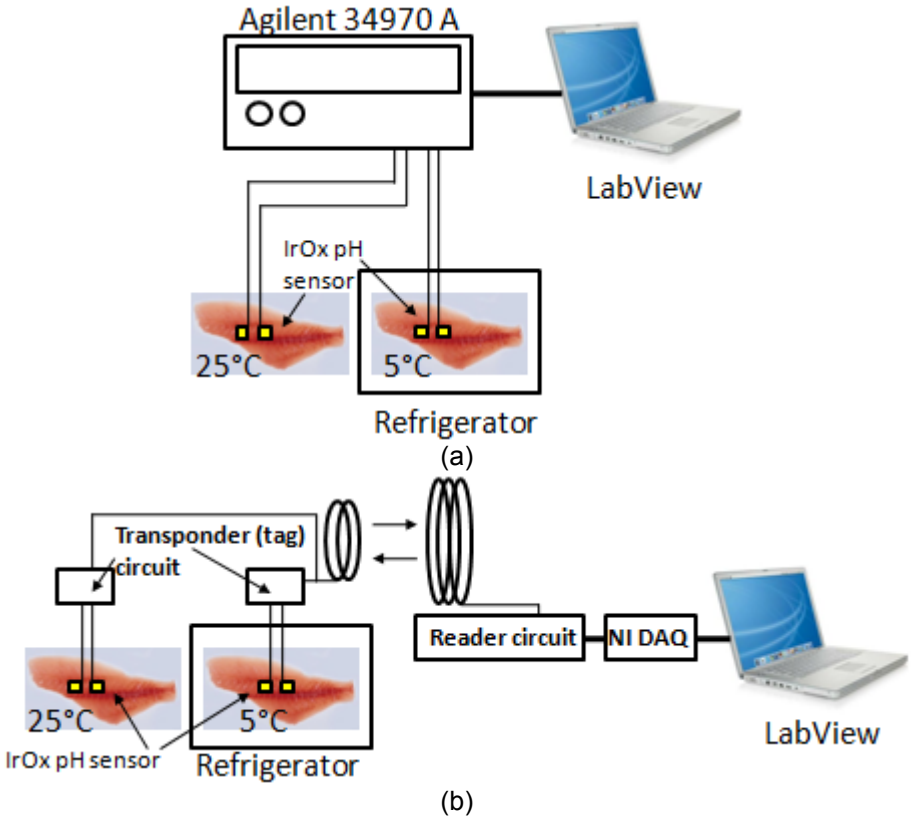

Figure 5.10 The experiment setup of (a) pH-freshness sensing system, and (b) pH-wireless-freshness sensing system.

Statistic and long term test results: In order to demonstrate the complete spoilage procedure, we did two tests by using the same pH sensor, and the Tilapia fillets were from the same purchase. Fig. 5.11 shows the results after 68 hours recording. The one stored in the refrigerator (black dash line) has no dramatic potential changes which mean the pH value kept constant around the same level. This may indicate that there were no microbes growing and no obvious odor was detected. However, the sensor attached on the fillet without the refrigeration (red solid line) has dramatic potential variations within the 68-hour period. The three spoilage stages of transition pattern were clearly showed in Fig. 5.11. The pH level changed probably

because of the chemical reaction and microbes growing as mentioned before as we described on 5.1.2 section.

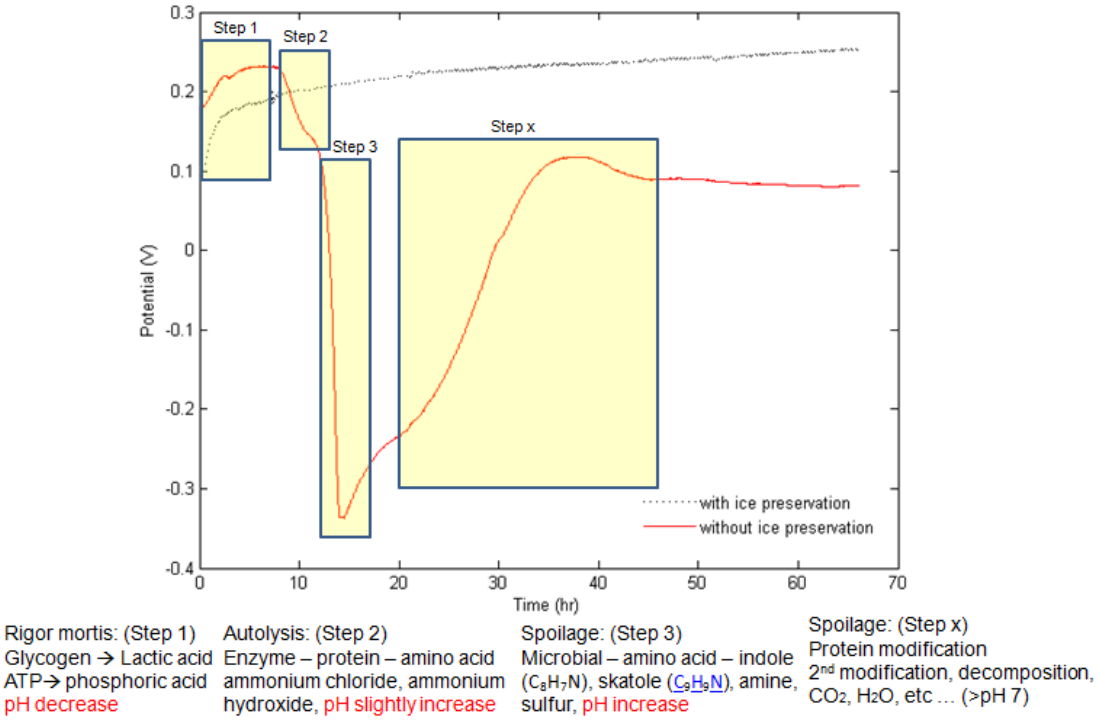

Figure 5.11 Long term monitoring of a tilapia fillet by our flexible IROF pH sensor.

Fig. 5.12 shows two tests of the spoilage procedure monitored by our IrO_x pH sensor. In these two tests, the spoilage fish meat all performed the tendency of the pH potential change as the low-high-low profile. The difference of the potential slope and happening event between two tests were compared in Table 5.1 and Table 5.2. The discrepancy on the potential changing rate may be caused by the room temperature or humidity of the air which will be the factors for the microbe growing. For example, in Fig. 5.12(b), it was the icy day that the room temperature was lower than the testing day of the Fig. 5.12(a). Therefore, the happening event in Fig. 5.12(b) was delayed for about an hour. This phenomenon represented that the lower growing rate of the yeast or microbe were because of the cold temperature. In this section, we presented a long term fish spoilage monitoring, and our sensor were able to sense the differences between the fresh and spoilage fish meet.

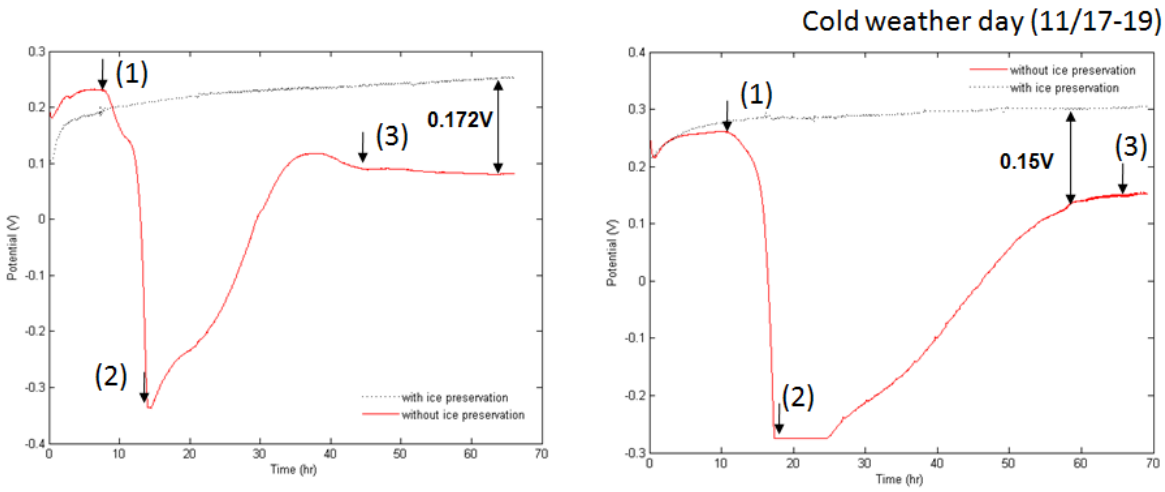

(a) (b)

Figure 5.12 Two times test for long term monitoring of a tilapia fillet on different days.

Table 5.1 Tilapia meat spoilage test No.1.

Time (second)	Potential (V)
(1) 1.56 hr	0.230
(2) 2.80 hr	-0.3275
(3) 6.79 hr	0.09814
Event	
lowest	-0.3275
Highest	0.230

Table 5.2 Tilapia meat spoilage test No.2.

Time (second)	Potential (V)
(1) 2.13 hr	0.26
(2) 3.46 hr	-0.2649
(3) 12.61 hr	0.145
Event	
lowest	-0.265
Highest	0.26

Short term test result: In the previous section, we demonstrated long term test. The complete spoilage process were monitored and proved by using our pH sensor. In this section, we define a spoilage window in 18 hours which is easier for spoilage judgment and monitoring procedure. According the data presented in Table 3 and Table 4, we observed that the potential changing event was happened obviously in 18 hours. Therefore, we can use the 18 hours as a standard spoilage moment (SSM) which the food quality may change and is not suitable for eating. In the SSM window as shown in Fig. 5.13, the sample stored in room temperature

without the ice preservation did follow the food spoilage procedure discussed in 5.1.2. In the first 11 hours, the potential increased from 45.8mV to 101.7mV which represented the pH level reduction caused by the releasing of lactic acid. We call the first step as “Rigor Mortis”. Right after 11 hours, the potential started to drop from 101.7mV to 96.4mV in one hour. The declined rate is –5.3mV/hour. This is the second step in the spoilage process called autolysis. The pH level will slightly increase because the releasing of amino group from dead muscle. From the 12th to 17th hour, the potential detected by our sensor dramatically dropped from 96.4mV to 34.8mV. The decline rate is –12.32mV/hour. This phenomenal will explain the last step in spoilage process. The pH level will increase very fast, because the microbes start to grow and absorb the amino and protein groups. Then the microbes will create different chemicals such as indole and skatole which are all alkaline making the pH level increase. However, the fish sample stored in the 5°C of refrigerator kept the potential rising slowly and constantly in 18 hours. This is a clear and distinct difference between the fresh and spoiled fish meat showing in the result. The pH-potential profile of the fish meat without the appropriate storing temperature represented the fluctuation of low-high-low tendency. The pH potential profile of the fish meat with the appropriate storing temperature represented a stable tendency. According to these pH potential profiles, we can simply recognize the food spoilage process, and easily apply on the real freshness monitoring system.

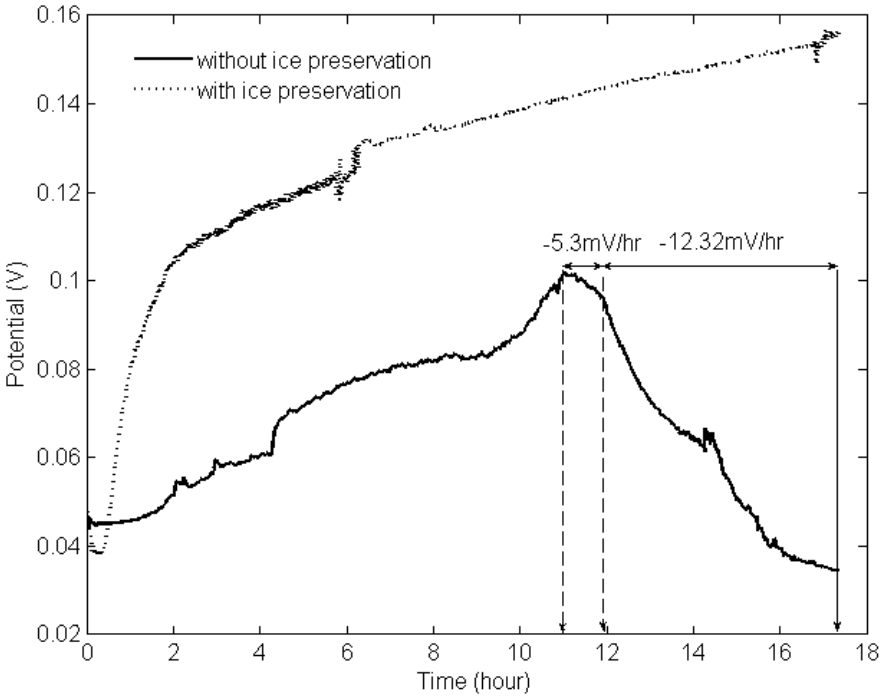

Figure 5.13 Spoilage potential monitoring result of our pH-freshness monitoring system.

5.1.5.4 Wireless freshness monitoring

In this test, our wireless freshness monitoring system was demonstrated as the setting showing in Fig. 5.10(b). Two Tilapia fillets were tested in two different storage temperatures which are in 25° of room temperature for spoilage monitoring and 5°C of refrigerator preservation for comparison by using our pH sensor. Two sensors were then connected to our transponder circuitry separately, and the sensing potential was then transferred to frequency in the tag circuitry. The frequency changes were transmitted by inducting coupling through the coil antenna to the reader circuit on another end. The detected frequency signals were monitored and recorded by NI 6210 USB data acquisition card with LabView program continuously in 18 hours for the sample treated as in room temperature. For the sample stored in refrigerator, the frequency signals were monitored and recorded by the system in each 2 to 4 hours.

Fig. 5.14 shows the result of wireless freshness monitoring procedure for two Tilapia samples. In the result, there are still two distinct frequency profiles showing the difference

between the fish sample treated by 25°C of room temperature and 5°C in refrigerator. The fish sample stored in 25°C of room temperature for 18 hours SSM presented the low-high-low frequency change showing the standard spoilage procedure mentioned in chapter 2. The frequency raised in first 6.39 hours from 17 kHz to 17.35 kHz corresponded to the rigor mortis step. From the 6.39th to 11.57th hour, the frequency drop from 17.35 to 16.99 kHz represented about –69.49 Hz/hour of frequency decline rate which explain the second step of the spoilage procedure. Right after the 11.57 hours, the frequency drop from 16.99 to 16.39 kHz represented the –123 Hz/hour of frequency decline rate. This phenomenal explains the pH level increased more in the last step of the spoilage process. In opposite, the frequency showed almost stable at about 17.3-17.4 kHz in 17 hours for the sample treated in the 5°C of refrigerator.

To compare with the calibration data in Fig. 5.7, we can roughly understand and calculate the change of pH level during the spoilage process. In Fig. 5.14, the pH level started at around 10 and rise to pH=9.35 in 6.39 hours. The pH level then drops back to 9.5, 10.5 and 11 in the rest of 10 hours profile.

In this experiment, we proved that our pH freshness system was able to recognize the food spoilage procedure in the long term monitoring by using RFID wireless technology. The low-high-low frequency profile is clearly defined as a spoilage condition comparing with the constant frequency for fresh sample. The food quality will be easily control and monitor by using our system.

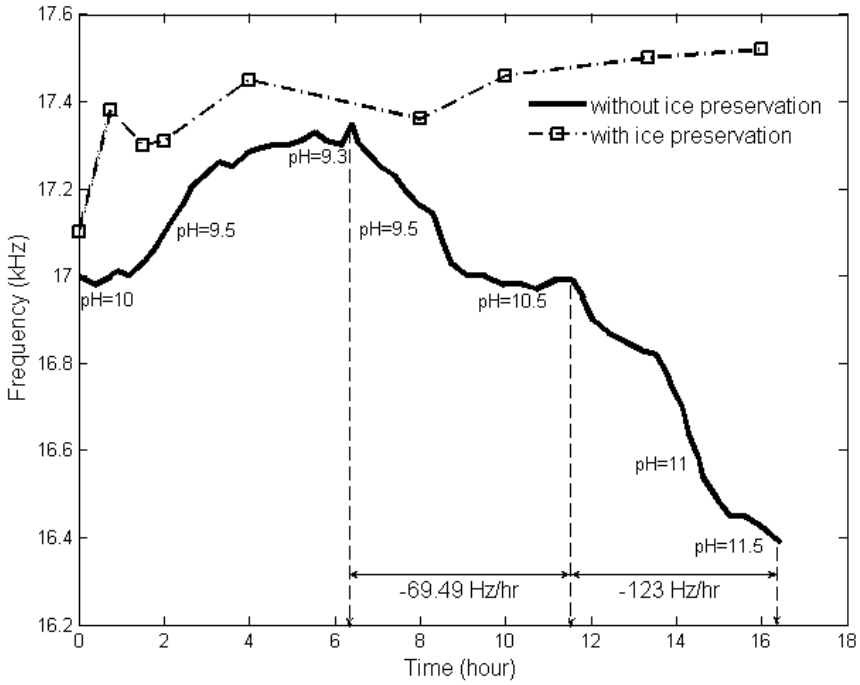

Figure 5.14 Spoilage frequency monitoring result of our wireless pH-freshness monitoring system.

5.1.6 Discussions and Conclusions

Our pH-freshness wireless monitoring system here is the first RFID based chemical sensor to apply electrochemical potential as the transduction on the target of food safety issue. The IrOx pH electrodes were fabricated on the biocompatible and flexible substrate which is easy to deform for food or medical applications. In the result, it shows good correlation between the measured pH, electrochemical potential, and frequency detected by using our sensor and wireless circuitry. The sensing system was applied and used on the detection of fish meat spoilage wirelessly, and the result matched with the spoilage procedure which is high-low-high of the pH changing profile. Comparing with the traditional freshness sensor such as the electronic nose, enzyme, and temperature sensor which we mentioned earlier, our sensor provide a simple fabrication, stable response, reusable material, and recordable data for the requirement of food safety control. The features of our pH sensor and wireless circuit are the passive, non-glass or silicon base, and machine-readable for the mass detection requirement. The sensitivity was presented as 633 Hz/pH in the range from pH level at 2 to 12. The stability

and dynamical test were also presented the sensor's ability in short and long term monitoring. Finally, our freshness wireless sensing module was applied on the detection of fish meat spoilage procedure. The pH level changing profile was monitored and recorded as pH=10-9.5-9.35-9.5-10.5-11 in 18 hours of SSM for the fish meat stored in 25°C of room temperature. The pH level of the fish sample stored in 5°C refrigerator kept at pH level at 8 to 9 in 18 hours. This result proved that our wireless sensing system was able to recognize the food spoilage wirelessly. The concept of our system design will reduce the risk of the food poison disease caused by the non-fresh or bad quality of the food. The customer and retailer will be able to use this sensing system to recognize the quality of the products wirelessly. To this end, the prototype of the pH-freshness wireless monitoring system is built and tested. The sensitivity, stability, response time and fish meat spoilage monitoring were presented and verified wirelessly. This design may be refined in the future applications of the wireless freshness monitoring as the commercial product that can be found in every super market.

5.2 Gastroesophageal Reflux Disease (GERD) Sensor

5.2.1 Motivation

Gastro-Esophageal Reflux Disease (GERD) is a condition in which food or liquid travels backwards from the stomach to the esophagus [5.21]. This unusual reflux can irritate the esophagus, and cause belching, heartburn, nausea, and other symptoms. The disease affects approximately 15% of the adult population in the United States, and is one of the most prevalent clinical conditions afflicting the gastrointestinal tract. GERD can also lead to complications such as esophageal cancer and lung damage. There are two common forms of esophageal cancer which are squamous cell carcinoma and adenocarcinoma. In the United States, esophageal carcinoma accounts for 10,000 to 11,000 deaths per year. The incidence of esophageal carcinoma is approximately 3-6 cases per 100,000 people. These increased rates are strongly related to GERD which is the primary risk factor recognized [5.22]. Over the past 25 years, the incidence of esophageal cancer has increased 350%, faster than any other malignancy in the western world. Therefore, to monitor the GERD symptoms comfortably and reliably is becoming the most important and popular issue for diagnosis of esophageal cancer.

5.2.2 Approach

For the GERD diagnosing system, we embedded our micro flexible pH sensor as shown in Fig. 5.15 on a surface size of 1.2cmx3.8cm in a wireless capsule sensor implant allowing to detect the pH changes of gastric juice reflux inside the esophagus. Based on the work [5.3, 5.20], the system consists of an implanted device and an external reader as shown in Fig. 5.16. Two approaches were proposed to realize passive sensing of the acid reflux. The first approach is using the application of resonance frequency shifting of passive components on the implant sensor capsule. The second approach utilizes RFID principles to detect the frequency generated from a circuitry on the capsule powered by an external reader. The action potential change generated by our pH sensor will represent by the change of frequency which can be monitored by the reader circuit.

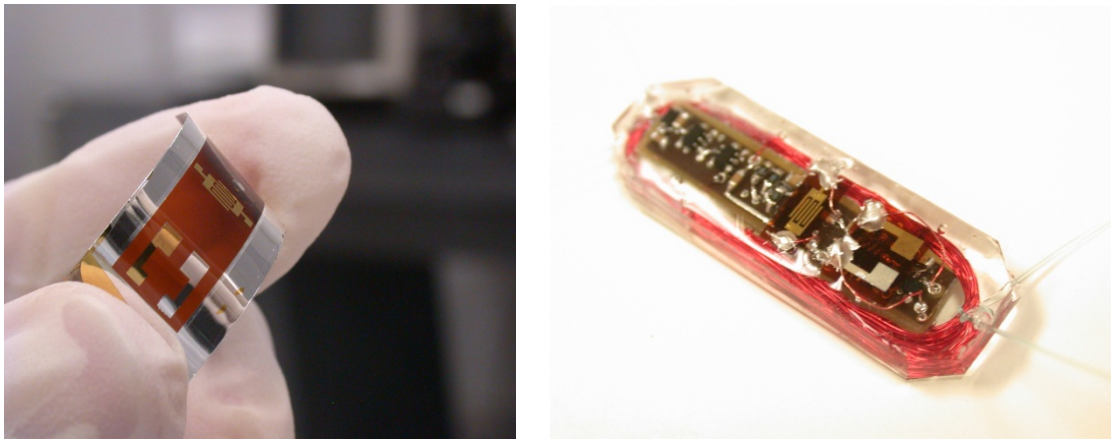

(a) (b)

Figure 5.15 Micro-fabricated (a) dual-sensors (pH and impedance) on flexible substrate and (b) pH/impedance RF-ID tag.

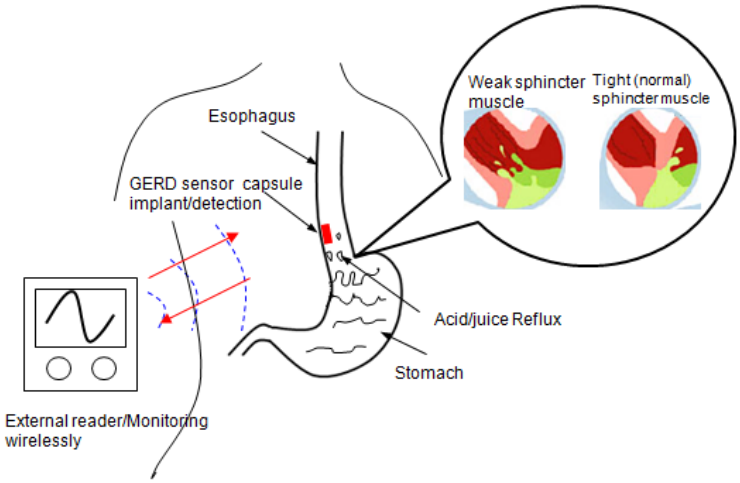

Figure 5.16 Schematics of an implant and an external reader for wireless GERD sensor.

5.2.3 Methods and Results

5.2.3.1 In vitro experiment

The experiment was done by putting the capsule in a 3-cm diameter glass tube to simulate conditions in the esophagus. The implant and Medtronic Bravo™ commercial pH sensor were attached on the wall of the tube simultaneously as shown in Fig. 5.17. The external coil was placed outside of the tube at a distance of 3 cm from the implant. The external coil was connected to an amplifier in a shield box. The different pH levels of solutions were supplied through another tube from the bottom to simulate the reflux from the human stomach. Fig. 5.18 shows the result of the in vitro test, our system responded to every simulated reflux episode immediately while commercially available pH sensor remained the same reading during the short test period. During the reflux of three pH episodes at levels of 2, 3, and 5, the frequency shows distinct down-shift from about 30 to 26 KHz which respond to each three clear reflux episode.

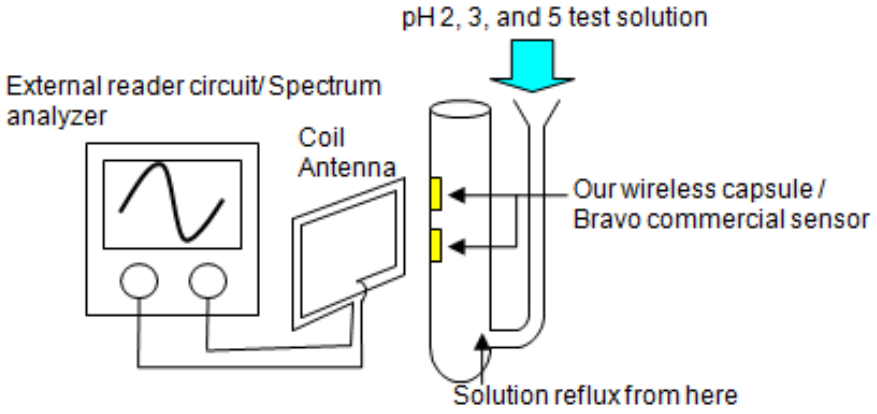

Figure 5.17 Schematic *in-vitro* experiment setup.

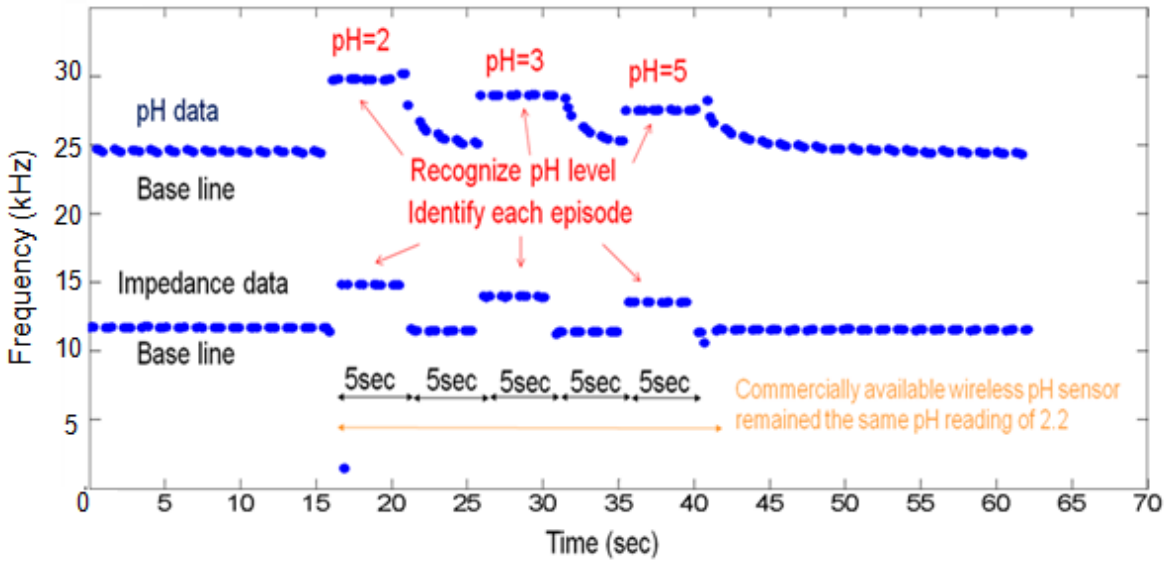

Figure 5.18 *In-vitro* GERD sensor test results.

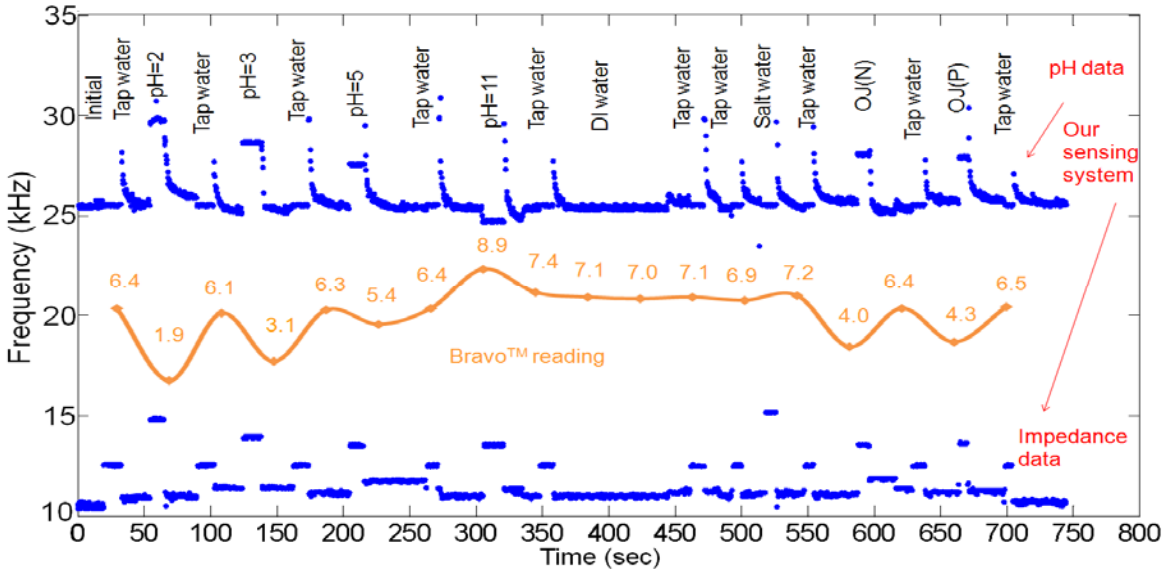

Figure 5.19 *In-vivo* GERD sensor test results.

5.2.3.2 In-vivo experiment

Our GERD sensor was also tested by three live animal experiments with the porcine model of female pigs weighted around 108 lbs., and the chest perimeter around 79cm. Our pH electrode was able to distinguish solutions with various pH levels from air so every reflux episode was detected. The pH value of each reflux episode was monitored with our pH sensor and Bravo^{TM} commercial pH sensor simultaneously. During the test, the Bravo^{TM} sensor did not detect water reflux episodes and failed to detect alkaline solutions with pH>10. Our pH sensor indicated the reflux episode at pH 2, 3, 5, and 11 clearly with the frequency shift down from 30 to 24 KHz. Our pH sensor not only can test on regular pH buffer solution, but also indicated the pH level of different solutions reflux such as the orange juice. The result shown in Fig. 5.19 represented our pH sensor indicated distinct pH sensing episodes much more precise, and quicker than commercial pH sensor.

5.2.4 Conclusions and discussions

In this section, a capsule size of GERD diagnosis system is designed, fabricated, and tested. The sensor includes two sensors which are impedance sensor and micro IrO_x/AgCl pH sensor. Our pH sensor is able to detect the electrochemical potential when different pH levels of solution reflux from the stomach, and the circuitry transfer the signal to frequency domain. The outside reader circuit is able to read the frequency shift. In this work, our flexible pH sensor embedded with the micro wireless transponder circuit design applied on GERD diagnosis was demonstrated and tested. The in vitro and in vivo tests were presented in this chapter.

CHAPTER 6

CONCLUSIONS AND FUTURE WORK

6.1 Conclusions

In this dissertation, a complete work of micro flexible IrO_x pH sensor has been investigated, fabricated, and applied on the real applications. To begin with, the literature, market, and production survey of the recent commercial pH sensor were reported and analyzed in order to design an innovated micro-pH sensor for bio-chemical or medical application. The comparisons of sensing mechanisms, material, fabrication, and performance evaluation of each pH sensing methods were also studied and considered. According to the result of literature survey and study, a flexible pH sensor based on economical sol-gel fabrication process by using the high stability of IrO_x sensing film were investigated and made.

About the sensor fabrication, a complete sensor fabrication including standard CMOS photolithography, economical sol-gel process, and anode electro-deposition were designed and proposed. For the working electrode, the IrO_x sol-gel process was applied on the flexible substrate. A stable and amorphous of IrO_x thin film was formed by this sol-gel method. The surface and material properties were then verified and compared by using the SEM, XRD and EDAX analysis. The different temperature affections to the surface were then proposed in this work. For the reference electrode, the electroplating process was applied to form AgCl thin film. The surface quality was verified by using SEM and EDAX as well. In this section, we fabricated a flexible pH sensor based on the IrO_x sensing film. The material and physical analyses of this sensor was considered and finished.

In the sensor test section, we performed different sensing properties of this flexible IrO_x pH sensor in order to verify the sensing performance. First, the sensitivity of the sensor was

measured by wide pH range from 2 to 12. Our sensor performed near Nernstian response which is about –51.5 mV/pH. Second, the response time of our pH sensor was measured by using acid-alkaline, alkaline-acid, and dry-acid titration method. In the result, less than one second of response time was presented in the tests. Third, the sensor's stability and repeatability were proposed by doing 5 minutes of test. In this measurement, the sensor performed stable and repeatable response for the long term test. Three parameters such as potential fluctuation, deviation, and drift potential were also defined and calculated in this testing section. Those factors represented the detail sensing performance of the pH sensor. After the stability test, the sensor was tested by continuous pH level titration in order to show the reversibility. Finally, the physical properties such as the cation selectivity and temperature dependence of our pH sensor were then proposed. In this sensor's in vitro test, our flexible pH sensor performed stable and repeatable sensing properties under different tests. Finally, a 4x4 pH sensor array was then fabricated and tested on multi-solution, temporal, and spatial experiment in order to focus on the micro- or nano- scale environment. In this section, a completely pH sensor test was applied and finished. An innovated micro-flexible pH sensor array was also performed in this section.

After the in vitro test, the sensor was then applied on two applications which are the food freshness monitoring and GERD diagnosis system. Our sensor was embedded with our batteryless, non-invasive wireless RF-ID circuit. The sensing pH level was able to transmit wirelessly through this circuitry.

For the freshness monitoring, the flexible pH sensor provided a stable, bio-compatible, and reversible sensing tool for food quality control system. A complete test procedure was performed which is from the sensor calibration to the fish meat spoilage test. Finally, we demonstrated wireless monitoring on fish spoilage in this section. Our freshness monitoring system was able to catch the signal caught by our pH sensor wirelessly.

For GERD diagnosis, our sensor was embedded with a wireless capsule which is suitable for implantation in esophagus. The complete in vivo and in vitro were purposed in this work. Our sensor was able to catch the reflux moment when the GERD syndrome happened unexpectedly.

In summary, an innovated flexible micro-IrO_x pH sensor was investigated and fabricated in this dissertation. A completely physical and chemical test were performed and confirmed for our pH sensor. Two real applications were then applied and tested. The performance of this sensor was not only able to reach the requirement of basic pH measurement, but also target on the novel application on bio-medical or chemical fields.

6.2 Future Work-Micro Scale of pH Sensing Test

In our recent research, the size of our sensing electrode is about 1mmx1mm. However, in order to target on the micro- or nano- scale of pH sensing environment such as the cell metabolism monitoring [6.1]. The size of electrode should be minimized to at least below 700-800 μm^2. Thus, we demonstrated the pH sensitivity test by using smaller exposure area on our electrode. The different exposure sensing areas were tested and compared its sensitivity performance of our pH sensor.

6.2.1 Test setup

In our sensor design, two types of the sensing electrode were made. One is 1.5mmx1.5mm, and another one is 1mmx1mm. In order to test the smaller exposure area, we covered a layer of Kapton polymer pocked by 500μm diameter of needle as shown in Fig. 6.1 (a) on the top of our 1.5mmx1.5mm sensing electrode. In sequentially, we also applied double and triple holes on the Kapton polymer in order to demonstrate and test the different exposure area for our IrO_x pH sensor. Fig. 6.1(b) shows that three holes of exposure area on the Kapton isolation layer.

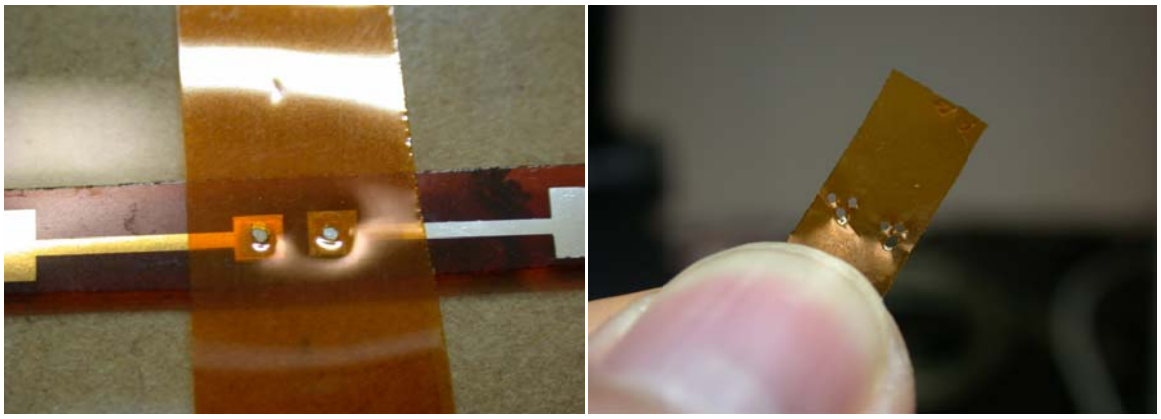

(a) (b)

Figure 6.1 Kapton isolation layer for (a) single hole, and (b) triple holes of exposure area.

6.2.2 Test result

In this experiment, we used the pH=2, 4, 7, 10, and 12 of test solutions to do the measurement. The test solution was dripped on the Kapton isolation layer, and the liquid just touched the sensor's surface depending on the size of exposure area as shown in Fig. 6.2. The sensor was then cleaned and dried after every measurement of each pH level of solution. Table 6.1 presented the sensitivity comparison between these three different exposure areas. The sensitivities were about from –56 to –57 mV/pH which is very close to Nerstian sensitivity, and the results show that our sensor still kept the same sensing performance eventually in the micro-scale of exposure area. Comparing with the size of the original electrode, Fig. 6.3 shows that the sensitivity didn't change much from –54.3 to –57.1 mV/pH, and keep at very high r^2 value from 0.98 to 0.99.

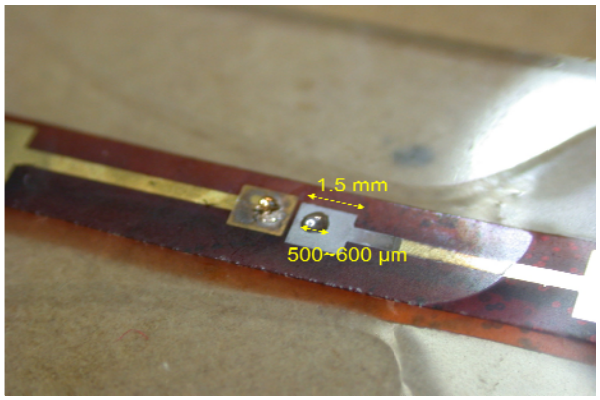

Figure 6.2 Exposed liquid for the single exposure area test.

6.2.3 Conclusions

In this section, we demonstrated the feature of small exposure size of IrO_x pH sensor test. The pH sensing sensitivity still kept at the similar result as the larger exposure size what we mentioned on chapter 3. According to the result, in the future work, the pH sensor can be able to make as the micro- or nano- size in order to treat or test for some spectacular applications such as the wound condition or cell milieu condition monitoring. Furthermore, micro- or nano- scale of pH sensor array can be embedded with micro-fluid channel that can monitor cell metabolism in cell culture volumes or other related applications.

Table 6.1 Sensitivity comparison between different exposure areas

Size (mm²)	Slope (mV/pH)	E° (mV vs. AgCl)	r^2
0.28	-56.7	531.7	0.9805
0.56	-57.1	550.7	0.9935
0.84	-57.3	521	0.9888

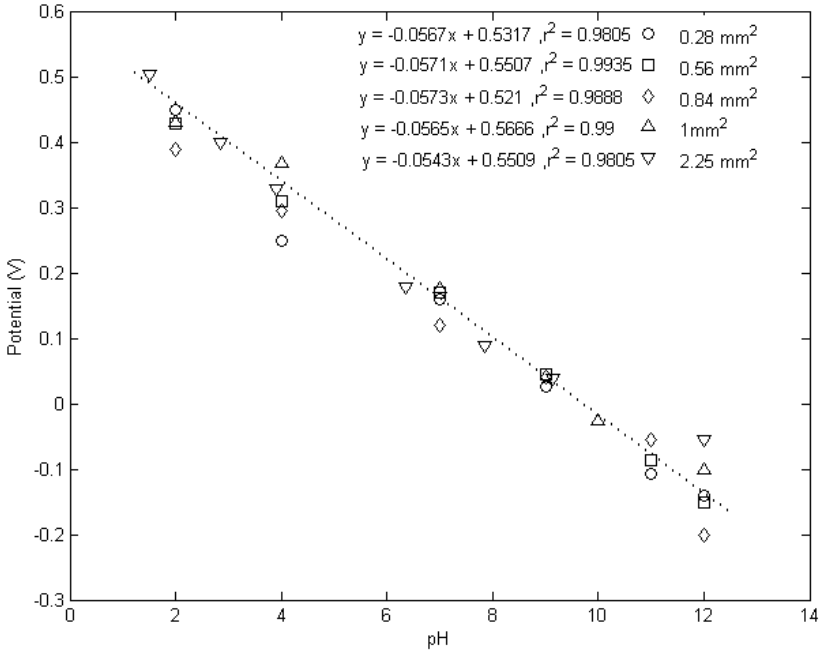

Figure 6.3 The comparisons of pH sensitivity between different exposure areas

6.3 Future Work- IrO_x material application

Generally speaking, iridium oxide has several features including low impedance, high charge capacity, and high porosity of physical properties. Furthermore, the IrO_x behaves as highly porous and high surface area redox metal similar to conductive polymers such as the polypyrrole and polyaniline. However, the IrO_x is unlike the polymer which is exceeding stable to irreversible reactions when the environment is fixed. The IrO_x can be oxidized and reduced over a wide range of pH which we already presented previously. These properties are able easily to be applied in some bio-medical or neural science field. On the following sections, two research future works are proposed, and discussed by showing the capability of the IrO_x material.

6.3.1 Micro neural stimulator

6.3.1.1 Motivation

In clinic application, there some body disorders caused by the nerve damage such as the blind vision and some paralyzation syndrome. Therefore, in order to recover or record the signal from our neural system, a good quality of the micro needle or stimulating system is required. There are some researches used the IrO_x material as the neural stimulator. Jessica [6.2] reported that the IrO_x stimulating electrode for the retinal and optic nerves. The concept of their prosthetic vision is using the electronic components to convert light into an electrical signal that stimulates neurons in the visual pathway. The neural signal is then processed by the brain to generate phosphenes. The IrOx electrode will be located on the bottom of the retinal in order to stimulate the nerve and transmit the electrical signal to the brain. Therefore, the IrOx played a very important role which should hold enough charge capacity current, and be a good conductive material in order to transmit the signal. The transformation between the different oxide state Ir(III)-Ir(IV) play a important role because the electrochemical redox energy releases the inflow-outflow current which is a good stimulation source and capability of the electrode for the nerve stimulation mechanism [6.3].

6.3.1.2 Proposed design

In the design of our next sensor generation, we proposed to coat an IrO_x film on a micron scale needle. The reference electrode such as the AgCl or Platinum will also be deposited as well. Fig. 6.4 shows the SEM picture of our design. In our design methodology, there are three 40μmx100μm of the open windows on an about 180μm width of micro needle. For the window No.2 in the center, we are going to deposit a layer of AgCl as a reference electrode. For the window No.1 and No. 3, the IrO_x and Platinum materials will be coated separately. In the future, this needle sensor can do the multi-sensing-stimulation function on the bio-medical and neural science application. For the IrO_x material, as introduced in previous section, it is an excellent porous and conductive material which can be a good stimulating electrode for neural science application. Furthermore, the IrO_x can also coordinate with the AgCl as a pH sensor which can monitor the cell milieu or other ion detections. The IrO_x can also be an immuno-sensor which we are going to propose on the next section. For the enzyme detection, the Platinum material can work as a good adhesion layer because its good stability and high surface charge properties.

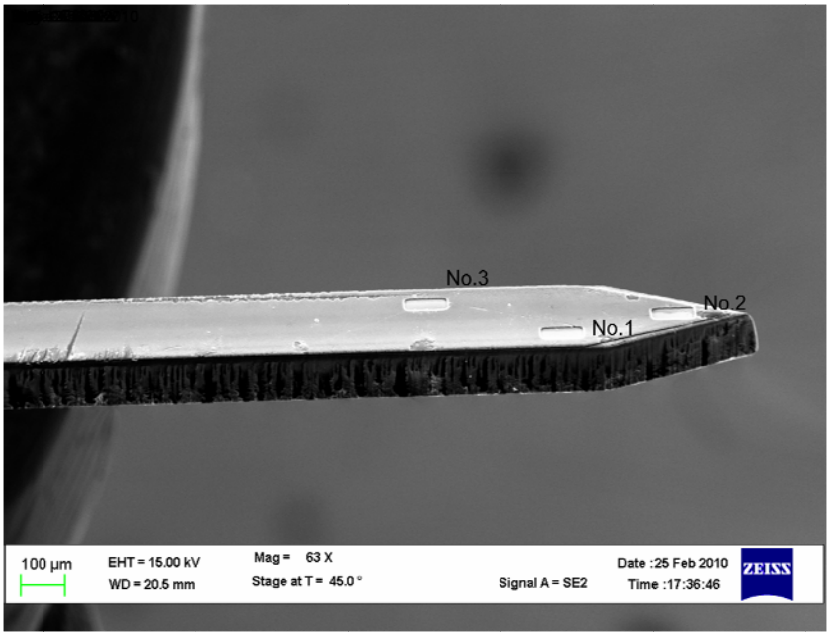

Figure 6.4 Multi-sensing-stimulation of micro scale needle by Hung Cao et.al.

6.3.2 Flexible Immuno-Sensor

6.3.2.1 Motivation

An immunosensor is a device comprising an antigen or antibody species coupled to a signal transducer, which detects the binding of the complementary species. An indirect immunosensor uses a separate labeled species that is detected after binding such as the fluorescence or luminescence. The immuno-device detects the binding by a change in potential difference, current, resistance, mass, heat, or optical properties.

Electrochemical immuno-sensor is the novel way to detect the virus, and may also design to trap the antigen. By using the porous feature of the IrO_x, the immunosensor is usually designed and fabricated by immobilizing antibodies onto the surface of the IrO_x by using the adsorption or entrapment process [6.4]. The three dimensional matrix of the iridium oxide film are available for immunological binding, and trap the antibodies as shown in Fig. 6.5.

6.3.2.2 Future Design

In the design methodology of the immunosensor, the surface porosity and the capability of capacity charge are the major issue for the immunosensor's performance. By using the economical sol-gel process as we mentioned before, the sensing performance is not only related to the thickness, but also related to the porosity of the surface. For the immunosensor, the quality of porous structure decides the capability of the antigen binding. The more uniform binding surface will create more stable sensitivity because the surface will be dominated by the binding of the antibody. On the other hand, the thickness also presents capability of the capacity charge. It represents the response time of the sensing performance.

During the sol-gel process, the precursor structure will explain the size and extent of branching of solution prior to film deposition. It also presents relative rates of evaporation and condensation during film deposition controlling the pore volume, pore size, and surface area of the final film. Fig. 6.6 shows the detail precursor steady-state deposition stage of the dip coating process [6.5]. The size of porous structure is addressed by the factors such as the size,

composition, pressure, and evaporation rate of the coating agent cluster. In order to make a good sensing film for immunosensor, the precise surface quality control is the first priority concern in the design methodology.

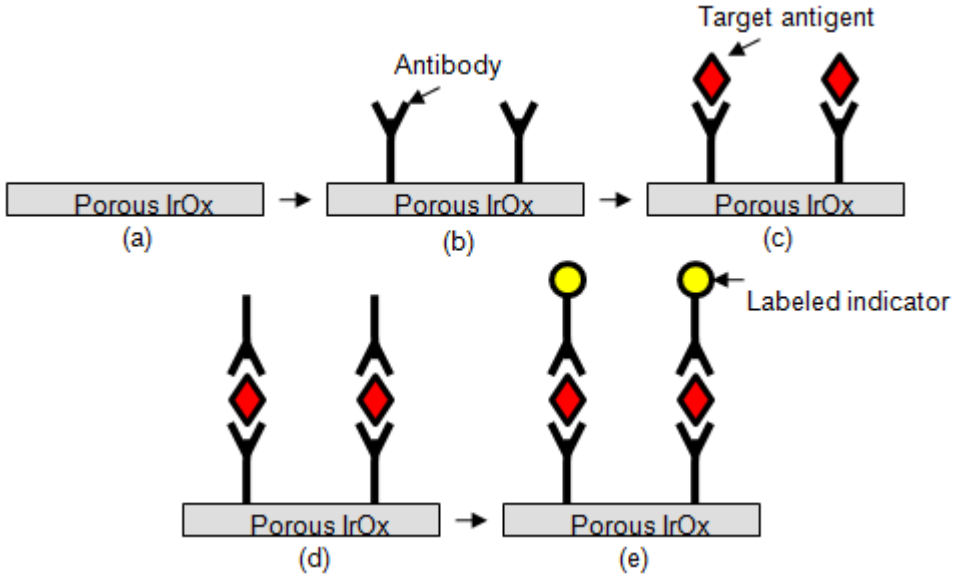

Figure 6.5 Sensing principle of IrO_x immune-sensor: (a)-(b) Antibody surface trap, (c) incubation of the sensor-target catching, (d) antibody bounding, and (e) labeled indication.

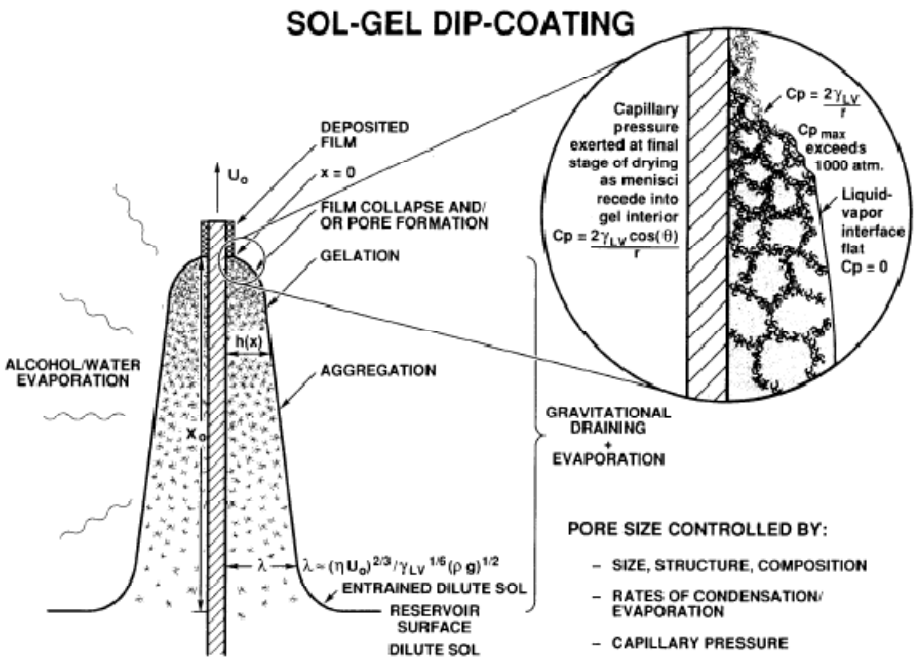

Figure 6.6 The schematic of the steady state sol-gel process [2.9].

6.4 Future Work- Wireless wound condition monitoring

6.4.1 Motivation

Wound healing is a sophisticated immune process which is represented by intercalating degradation, tissue re-assembly, and epidermal layer [6.6]. It is important to monitor the wound condition while the patient wears a bandage for two reasons: (1) the bandage should be changed according to the wound conditions, and (2) the different therapy agents need to be applied with respect to the wound conditions during various stages in wound healing.

For serious wound conditions, the bandage changes are done by doctors or nurses. In a hospital or trauma center, frequent changes of bandage add significant manual labors and therefore costs. Currently, the changes of bandages are done at fixed time schedules. This is not cost effective since sometimes the bandages may not need to be changed. Unnecessary changes of bandages may cause further damage to the wounds. It is also not result effective since some of the bandages need more frequent changes at certain stages of therapy, while others should not be changed in order to avoid tissue damages. However, the caretakers may not know when is the best time to change the bandages since most of the bandages are not transparent. The bandages need to be removed in order to examine the conditions of the wounds. In addition, the frequently removal of bandage will not only lose the efficiency and cost, but also result the high rate of wound infection. The patients may be infected by different yeast or microbe during the removal or change of the bandage. Therefore, with the fast growing of healthcare costs, active wound monitoring and infection management are crucial during this stage to ameliorate the likelihood and severity of infections.

6.4.2 Proposed Methods

For normal wound conditions, patients who wear bandages also need to know the wound conditions before replacement or seeking for further medical cares. This can be categorized into two general applications. For therapy purposes, wound conditions are monitoring to reduce scar forming and promote stable tissue regrowth. For protection purposes,

the wounds are monitored to prevent infection. Current solutions rely mainly on passive bandages for wound management without a monitoring mechanism. There is a strong need for a continuous, systematic yet flexible and reconfigurable wound monitoring that is lightweight, easy to implement and that provides ability to track patient's conditions.

pH value is an important indication to determine wound conditions with respect to its bacterial level. The pH distribution in the large wound area is useful information during the recovering and therapy procedures. Our pH sensor array on flexible substrates can be used to monitor pH level changes across an area of wound site. The metal oxide pH sensors allow continuous and long-term monitoring of pH, compared to the short lifetime disadvantage in enzyme-based or electrochemical sensing. The sensor is in an array configuration and on a flexible substrate allowing the sensor array to deform onto body parts to monitor multiple points in an area as shown in Fig. 6.7. The invented pH sensor produces a linear relationship between pH and potentials, which can be used in our batteryless wireless telemetry system. By detecting the responding shifted frequency of the modulated signals, we can remotely monitor the pH changes on the tissue.

6.4.3 The pH level of different skin conditions

1. pH value of normal skin

The normal pH level of human skin is between pH 4-7 [6.6] which depends on age, sex, and race of the person. The different location of skin also performs different pH value. Harrison and Walker mentioned that the pH of human's dermis was 7.54±0.09 tested by glass pH electrode [6.7]. The physiological pH value is caused by amino acids, fatty acids, and others produced by the skin appendages [6.6].

2. pH value and Bacterial Infection

In the beginning of infection, the pH level of tissue may decrease because the bacteria share the nutrients and oxygen with the tissue cells. The phenomenon is called ischemic

condition which may result the metabolism of tissue cells becoming anaerobic and therefore acidic [6.8].

3. pH value and Bacterial Thriving

In chronic wound, there are different bacteria as staphylococcus aureus and enzymes as staphylococci may contaminate the wound area and delay the healing process. Those microbes perform the overgrowth and highly activity in higher pH level milieu during the in-vitro experiment [6.6]. In other present study, the high level pH environment will slow down the cell migration and DNA synthesis during the healing process [6.9].

4. Result from the literature

In [6.8], the animal and clinical study has been done and shown the approximate linear response with the number of bacteria and pH level. With increasing of bacteria counts, the pH level decreased. In [6.6], the wound pH was measured by invasive glass electrode. The pH value drop from 7.4 to 6.6, and the wound condition was improved with the pH decreased.

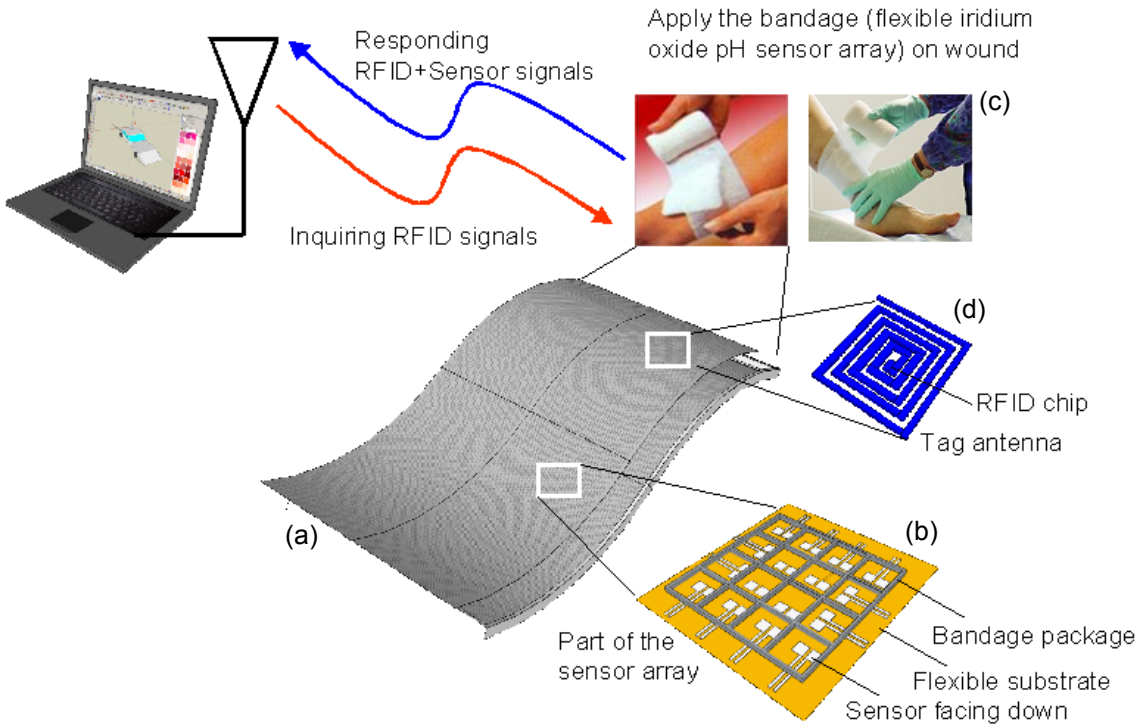

Figure 6.7 The novel flexible wound condition monitoring system is on (a) flexible substrate, (b) pH sensor array configuration across the wound area, (c) monitor pH values across the wound area to prevent infection, (d) batteryless and wireless communication.

APPENDIX A

CYCLIC VOLTAMMETRY ANAYSIS OF IRIDIUM OXIDE pH ELECTRODE

A.1 INTRODUCTION

Cyclic Voltammetry (CV) is the most effective and versatile electro-analytical technique for the mechanistic study of redox systems. It enables the electrode potential to be rapidly scanned in search of redox couples. The repetitive triangular potential excitation signal for CV causes the potential of the working electrode to sweep back and forth between two designated values. To obtain a cyclic voltammogram, the current (*i*) at the working electrode is measured during the potential scan as shown in Fig. A.1. Once located, a couple can then be characterized from the potentials of peaks on the cyclic voltammogram and from changes caused by variation of the scan rate. CV is often the first experiment performed in an electrochemical study. Therefore, we can use the CV analysis to verify the performance of our IrOx film in the redox system.

Consider an overall electrode reaction, $O + ne \Leftrightarrow R$, composed of a series of steps that cause the conversion of the dissolved oxidized species, *O*, to a reduced form, R. General speaking, the electrode reacting performance can be presented by the current which is governed by the processes such as the mass transfer, electron surface transfer, chemical reaction, and other surface reactions as shown in Fig. A.2 [6.10].

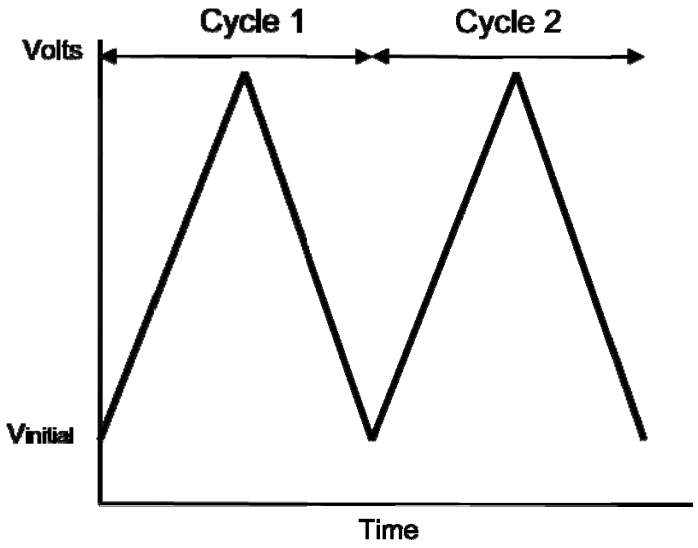

Figure A.1 Typical excitation signal for cyclic voltammetry.

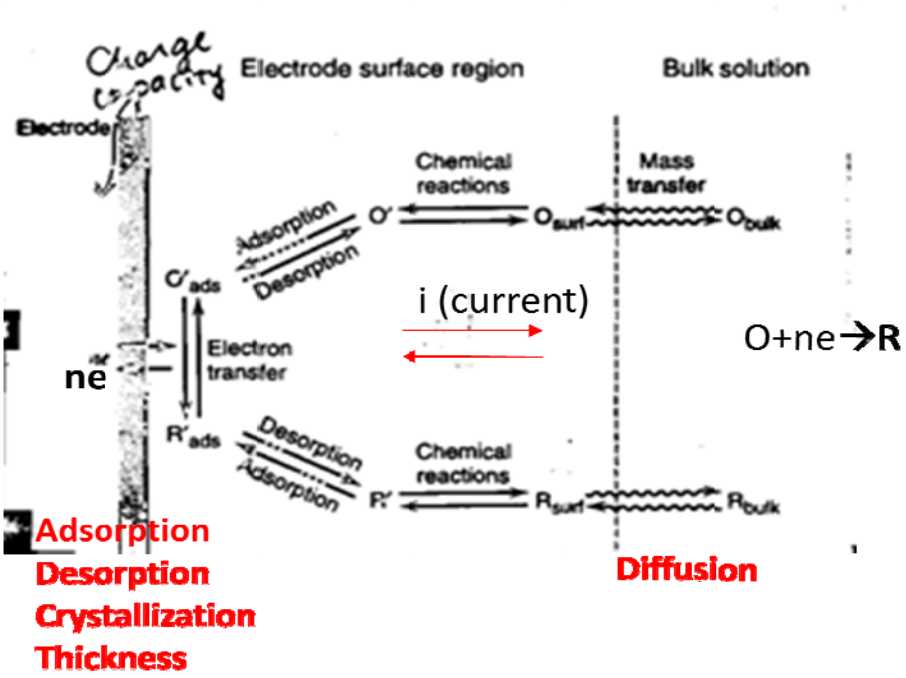

Figure. A.2 General electrode reaction in the solution [6.10].

A.2 Surface current calculations

From the Fig. A.2, the current (*i*) between the bulk solution and surface can be explained and calculated by understanding the rate of reaction, *v*, which associates with mass transfer process. By using the charge density, *q*, the reaction rate can be derived as below:

$$i = {dQ}/{dt}, \frac{Q}{nF} = N(mol) \quad \text{A.1}$$

$$v = Rate(mol/s) = \frac{dN}{dt} = \frac{i}{nF}, v(mol/(s*cm^2)) = \frac{i}{nFA} \quad \text{A.2}$$

which *n* is the number of electron consumed in the electrode reaction, and *A* is the electrode surface area. Such electrode reactions are often called reversible or nernstian. The principal of the reaction is based on thermodynamic relationships at the electrode surface. Therefore, the mass transfer equation could be simplified by [6.10]:

$$v = \frac{i}{nFA} = m_0 C, \quad \text{A.3}$$

$$i = nFAm_0 C \quad \text{A.4}$$

which m_0 is the mass-transfer coefficient, and the C is the surface charge as the voltage. Therefore, from the equation A.3 and A.4, we know the information of the surface charge when the electrode reacts with the agents. The electrochemical potential and current were also presented in these equations. After the definition of the surface current, if the kinetics of electron transfer are rapid, the charge of the surface (C_0) and bulk solution (C_R) can be assumed to be at equilibrium with the electrode potential as governed by the Nerestian equation which we mentioned at the chapter 2 as shown in equation A.5:

$$E = E^0 + \frac{RT}{nF}\ln\frac{C_0}{C_R} \qquad \text{A.5}$$

$$\frac{C_0(0,t)}{C_R(0,t)} = f(t) = \exp[\frac{nF}{RT}(E_i - vt - E^0)]$$

$$i_p = (2.69\times10^5)n^{3/2}AD^{1/2}{}_0C^*{}_0v^{1/2} \qquad \text{A.6}$$

$$E_p = E_{1/2} - 1.109\frac{RT}{nF} = 28.5/n \ \ (mV)$$

$$E_{1/2} = E^0 + (RT/nF)\ln(\frac{D_R}{D_0})^{1/2} \qquad \text{A.7}$$

where D is diffusion coefficient. In equation A.6, the diffusion equation between the electrode surface region and bulk solution is concerned. However, the surface not only includes linear but also includes the other coordinates system such as the spherical electrode. Therefore, the complete current also can be derived by:

$$i = i(plane) + i(spherical) \qquad \text{A.8}$$

$$i = nFAD^{0.5}{}_0C_0v^{1/2}\pi^{1/2}x(\sigma t) + nFAD_0C_0(1/r_0)\phi(\sigma t) \qquad \text{A.9}$$

A.3 CYCLIC VOLTAMMETRY

On the last section, we derived the surface current which will happen in the electrode redox process. In this section, the complete cyclic voltammetry will be presented and explained. In our application, what we care is the surface quality which is the sensor's response rate (v) and the performance of the redox ability. As shown in Fig. A.3, the basic volammograms chart is presented as two different oxidation states in the surface redox process. Basically, the different

material will have different redox performance such as the surface potential and number of the oxidation states. For IrO_x material, basically at least three oxidation states will be found during the complete CV analysis. In each approach of the oxidation state, the current and surface charge will add to the original charge, which means the current and surface charge will be larger than the original oxidation state. The phenomenon also represents the difference of sensitivity happened in different fabrication method due to the surface quality controlled by the change of thickness and porosity parameters. Fig. A.4 shows one of the CV analyses from [A.1].

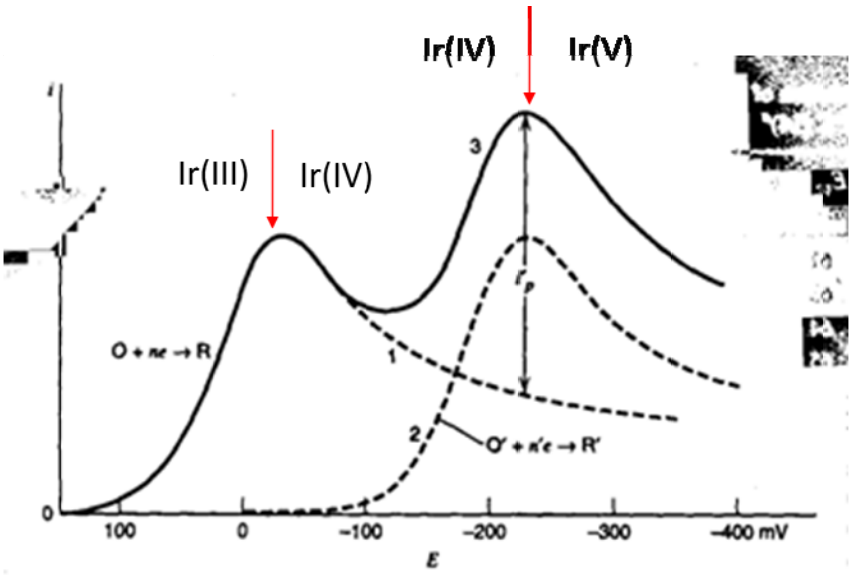

Figure A.3 Different oxide state creates (releases) different potential [6.10].

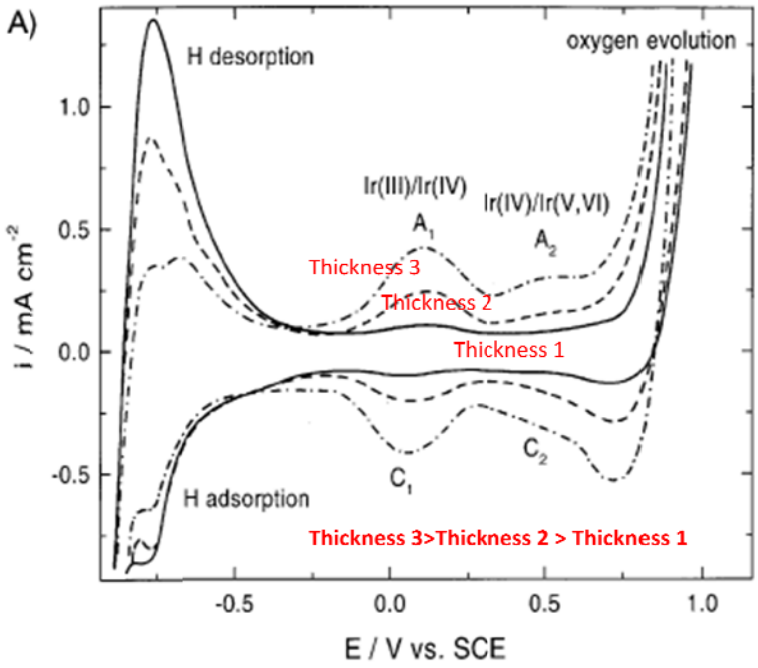

Figure A.4 Complete IrOx CV redox analysis by [A.1].

A.4 EXPERIEMENT

A.4.1 Experimental set up

The standard three-electrode cell was used for the electrochemical C-V measurements. The IrO_x films of 0.01 cm^2 area were used as working electrode (WE), Platinum was a counter electrode (CE), saturated AgCl electrode was reference electrode (RE) and 0.5 M of H_2SO_4 served as an electrolyte. The voltages were measured with reference to the saturated AgCl electrode. Cyclic voltammetry was carried out and recorded by using Agilent potentiostat. The variation of current with respect to time was with the potential from –0.4V to 1.2V at the potential sweep rate at 100 mV/s.

A.4.2 Experimental result

In this section, we calculated the surface current by using the equation A.5-A.9, and compare with the C-V curve recorded from the potentiostat. In our experiment, we use 10 min/cm as the withdraw rate, and the electrode area is about 0.01 cm^2. The surface current was derived as followed:

$$i_p = (2.69\times10^5)n^{3/2}AD^{1/2}{}_0C^*{}_0v^{1/2}$$

$$E_p = E_{1/2} - 1.109\frac{RT}{nF} = 28.5/n \quad (mV)$$

$$i_p = (2.69e5)*1*0.01(cm^2)*(34.5e-10)^{0.5}*(0.5e-3)(mol/ml)*(100mV)^{0.5}$$

$$= 0.025mA = 2.5\times10^{-5}A$$

where the i_p is the peak current, and E_p is the peak potential. To compare with the theoretical data in Fig. A.5, the hydrogen underpotential deposited peak (upd) peak current is about 0.042mA which is close with our theoretical data. Normally, higher upd peak value (about 1mA) is easy to find in AIROF (anodic electrodeposition) fabrication process, because the high degree of porosity of the films done by electrodeposited process. In our case, the Ir nanoparticle is converted to IrO_x completely by sol-gel process. Therefore our upd peak is much lower than 1mA. General speaking, when the H upd peak is higher, the charge density is lower. The phenomenon also presented that the IrO_x film is not covered well. In the Fig. A.5, it showed clear peak at the 1st and 2nd oxidation states which are from Ir(III) to Ir(IV), and from Ir(IV) to Ir(V). The current and surface charges are all clear and obvious. The result shows that our sol-gel IrO_x film has a good oxidation performance. In the reduction peak, the value is not clear but still can be recognized. The phenomenon may show that our sensor have weaker surface charge during the reduction process. However, for the reduction reaction, our pH sensing potential is showing the negative potential which matches with the negative surface charge showing in CV analysis. By using the CV curve, we can easily inspect the sensor's performance by the scientific way.

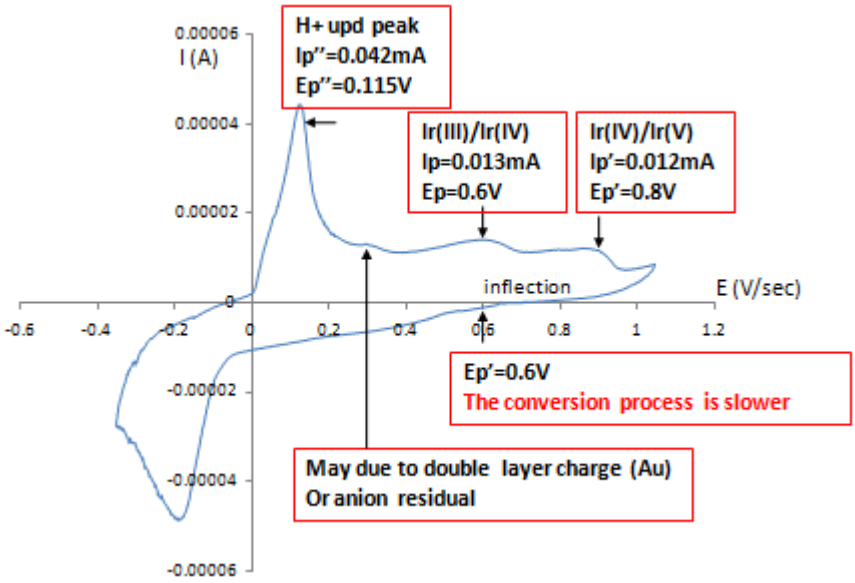

Figure A.5 Experimental CV curve of our IrO_x thin film.

A.4.3 Discussions

In this section, we demonstrated an electrochemical analysis method which can be easily applied on the deposited reversible redox material. The sensing performance and chemical event can easily be inspected by using the cyclic voltammetry analysis method. In the future work, the CV analysis is a necessary tool to verify the film quality and capability. For example, the thickness, and surface porosity are related to the sensing performance. The CV curves can easily identify the special event happen and compare the difference between the variety of parameters in fabrication process in order to find the properly recipe.

REFERENCES

[1.1] John G. Webster, "The measurement, instrumentation and sensors handbook," *CRC Press and IEEE Press,* pp. 71-1, Florida, 1999.

[1.2] Young-Jin Kim, Young-Chul Lee, Byung-Ki Sohn, Jung-Hee Lee, and Chang-Soo Kim, "A novel pH microsensor with a buile-in reference electrode," *Journal of the Korean Physical Society*, Vol. 43, pp. 769-772, 2003.

[1.3] Yi Liu, Tianhoung Cui, "Ion-sensitive field-effect transistor based pH sensors using nano self-assembled polyelectrolyte/nanoparticle multilayer films," *Sensors and Actuators B*, Vol. 123, pp. 148-152, Aug., 2006.

[1.4] Jinghong Han, Dafu Cui, Yating Li, Hong Zhang, Yuzi Huang, Zipan Zheng, Yaming Zhu and Xiangming Li, "A gastroesophageal tract pH sensor based on the H-ISFET and the monitoring system for 24 h," *Sensors and Actuators B*, Vol. 66, pp. 203-204, July, 2000.

[1.5] Kalman Pasztor, A. Sekiguchi, N. Shimo, N. Kitamura and H. Masuhara, "Iridium oxide-based microelectrochemical transistors for pH sensing," *Sensors and Actuators B*, Vol. 12, pp. 225-230, 1993.

[1.6] Otto S. Wolfbeis, "Fiber-optic chemical sensors and biosensors," *Anal. Chem*., Vol. 76, pp. 3269-3284, 2004.

[1.7] Sheila A. Grant, Robert S. Glass, "A sol-gel based fiber optic sensor for local blood pH measurements," *Sensors and Actuators B*, Vol. 45, pp. 35-42, 1997.

[1.8] Saying Dong, Ming Luo, Gangding Peng, and Wenhua Cheng, "Broad range pH sensor based on sol–gel entrapped indicators on fiber optic," *Sensor and Actuators B: Chem.* Vol.129, pp. 94-98, Jan., 2008.

[1.9] Zhe Jin, Yongxuan Su, and Yixiang Duan, "An improved optical pH sensor based on polyaniline," *Sensors and Actuators B*, Vol. 71, pp. 118-122, Nov., 2000.

[1.10] Afsaneh Safavi, Mozhgan, "Novel optical pH sensor for high and low pH values," *Sensors and Actuators B*, Vol. 90, pp. 143-150, April, 2003.

[1.11] E. Alvarado-Mendez, R. Rojas-Laguna, J.A. Andrade-Lucio, D. Hernandez-Cruz, R.A. Lessard, and J.G. Avina-Cervantes, "Design and characterization of pH sensor based on sol–gel silica layer on plastic optical fiber," *Sensors and Actuators B*, Vol. 106, pp. 518-522, May, 2005.

[1.12] Norman F. Sheppard, Jr., Matthew J. Lesho, Philip McNally, and A. Shaun Francomacaro, "Microfabricated conductimetric pH sensor," *Sensors and Actuators B*, Vol. 28, pp. 95-102, Aug., 1995.

[1.13] Gerald Gerlach, Margarita Guenther, Joerg Sorber, Gunnar Suchaneck, Karl-Friedrich Arndt, and Andreas Richter, "Chemical and pH sensors based on the swelling behavior of hydrogels," *Sensors and Actuators B*, Vol. 111-112, pp. 555-561, Nov., 2005.

[1.14] R.Bashir, J.Z. Hilt, O.Elibol, A.Gupta and N.A. Peppas, "Micromechanical cantilever as an ultrasensitive pH microsensor," *Applied Physics Letters*, Vol. 81, pp. 3091-3093, 2002.

[1.15] Agner Fog, and Richard P. Buck, "Electronic semiconducting oxides as pH sensors," *Sensors and Actuators*, Vol. 6, pp. 137-146, 1984.

[1.16] T. Mikolajick, R. Kuhnhold, and H. Ryssel, "The pH-sensing properties of tantalum pentoxide films fabricated by metal organic low pressure chemical vapor deposition," *Sensors and Actuators B*, Vol. 44, pp. 262-267, 1997.

[1.17] Patrick J. Kinlen, John E. Heider, and David E. Hubbard, "A solid-state pH sensor based on a Nafion-coated iridium oxide indicator electrode and a polymer-based silver chloride reference electrode," *Sensors and Actuators B*, Vol. 22, pp. 13-25, Oct.,

1994.

[1.18] H. Neil McMurray, Peter Douglas, and Cuncan Abbot, "Novel thick-film pH sensors based on ruthenium dioxide-glass composites," *Sensors and Actuators B*, Vol. 28, pp. 9-15, July, 1995.

[1.19] Wouter Olthuis, "Chemical and physical FET based sensors or variations on an equation," *Sensor and Actuator B*, Vol. 105, pp. 96-103, 2005.

[1.20] Yi-Hung Liao and Jung-Chuan Chou, "Preparation and characteristics of ruthenium dioxide for pH array sensors with real-time measurement system," *Sensor and Actuators B*, Vol.128, pp. 603-612, Jan., 2007.

[1.21] Chu-Neng Tsai, Jung-Chuan Chou, Tai-Ping Sun, and Shen-Kan Hsiung, "Study on the sensing characteristics and hysteresis effect of the tin oxide pH electrode," *Sensors and Actuators B*, Vol. 18, pp. 877-882, July, 2005.

[1.22] Sheng Yao, Min Wang, and Marc Madou, "A pH electrode based on melt-oxidized iridium oxide," *Journal of the Electrochemical Society*, Vol. 148, pp. 29-36, 2001.

[1.23] J. V. Dobson, P. R. Snodin and H. R. Thirsk, "EMF measurements of cells employing metal-metal oxide electrodes in aqueous chloride and sulphate electrolytes at temperatures between 25–250°C," *Electrochemical Acta*, Vol. 21, pp. 527-533, 1976.

[1.24] C. Jefferey Brinker, George W. Scherer, "Sol-gel science: The physics and chemistry of sol-gel processing," *Academic Press*, pp. 788-798, Boston, 1990.

[2.1] M. Pourbaix, "Atlas of electrochemical equilibria in aqueous solutions," *National Association of Corrosion Engineers*, 1974.

[2.2] Jiang-Tsu, and Ying-Sheng Huang, "Electron paramagnetic resonance of a molecular defect in γ-irradiated IrO2 single crystals," *Physical Review B*, Vol. 40, pp. 4281-4288, 1989.

[2.3] Scott Brewer, Dwi Wicaksana, Jon-Paul Maria, Angus Kingon, and Stefan Franzen, "Investigation of the electrical and optical properties of iridium oxide by reflectance

FTIR spectroscopy and density functional theory calculations," *Chemical Physics*, Vol. 313, pp. 25-31, 2005.

[2.4] Akiyoshi Osaka, Toru Takatsuna, and Yoshinari Miura, "Iridium oxide films via sol-gel processing," *Non-Crystalline Solds*, Vol. 178, pp. 313-319, 1994.

[2.5] Kazusuke Yamanaka, "Anodically electrodeposited iridium oxide films (AIROF) from alkaline solutions for electrochromic display devices," *Japanese Journal of Applied Physics*, Vol. 28, pp. 632-637, 1989.

[2.6] Michael S. Wilson, and R. David Rauh, "Novel amperometric immunosensors based on iridium oxide matrices," *Biosensor and Bioelectronics*, Vol. 19, pp. 693-699, 2004.

[2.7] Michael L. Hitchman, and Subramaniam Ramanathan, "A field-induced poising technique for promoting convergence of standard electrode potential values of thermally oxidized iridium pH sensors," *Talanta*, Vol. 39, pp. 137-144, 1992.

[2.8] Keishi Nishio and Toshio Tsuchiya, "Electrochromic thin films prepared by sol-gel process," *Solar Energy Materials& Solar Cells*, Vol. 68, pp. 279-293, 2001.

[2.9] C. Jefferey Brinker, George W. Scherer, "Sol-gel science: The physics and chemistry of sol-gel processing, " *Academic Press*, pp. 788-798, Boston, 1990.

[2.10] M. Pourbaix, "Atlas of electrochemical equilibria in aqueous solutions," *National Association of Corrosion Engineers*, pp. 374-377, 1974.

[2.11] Erno Pungor, "The theory of ion-selective electrodes," *Analytical Sciences*. Vol. 14, pp. 249-256, 1998.

[2.12] L.D. Burke, M.E. Lyons, E.J.M. O'Sullivan, and D.P. Whelan, "Influence of hydrolysis on the redox behaviour of hydrous oxide films," *J. Electroanal. Chem.*, Vol. 122, pp. 403-407, 1981.

[2.13] W. Olthuis, M. A. M. Robben, P. Bergveld, M. Bos and, W. E. van der Linden, "pH sensor properties of electrochemically grown iridium oxide," *Sensor and Actuators B*, Vol. 2, pp. 247-256, 1990.

[3.1] H. Andreas, H. Elzanowska, I. Serebrennikova, and V. Birss, "Hydrous Ir oxide film properties at sol-gel derived Ir nanoparticles," *Journal of The Electrochemical Society*, Vol. 147, pp. 4598-4604, 2000.

[3.2] A.W.J.Cranny, J. K. Atkinson, "Thick film silver–silver chloride reference electrodes," *Meas. Sci Technol*, pp. 1557-1565, 1998.

[4.1] R.H. Horng, D.S. Wuu, L.H. Wu, and M.K. Lee, "Formation Process and Material Properties of Reactive Sputtered IrO_2 Thin Films," *Superficies y Vacio*, Vol. 9, pp. 139-142, 1999.

[4.2] Yu. E. Roginskaya, M. D. Gol'dshtein, O. V. Morozova, and L. D. Glazunova,"Charge Accumulation in Nanoheterogeneous Iridium Oxide Films," *Russian Journal of Electrochemistry*, Vol. 37, No. 10, pp. 1065–1071, 2001.

[4.3] T. Katsube, I. Lauks and J. N. Zemel, "pH-sensitive sputtered iridium oxide films," *Sensors and Actuators*, Vol. 2, pp. 399-410, 1981.

[4.4] Hassan Y. Aboul-Enein, Xian Xiang Sun, and Cheng Jun Sun, "Ion selective PVC membrane electrode for the determination of methacycline hydrochloride in pharmaceutical formulation," *Sensors*, Vol. 2, pp.424-431, 2002.

[4.5] Lee Yook Heng, Loh Han Chern and Musa Ahmad, "A hydrogen ion-selective sensor based on non-plasticised methacrylic-acrylic membranes," *Sensors*, Vol. 2, pp. 339-346, 2002.

[4.6] Hongmei Quan, Won Kim, Koo-Chun Chung, and Jongman Park, "Surface renewable hydrogen ion-selective polymeric composite electrode containing iridium oxide," *Bull. Korean Chem. Soc.*,Vol. 26, pp. 1565-1568, 2005.

[4.7] S. Ardizzone, A. Carugati, and S. Trasatti, "Properties of thermally prepared iridium dioxide electrodes," *J. Electroanal. Cheml.*, Vol. 126, pp. 287-292, 1981.

[4.8] J. Hendrikese, W. Olthuis, and P. Bergveld, "A method of reducing oxygen induced drift in iridium oxide pH sensor," *Sensor and Actuator*, Vol. 53, pp. 97-103, Nov., 1998.

[4.9] G. Papeschi, S. Bordi, C. Beni, and L. Ventura, "Use of an iridium electrode for direct measurement of pI of proteins after isoelectric focusing in polyacrylamide gel," *Biochimica et Biophysica Acta,* Vol. 453, pp. 192-199, 1976.

[4.10] G.M. da Silva, S.G. Lemos, L.A. Picrifka, P.D. Marreto, A.V. Rosario, and E.C. Pereira, "Development of low-cost metal oxide pH electrodes based on the polymeric precursor method," *Analytica Chimica Acta*, Vol. 616, pp. 36-41, 2008.

[4.11] Fang Yue, Tan Swee Ngin, and Ge Hailin, "A novel paper pH sensor based on polypyrrole," *Sensor and Actuators B*, Vol.32, pp. 33-39, April, 1996.

[4.12] Kenneth G. Kreider, Michael J. Tarlov, and James P. Cline, "Sputtered thin-film pH electrode of platium, palladium, ruthenium, and iridium oxides," *Sensors and Actuators B*, Vol. 28, pp. 167-172, 1995.

[4.13] M. L. Hitchman and S. Ramanathan, "A field-induced poising technique for promoting convergence of standard eletrode potential values of thermally oxidized iridium pH sensors," *Talanta*, Vol. 39, pp. 137-144, 1992.

[4.14] Eric Bakker, "selectivity of liquid membrane ion-selective electrodes," *Electroanalysis*, vol. 9, No. 1, pp. 7-12, 1997.

[4.15] Lee Yook Heng, Loh Han Chern and Musa Ahmad, "A hydrogen ion-selective sensor based on non-plasticised methacrylic-acrylic membranes," *Sensors*, Vol. 2, pp. 339-346, 2002.

[4.16] Mohsen M. Zareh, "Relative selectivity coefficient as a new concept for evaluating electrochemical dopamine sensors," *Journal of Applied Sciences*, Vol. 8, pp.3654-3661, 2008.

[4.17] Ramin Maleki, Amir Abbas Matin, and Abolghasem Jouyban, "A membrane sensor for selective determination of bisacodyl in tablets," *Journal of the Chinese Chemical Society*, Vol. 53, pp. 613-618, 2006.

[4.18] Vasilios A. Krargounis, Chung Chiun Liu, Michael R. Neuman, Lubomyr T. Romankiw,

P. A. Leary and J. J. Cuomo, "A Pd-PdO film potentiometric pH sensor," *IEEE Transactions on Biomedical Engineering*, Vol. 33, pp. 113-116, 1986.

[5.1] J. C. Buzby and T. Roberts, "Economic costs and trade impacts of microbial foodborne illness," *World Health Statistics Quarterly*, Vol. 50, pp. 57-66, 1997.

[5.2] G. Sberveglieri, Gas Sensors, Principles, Operation and Developments, G. Sberveglieri , Italy, New York: Springer, 1992.

[5.3] Saverio Mannino, S. Benedetti, S Buratti, M.S. Cosio and Matteo Scampichio, "Electrochemical sensors for food authentication", Wilson and Wilson's comprehensive analytical chemistry, Vol. 49, pp. 755-770, 2007.

[5.4] Alexis Pacquit, June Frusby, Danny Diamond, King Tong Lau, Alan Fqrrell, Brid Quilty, and Dermot Diamond, "Development of a smart packaging for the monitoring of fish spoilage," Food Chemistry, Vol. 102, pp. 466-470, 2007.

[5.5] J. Oehlenschlager, "Volatile amines as freshness/spoilage indicators: a literature review, " 25th WEFTA international seafood conference, Vol. 38, pp. 571–586, 1997.

[5.6] Ivo Frebort, Lenka Skoupa, and Pavel Pec, "Amine oxidase-based flow biosensor for the assessment of fish freshness," Food Control, Vol. 11, pp. 13-18, 2000.

[5.7] Ching Mail Keow, Fatimah Abu Bakar, Abu Bakar Salleh, Lee Yook Heng, Rahman Wagiran, and Low Sim Bean, "A amperometric biosensor for the rapid assessment of histamine level in tiger prawn spoilage," Food Chemistry, Vol. 105, pp.1636-1641, 2007.

[5.8] June Frisby, Declan Raftery, Joe P. Kerry, and Dermot Diamond, "Development of an autonomous, wireless pH and temperature sensing system for monitoring pig meat quality," Meat Science, Vol. 70, pp.329-336, 2005.

[5.9] Lone Gram, and Hans Herik Huss, "Microbiological spoilage of fish and fish products," Food Microbiology, Vol. 33, pp. 121-137, 1996.

[5.10] Beatriz Serra, Angel Julio Reviejo, and Jose Mannuel Pingarron, "Application of

electrochemical enzyme biosensors for food quality control," Electrochemical Sensor Analysis, Vol. 13, pp. 255-298, 2007.

[5.11] Natali Chen, Nadav Chen, and Naaman Chen, "Food freshness indicator," *U .S. Patent 6723285 B2*, 2004.

[5.12] Alexis Pacquit, June Frisby, Danny Diamond, King Tong Lau, Alan Farrell, Brid Quilty, and Dermot Diamond, "Development of a smart packaging for the monitoring of fish spoilage," *Food Chemistry*, Vol. 102, pp. 466-470, 2007.

[5.13] T. Ativanishayaphong, J. Wang, W. Huang, S. Rao, and J.C. Chiao, "A simple wireless batteryless sensing platform for resistive and capacitive sensor," *IEEE Sensors*, Vol. 1 ,pp. 139-142, 2007

[5.14] J.J. Rodriguez-Jerez, M.M. Hernandez, and A.X. Roig-Sagues, "New methods to determine fish freshness in research and industry," *Cahiers Options Mediterraneennes*, pp. 63-69, 2000.

[5.15] S. Chen and V. Thomas, "Optimization of inductive RFID technology," *IEEE International Symposium on Electronics and the Environment*, pp. 82-87, 2001.

[5.16] E. Haile and J. Lepkowski, "Oscillator Circuits for RTD Temperature Sensors," Application notes AN895, Microchip Technology Inc., 2004.

[5.17] P. R. Troyk and G. A. DeMichele, "Inductively-coupled power and data link for neural prostheses using a class-E oscillator and FSK modulation, " *IEEE International Conference Engineering in Medicine and Biology Society*, Vol. 4, pp. 3376-3379, 2003.

[5.18] N. Chaimanonart, D.J. Young, "Remote RF powering system for wireless MEMS strain sensors," *IEEE Sensors Journal*, Vol. 6, pp. 484-489, 2006.

[5.19] Nathan O. Sokal, "Class-E RF power amplifiers," ARRL Technical Inc., pp. 9-20, 2001.

[5.20] Thermpon Ativanichayaphong, Wireless devices for medical applications, Ph.D. dissertation, University of Texas at Arlington, 2007.

[5.21] P. Kahrilas, "Surgical therapy for reflux disease," *The Journal of the American Medical Association, JAMA.*, Vol. 285, Issue 18, pp. 2376-2378, 2001.

[5.22] H. Mattox III and J. Richter, "Prolonged ambulatory esophageal pH monitoring in the evaluation of gastroesophageal reflux disease," *The American Journal of Medicine*, Vol. 89, Issue 3 , pp. 345-356, 1990.

[6.1] Igor A. Ges, Borislav L. Ivanov, David K. Schaffer, Eduardo A. Lima, Andreas A. Werdich, and Fran J. Baudenbacher, "Thin-film IrOx pH microelectrode for microfluidic-based microsystems," *Biosensors and Bioelectronics*, Vol. 21, pp. 248-256, 2005.

[6.2] Jessica Winter, Stuart Cogan, and Joseph Rizzo, "Retinal prostheses: current challenges and future outlook," *J. Biomater, Sci*., pp. 1-25, 2007.

[6.3] Ross D. Meyer, Stuart Cogan, and R. David Rauh, "Electrodeposited iridium oxide for neural stimulation and recording electrodes," *IEEE Transactions on neural system and rehabilitation engineering*, Vol. 9, pp. 2-11, 2001.

[6.4] Michael S. Wilson, and R. David Rauh, "Novel amperometric immunosensors based on iridium oxide matrices," *Biosensors & Bioelectronics*, Vol. 19, pp. 693-699, 2004.

[6.5] C. J. Brinker, G.C. Frye, A.J. Hurd, and C.S. Ashley, "Fundamentals of sol-gel dip coating," *Thin Solid Film*, Vol. 201, pp. 97-108, 1991.

[6.6] Lars Alexander Schneider, Andreas Korber, Stephan Grabbe, and Joachim Dissemond, "Influence of pH on wound-healing: a new perspective for wound-therapy?" *Arch Dermatol Res,* Vol. 298, pp. 413-420, 2007.

[6.7] Harrison DK, Walker WF, "Micro-electrode Measurement of Skin pH in Humans During Ischaemia, Hypoxia and Local Hypothermia," *Journal of Physiology*, Vol. 291, pp. 339-350, 1979.

[6.8] Susan Margaret Shorrock, "The exploration of tissue pH in wounds and its relationship to bacterial contamination," *Master Degree Thesis, Worcester Polytechnic Institute*, pp. 20-24, 2000.

[6.9] Lengheden A, and Jansson L, "pH effect on experimental wound healing of human fibroblasts in vitro, " *Eur J Oral Sciences*, Vol. 103, pp. 148-155, 1995.

[6.10] Allen J. Bard, *Electrochemical methods: fundamentals and application*, Wiley, New York, 2006.

[7.1] Hanna Elzanowska, Erfan Abu-Irhayem, Beata Skrzynecka, and Viola Briss, "Hydrogen peroxide detection at electrochemically and sol-gel derived Ir oxide films," *Electroanalysis*, Vol. 16, 2004, pp. 478-490.

BIOGRAPHICAL INFORMATION

WEN-DING HUANG received his Bachelor degree in Automatic Control Department from Feng Chia University, Taichung, Taiwan in 1999. Subsequently, he worked at Aerospace Industrial Development Corporation (AIDC) for 2 years as a R&D engineer for the invention of the train and flight simulator technology. After the end of the project, he continued the education and finished M.S. degree in Electrical Engineering Department from University of Texas at Arlington on 2005. He then joined the iMEMS group advising by Dr. J.C. Chiao, and worked on the research of miniature bio-medical devices. In 2010, he received his Ph.D. from the Department of Electrical Engineering in the University of Texas at Arlington. During his Ph.D. study, he has authored and coauthored more than 20 papers in technical journals and conferences, and obtained a pending patent. His research interests include medical devices, MEMS, sensors, wireless technologies, systematic characterization methods.